

EXPERT REPORT
U.S v. BP Exploration & Production, Inc., et al.

Oil Release from the MC252 Macondo Well

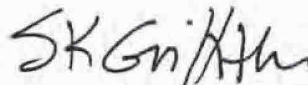
Prepared on Behalf of the United States

Prepared by:

Stewart K. Griffiths

████████████████████
Albuquerque, New Mexico 87122

March 22, 2013



Stewart K. Griffiths

11485
Exhibit No. _____
Worldwide Court Reporters, Inc.

CONTENTS

Personal Background	3
Involvement in Deepwater Horizon Response	3
Executive Summary	4
Methodology and Model	5
Best Estimates of Flow Rates and Discharge	7
Conditions Used for Best Estimate	8
Discussion of Uncertainties	10
Alternative Calculation of Flow Rates and Discharge	10
Validity of Model and Data	12
Information Required by the Federal Rules of Civil Procedure.....	15
Appendix A: Main Assumptions	16
Appendix B: Mathematical Model	18
Appendix C: Technical Basis for Constant Discharge Coefficients	20
Appendix D: Parameter Estimation	30
Appendix E: BOP gauge Offset	32
Appendix F: Long Term Shut-In Pressure	39
Appendix G: Discussion of Uncertainties	40
Appendix H: Flow Rates Based on Reservoir and Ambient Pressures	45
Appendix I: Flow Rates and Discharge Prior to May 8	46
Appendix J: Correlation of BOP and Reservoir Pressures	50
Appendix K: Curriculum Vitae for S. K. Griffiths	51
Appendix L: S. K. Griffiths Publications, Reports and Patents	52
Appendix M: List of Consideration Materials.....	61

PERSONAL BACKGROUND

I worked at Sandia National Laboratories for 31 years prior to retirement in December of 2011. Sandia is a U.S. Department of Energy national laboratory devoted to work on nuclear weapons, broader defense and deterrent systems, homeland security, and a variety of energy programs.

While at Sandia, I was responsible for a broad range of theoretical, computational, and experimental research in a great many areas, including:

- multi-phase flow in heat pipes and porous media, including geological materials
- gas transfer systems for nuclear weapons
- containment of underground nuclear explosions
- fractures in geological materials driven by single and multi-phase flows (hydraulic fracturing)
- optimization and parameter estimation
- analysis of data through development and application of physically-based models

During this time, I also served as a member the U.S. Nuclear Emergency Search Team, providing analysis, countermeasures, and field response to terrorist threats involving nuclear weapons.

Eleven years before retirement, I was promoted to the special appointment of Senior Scientist. In that capacity, I was additionally responsible for leadership of Sandia's ~\$12M/year laboratory-directed R&D program in nuclear weapons and served as a member of Sandia's Science Advisory Board responsible for ~\$150M annual investments in discretionary research. As a Senior Scientist, I also served as a technical resource for the laboratory and was asked on numerous occasions to address urgent, highly challenging problems across multiple disciplines, including fluid dynamics. Such requests were based on my technical judgment, ability to examine data carefully, and my ability to draw useful conclusions from data through specialized mathematical models. I used these skills in my analysis of oil discharged from the Macondo well, just as I did in my career at Sandia.

I have authored over 50 refereed journal publications, more than one hundred corporate technical reports, and hold 12 U.S. and international patents.

I received my B.S., M.S. and Ph.D. degrees in Mechanical Engineering from the University of Illinois at Urbana-Champaign in 1976, 1977 and 1980. My area of specialization was fluid dynamics and thermal sciences.

INVOLVEMENT IN DEEPWATER HORIZON RESPONSE

I participated in Sandia's contribution in the Department of Energy response to blowout of the Macondo well beginning in June of 2010. As part of that work, I developed the methodology used here and computed flow rates and the cumulative discharge of oil based on the data available to me at the time. I documented those studies in Sandia Report SAND2011-3800 released in June 2011. This work was later peer reviewed and published in the journal *Environmental Science and Technology*. The conclusions I express in this report are based largely on this modeling and analysis conducted while a Sandia employee.

My conclusions are also based in part on further research following my retirement from Sandia. This additional study enabled the discovery and analysis of additional data, resulting in refinement of the conditions used in my calculations and deeper understanding of the events immediately following the blowout. My methodology, however, has remained the same as that developed at Sandia. With this additional effort and new data, my estimate of the cumulative discharge has been revised downward by roughly 2% relative to my "most likely" discharge previously determined and documented.

EXECUTIVE SUMMARY

The purpose of my study was to quantify flow rates and the cumulative discharge of oil from the Macondo well over the roughly 86 days following blowout. I conclude that the cumulative discharge was 5.0 million stock-tank barrels (mmstb). Quantified uncertainties in this value are -13.9% and +9.7%, leading to bounds on this nominal value of 4.3 to 5.5 mmstb. The flow rate just following blowout was approximately 63,000 stock-tank barrels per day (stbd). This flow rate decayed to approximately 55,000 stbd just prior to installation of the capping stack.

To obtain these values, I developed a physically-based empirical model describing flow in the reservoir, wellbore, BOP, and capping stack. This model is physically-based because it is built on two underlying principles of fluid dynamics. The first of these is conservation of mass. That is, the mass of stock-tank oil entering any segment along the flow path must also exit that segment. The second is that flow rates exhibit certain specific relations to the frictional pressure drop, depending on whether the flow is laminar or turbulent.¹ For laminar flows, as in the reservoir, the flow rate is simply proportional to the pressure drop. For turbulent flows, as in the wellbore, BOP, and capping stack, flow rates are proportional to the *square-root* of the pressure drop. Provided a measured flow rate and pressure drop at one condition, I can therefore calculate flow rates at other conditions for which just the pressure drop is known. This model is also empirical in nature because I determined the constants of proportionality relating flow rates to pressure drops from pressures and flow rates that were actually measured. All pressures and flow rates discussed in my report were measured by BP.

Through this methodology, utilizing a combination of theory and empiricism based on BP data, I believe the model very accurately represents the well from a perspective of flow without the need for details of the flow path or physical dimensions along it. And because the model conserves mass along the flow path, the pressure drop between any pair of known or measured pressures can be used to compute flow rates over the 86 days of interest.

My best estimate of the discharge was calculated using this model along with pressure differences (drops) between reservoir pressures and pressures measured at the bottom of the BOP periodically over the 86 days. An important advantage of using this particular pair of pressures is that resulting calculated flow rates and the cumulative discharge automatically account for the many alterations of the wellhead geometry downstream of the BOP gauge through their influence on BOP pressures. Removal of the marine riser, installation of the top-hat, and even erosion of the BOP rams are all therefore dealt with in a rigorous manner without need for detailed knowledge of the changing wellhead geometry.

Related key findings of my study are that:

- The top-kill activities between May 26 and 29 had essentially no lasting influence on flow rates and very little impact on the cumulative discharge.
- Removal of the marine riser increased flow rates from the well by roughly 3%.
- Any significant erosion of the BOP rams, pipe, riser, and cement barrier in the bottom of the well occurred rapidly over the first few days following blowout. Subsequent erosion had little impact on flow rates or on the cumulative discharge.

I established the validity of this model and its underlying assumptions through comparison with various measured pressures and flow rates, comparison with well-established models of two-phase flow, and comparison with calculations done by BP. Validity of the model was further established through two alternative calculations using the fixed ambient sea pressure to calculate historical flow rates, both of which yield a cumulative discharge that is within 2% of my best estimate. I established accuracy of the model and my best estimate of the discharge through a quantitative analysis of uncertainties.

¹ The frictional pressure drop is simply the difference in pressure between two points along a flow path, excluding the difference due to gravity. This difference due to gravity is usually referred to as the elevation head. Laminar flows are characterized by smooth orderly behavior as one layer of fluid slides past another. Turbulent flows are characterized by extensive mixing, folding, and chaotic motion.

METHODOLOGY AND MODEL

Calculation of the cumulative oil discharged from the well requires the calculation of flow rates periodically over the 86 days between blowout on April 20 and shut-in on July 15.² Any calculation of these flow rates in turn requires pressures at two points somewhere along the flow path from reservoir to sea. These pressures may be measured over the 86 days or known by other means. General-purpose theoretical models used in such calculations also require a detailed description of the geometry between the two points at which pressures are specified, including lengths and apertures at every position along the path. They additionally require an equation of state describing the fluid as a function of the pressure and temperature, some model describing fluid temperatures, and constitutive equation relating the flow rate of a two-phase fluid to local pressure gradients as a function of local fluid properties.

Most of this required information is available, and the geometry and dimensions of the wellbore and capping stack are well characterized. The geometry, lengths, and apertures of the paths into the bottom of the well and through the BOP, however, cannot be characterized with sufficient accuracy to yield accurate estimates of the flow rates. Under such circumstances, a good alternative to the theoretical approach employed in general-purpose models is the hybrid methodology used here. I refer to this as a physically-based empirical model. Here the reservoir, wellbore, BOP, and capping stack are all characterized from the perspective of flow using measured pressures and flow rates, without the need for a detailed description of their geometries or dimensions. Assumptions underlying the model are described in Appendix A. Details of the mathematics are provided in Appendix B.

This model combines pressures measured by BP with two underlying principles of fluid dynamics in a manner that enables me to calculate flow rates over the 86 days following blowout of the well. The first of these principles is conservation of mass, requiring that any oil entering the wellbore must also exit the wellbore at some point along the flow path. The second principle is that flow rates vary with the pressure drop between two points along the flow path according to certain well-established relationships.

In my model, the relationship between the pressure drop and flow rate of oil in the reservoir is described by an industry-standard productivity index. Here the relationship is linear such that the flow rate is simply proportional to the pressure drop, as appropriate for laminar flow in a porous material, and the constant of proportionality is the productivity index. Flow in the wellbore, BOP, and various paths through the capping stack (when present) is described by a series of discharge coefficients relating the flow rate to the *square-root* of the pressure drop, as appropriate for the turbulent flow that occurs in these segments along the path. In this sense, the model is physically based in that flow rates are related to pressure drops according to well-established principles of fluid dynamics. The technical basis for use of these discharge coefficients is described in Appendix C. There I demonstrate that constant discharge coefficients very accurately reproduce flow rates computed using more complex general-purpose models of two-phase flow for the conditions of interest here.

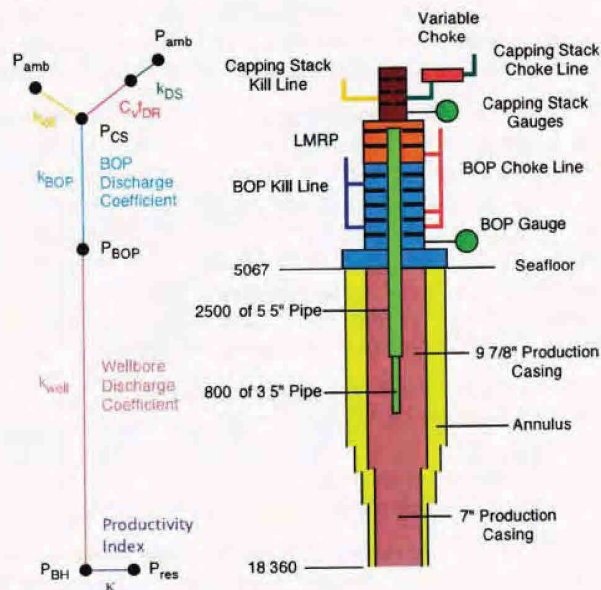
A schematic of this model is shown on the left of Fig. 1 below, along with a diagram of the well. Each black dot along the schematic represents a point at which pressures are known, measured, or can be calculated. Colored lines between these represent flow paths that are characterized by the productivity index or one of five discharge coefficients. These discharge coefficients, constants of proportionality, are not known beforehand. In a purely theoretical approach they are calculated for each phase using lengths and apertures along each segment of the path, along with the equation of state and models describing heat transfer and two-phase flow. Here I determine them empirically from pressures measured during shut-in and from pressures and flow rates of collected oil measured earlier the same day.

The method for determining the productivity index and five discharge coefficients is built on the fundamental principle of conservation of mass. During shut-in, pressures were measured at the BOP

² There are 87 calendar days between April 20 and July 15, 2010, including the start and end dates. However, the duration of flow between blowout and shut-in was 85 days and 17 hours, or approximately 86 days.

(PT-B) and capping stack (PT-3K-2) at each of 15 steps as the capping-stack variable choke was closed. At each of these steps, flow rates are calculated using the six parameters and the measured BOP and capping stack pressures, the reservoir pressure, and the known ambient pressure at the seafloor. Conservation of mass requires that the calculated flow rate from the reservoir through the wellbore must equal the flow rate through the BOP. And, the flow rate through the BOP must equal that through the variable choke and choke line of the capping stack. Together these provide 30 conditions that must be satisfied by the productivity index and discharge coefficients.

Figure 1. Diagram of the Macondo well, blowout preventer, and capping stack.³ The overall height of the capping stack is about 12 feet; that of the BOP is about 54 feet. Depth of well from the seafloor is roughly 13,300 feet. Capping stack was added on July 12, 2010. For purposes of this analysis, the lower marine riser package (LMRP) is considered to be part of the BOP. The schematic at left shows relative positions of pressures and flow coefficients used in calculating flow rates. Each coefficient relates local flow rates to the pressure difference over the line segment of corresponding color.



Pressures were again measured at the BOP and capping stack during oil collection preceding shut-in, and these are again used to calculate flow rates based on the six parameters. Here, the calculated flow rate up the wellbore must equal the sum of the measured flow rate of collected oil *plus* the calculated flow rate through the open kill line on the capping stack. Taking one case in which oil was collected and one case in which it was not, this adds two additional constraints that the productivity index and discharge coefficients must satisfy. These constraints establish the overall magnitude of the flow rate based on the actual measured rate of collected oil.^{4,5} This again reflects the empirical nature of my method and its reliance on the actual measured behavior of the well via data provided by BP.

Because there are more conditions to be satisfied than there are parameters in the model, this becomes a problem of least-squares estimation in which the six parameters are chosen to satisfy all of the conditions as best as is possible given the physical reality of the measured pressures and flow rates of collected oil.⁶ Here I estimate all six parameters simultaneously using a non-linear least-squares optimization algorithm, TJMAR1.⁷ Details of this process are provided in Appendix D.

³ Dimensions from BP file "Macondo_Relief_Well_Wall_Plot-Review_Pre-read.xls", SNL044-002450.

⁴ From BP file "Collection rates during well integrity test w_Vx-1.xls". BP-HZN-2179MDL04884268.

⁵ From BP file "Tab 03-BP-HZN-2179MDL07266155.XLS." Q4000 mean flow rate for the period 01:30-02:30 on July 15 is 8040 stbd, leading to a total collected oil flow rate of 20,296 stbd based on HP1 collection per "Tab 04-BP-HZN-2179MDL07265827.XLS".

⁶ In contrast, we are most familiar algebraic systems in which the number of unknowns equals the number of equations and the solution satisfies all of the equations exactly.

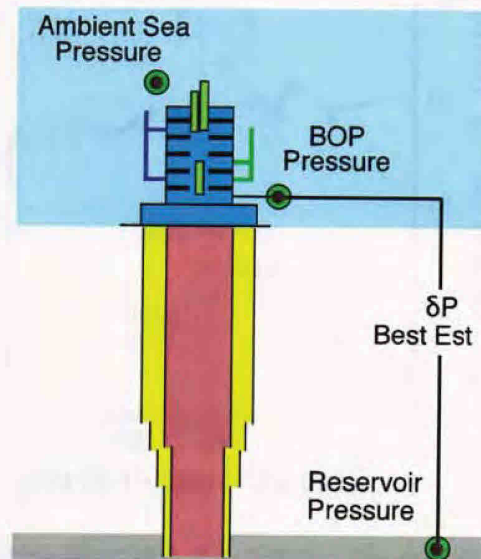
⁷ Jefferson, T. H., "TJMAR1-A Fortran Subroutine for Nonlinear Least Parameter Estimation," Sandia National Laboratories Report, SLL-73-0305, 1973.

Once the six parameters are determined, my model is capable of describing flow through all points in the well, BOP, and capping stack given appropriate known or measured pressures. Historical flow rates over the 86 days can then be calculated using pressure differences based on any combination of the reservoir, BOP, and ambient sea pressures. These flow rates are then integrated over time to yield the cumulative discharge.

My best estimate of the cumulative discharge is based on flow rates calculated using the difference between the reservoir pressures and pressures at the bottom of the BOP that were measured periodically over the 86 days. This is illustrated in Fig. 2. The basis for this choice is that flow rates calculated using the reservoir and BOP pressures automatically account for alterations of the wellhead downstream of the BOP gauge through their influence on BOP pressures. Removal of the marine riser, installation of the LMRP top-hat, installation of the final capping stack, and even erosion of the BOP rams are all therefore dealt with in a rigorous manner without need for detailed knowledge of the changing wellhead geometry.

Figure 2. Schematic of well showing the pressure difference (δP) used in my best-estimate calculations of historical flow rates and cumulative discharge. This is illustrated by the black line joining the reservoir and the BOP at the location of the BOP gauge.

Alterations of the wellhead downstream of the BOP gauge (PT-B) affect the measured BOP pressures and so affect my calculated flow rates. Any such alterations, including erosion within the BOP, are therefore properly accounted for.



BEST ESTIMATES OF FLOW RATES AND DISCHARGE

Using the difference between reservoir and BOP pressures, as illustrated in Fig. 2, my calculated cumulative discharge of oil from the well is 5.0 million stock-tank barrels (mmstb). The average flow rate from the well over the period from blowout to shut-in was 58,300 stbd.

Quantified uncertainties in my cumulative discharge are -13.9% and +9.7%. As discussed below, these values arise from twelve distinct contributions. Applying these uncertainties to my nominal best-estimate discharge of 5.0 mmstb yields a range from 4.3 to 5.5 mmstb. Based on the investigation documented in this report regarding validity of the model and data, I have very high confidence that the true discharge from the well lies within these bounds.

The calculated flow rates on which my cumulative discharge is based are shown in Fig. 3. Each point on this plot (with the sole exception of time zero) represents a measured BOP pressure and the corresponding calculated flow rate. Although difficult to discern, this plot displays over 94,000 calculated flow rates. The initial flow rate from the well is slightly over 63,000 stock-tank barrels per day (stbd). This decays to about 55,000 stbd just before installation of the capping stack. Following

installation of the capping stack, the flow drops further depending on whether the choke, kill line or both are open.

Figure 3 shows that the flow rate decays fairly smoothly with little evidence of any significant lasting effects from the various wellhead activities, except perhaps removal of the original marine riser. Linear fits to flow rates just before and after removal of the riser show an increase in flow rate of about 1800 stbd or 2.8%. Calculated flow rates just before and after the top-kill effort are continuous along the trend, indicating that the injection of mud and debris had no significant lasting effect on flow rates. Linear fits to these rates just before and after top-kill are offset by just 0.1%.

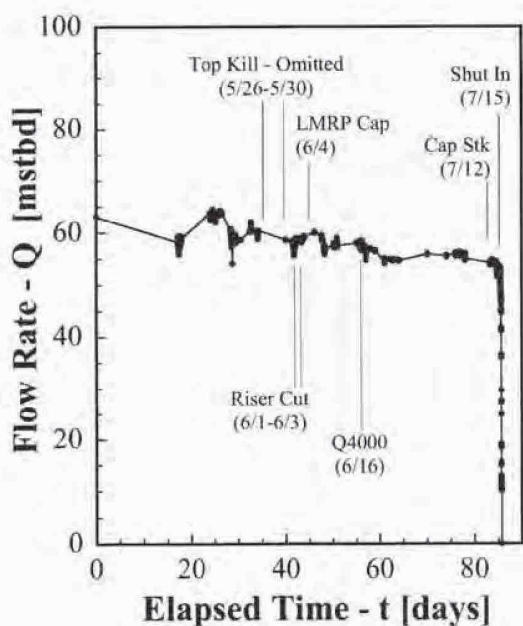


Figure 3. Best-estimate flow rates in thousands of stock-tank barrels per day. These are calculated using measured BOP pressures and the reservoir pressure history shown in Fig. 5.

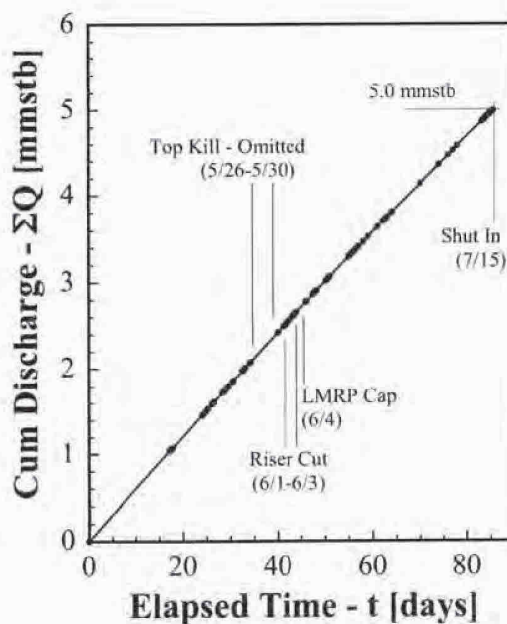


Figure 4. Calculated best-estimate cumulative discharged oil. Nominal cumulative discharge over the 86 days is 5.0 mmstb. The range due to uncertainties is 4.3 to 5.5 mmstb.

I calculated the cumulative discharge of oil directly from the results of Fig. 3. This was done using a trapezoid algorithm to integrate the instantaneous flow rate from one measured BOP pressure to the next. These results are shown in Fig. 4. Note that the history of the calculated cumulative discharge is much smoother than that of the flow rates because brief excursions in the flow rate do not contribute significantly to the cumulative total. Again, over 94,000 points are represented in this plot. The cumulative discharge at the last point is 5.0 mmstb.

CONDITIONS USED FOR BEST ESTIMATE OF DISCHARGE

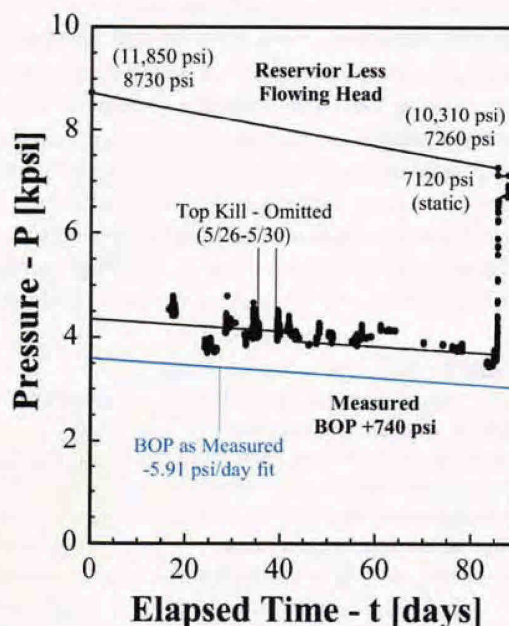
As already mentioned, my calculated cumulative discharge is based on differences between the reservoir and BOP pressures over the 86 days following blowout. The BOP pressures I used for these calculations are corrected by +740 psi from the reported values to account for a persistent offset in the PT-B transducer. As discussed in Appendix E, this correction is based on reference of the PT-B gauge to

four other gauges, as well as calibration of the PT-B gauge following recovery of the BOP. My estimate of the discharge is also based on a reservoir pressure history determined by the initial value of 11,850 psi measured by BP before the blowout and by my own estimate of the final long-term wellhead shut-in pressure of 7120 psi. This corresponds to a final reservoir pressure of 10,310 psi and depletion of the reservoir by 1540 psi over the 86 days of flow. This shut-in pressure and depletion are discussed further in Appendix F.

Figure 5. Best-estimate reservoir and measured BOP pressure histories. Per Appendix E, reported BOP pressures are offset by +740 psi prior to July 12 and by -620 psi thereafter.

Reservoir pressures less flowing elevation head (upper black curve) are obtained from the indicated initial and final values with a decay in between based on cumulative flow from the well. This leads to a reservoir pressure history that is very slightly concave upwards owing to flow rates that are initially high but fall as the reservoir pressure decays.

Over 94,000 measured BOP pressures are shown (black symbols). These were all provided by BP.



Corrected BOP pressures used in my calculations are shown in Fig. 5 along with my best estimate of the reservoir pressure history less the flowing elevation head.⁸ Elevation heads are pressure differences due to gravity and fluid density. They are excluded in my analyses because they do not contribute to flow. The difference between these measured BOP pressures and the continuous reservoir pressure history is used with the productivity index and discharge coefficient for the wellbore to calculate my best estimate of flow rates and cumulative discharge over the 86 days.

The solid blue line in Fig. 5 represents a linear least-squares fit to the measured pressures between May 8 and July 14, 2010.⁹ The slope of this fit is -5.91 psi/day, with an intercept at the origin of 3560 psi. This corresponds to a true pressure of 4300 psi based on my estimate of -740 psi for the offset in the PT-B gauge. This is the initial pressure (at zero elapsed time) used in my best estimate of the cumulative discharge. Absent additional information, I believe this provides the best estimate of BOP pressures before May 8. The slope of -5.91 psi/day is used in a later discussion related to decay of the reservoir pressure as part of model and data validation.

⁸ Measured BOP pressures are from the BP files: "MC252_DataDump_071810.xls", SNL087-001206; "05_14 - 23 May.xls", SNL088-072912; "034a_20100516_0201_BPD410-49632-49632.xls", BP-HZN-2179MDL06336851; "033b_20100516_0201_BPD407-30430-30430.xls", BP-HZN-2179MDL06089077; and "PT_B Offset 2 15 Jun thru 14 Jul.xls", SNL022-007753.

⁹ The measured values were first interpolated onto uniform intervals of one day for each point to eliminate biases associated with highly episodic data having variable numbers of points within each measurement period.

DISCUSSION OF UNCERTAINTIES

In calculating uncertainties of -13.9% and +9.7%, I have considered twelve distinct sources of potential error. As summarized in Table 1, these arise either from sources associated with parameter estimation (yellow) or from uncertainties or variations over the 86-day period (blue). The uncertainties associated with parameter estimation in turn arise largely from variations in density, viscosity, and/or quality of the gas-oil mixture that are not accounted for in my model. In Table 1, for example, the estimated variation in flow rates through the BOP due to density variations is $\pm 3.4\%$, and this leads to uncertainties in the calculated cumulative discharge of -1.6% and +1.8%. These values were calculated by perturbing the BOP discharge coefficient by $\pm 3.4\%$, estimating all other parameters holding this perturbed value constant, and calculating the cumulative discharge that results. Uncertainties arising from density-induced variations in flow rates through the capping-stack choke and kill lines were computed in a similar manner. Additional details on my uncertainty analysis are presented in Appendix G. Note in Table 1 that uncertainties associated with each source are simply grouped together according to sign and so represent a worst-case scenario. We might reasonably expect that some of these uncertainties would offset one another and so result in a somewhat lower total range.

Table 1. Summary of uncertainties in my cumulative discharge due to various sources. The numbers immediately following each source represent uncertainty in flow rate associated with that source. Values listed in the last two columns represent resulting uncertainties in the calculated historical flow rates and cumulative discharge of oil from the well. These are grouped according to their signs without regard to signs in the source.

The origin of these values is discussed in Appendix G.

Source of Uncertainty	Negative (%)	Positive (%)
BOP $\pm 3.4\%$	-1.6	+1.8
Choke Dwn-Strm Tubing $\pm 4.5\%$	-0.3	+0.3
Kill Line $\pm 1.9\%$	-0.3	+1.0
Choke 2- ϕ Factor +250/-0%	-1.7	
Measured Flow Rates	-1.6	+1.8
Res Press (7260 vs 6605 psi)		+0.6
Head Variation During Shut-In	-0.7	
Wellbore Density +3.4/-4.0%	-1.3	+1.1
Res Density & Viscosity +0/-12%	-1.0	
Reservoir Pres Decay (± 50 psi)	-0.3	+0.3
BOP Gauge Offset (± 130 psi)	-1.8	+1.9
Flow Rate Before May 8	-3.3	+0.9
Total	-13.9	+9.7

ALTERNATIVE CALCULATIONS OF FLOW RATES AND DISCHARGE

I have calculated my estimated discharge above using differences between the reservoir and BOP pressures. Alternate calculations are possible, however, using the difference between the reservoir pressure and fixed ambient pressure of ~ 2200 psi at the seafloor. This method is discussed further in Appendix H. Flow rates and the cumulative discharge can also be calculated using the difference between the measured BOP pressures and the fixed ambient sea pressure. The pressure differences used in these two alternative calculations are illustrated schematically in Fig. 6.

Comparing my best-estimate cumulative discharge with estimates based on these alternative methods has provided me with significant insight into historical flow rates and potential mechanisms affecting these flow rates. I first consider the alternative result based on differences between the reservoir and ambient pressures (indicated by the blue line in Fig. 6). The calculated discharge using this alternative pressure difference is 5.1 mmstb, which agrees with my best estimate of 5.0 mmstb to within 2%. Such good agreement indicates that the various wellhead alterations, other than removal of the riser, did not significantly affect flow rates. This good agreement also indicates that flow rates over the 86-day period

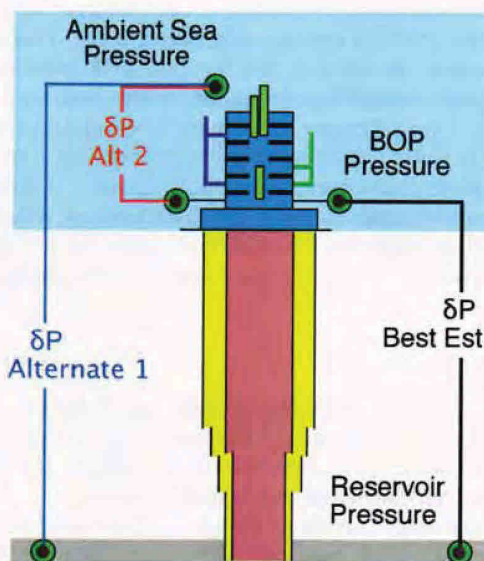
were not significantly affected by erosion within the BOP since use of the reservoir and BOP pressures accounts for this possibility while use of the reservoir and ambient pressures does not. Any erosion in the BOP that affected flow rates therefore had to occur over the first few days such that the state of the BOP over the great majority of the 86 days was comparable to that at shut-in on July 15. If not, the alternative discharge based on the reservoir and ambient pressures would significantly exceed my best-estimate value of 5.0 mmstb, and this is not the case.

Figure 6. Schematic showing pressure differences (δP) used in my best estimate and alternative calculations.

Best estimate calculations are based on the difference between the reservoir pressure and pressures measured at the BOP using PT-B. This is illustrated by the black line on the right.

The first alternative calculation uses the difference between the decaying reservoir pressure and the fixed ambient pressure of ~2200 psi at the seafloor, as indicated by the blue line at the left.

Second alternative calculation uses the difference between the measured BOP pressures and ambient seafloor pressure. This is indicated by the red line on the left.



Given that the state of the BOP remained relatively constant over most of the 86 days, further conclusions about the state of the wellbore and reservoir can be reached. I now consider the alternative calculation of discharge based on the difference between the BOP and sea ambient pressures (indicated by the red line of Fig. 6). This also yields 5.1 mmstb, and this result does not involve the wellbore discharge coefficient or productivity index. In this case, my best estimate of 5.0 mmstb would significantly exceed the alternative value if the wellbore discharge coefficient or productivity index had increased significantly over the 86 days. Again, this is not the case. Any variation in the wellbore discharge coefficient or productivity index therefore also occurred within the first day or so such that the state of the reservoir and wellbore over most of the 86 days were substantially the same as the state on July 15. And, this includes the state of the cement barrier in the bottom of the well. This view is also supported through calculations performed for BP by Add Energy that address the period just preceding the initial explosion. Under conditions that most closely replicate measured pressures and observable events, their analyses indicate that the effective productivity index increased by over 25% between 21:00 and 21:30 on April 20.¹⁰ This indicates that whatever down-hole restriction existed at that time was failing rapidly, regardless of whether this restriction resided in wellbore debris, the float collar, or cement barrier. For continued failure at this rate, I estimate that the productivity index would further increase to my best-estimate value

¹⁰ From "Deepwater Horizon Accident Investigation Report," September 8, 2010. Appendix W, Case 7, Page 54. To match data and observations, the pay zone was increased from 13 and 16.5 feet, corresponding to effective productivity indices of 7.4 and 9.4 stbd/psi based on the nominal value of 49 stbd/psi and maximum pay zone of 86 feet used in that report. At this rate, the productivity index would reach 43.8 stbd/psi in 8.6 hours.

in less than 9 hours.¹¹ At this point, the cement barrier or other impediments would provide no significant restriction to flow from the reservoir into the casing. Subsequent erosion in this region therefore could not have influenced later flow rates.

These conclusions rigorously apply only for the period from May 8 to July 15, the dates over which BOP pressures were measured. While I conclude that erosion in the BOP during this period did not significantly affect flow rates or the cumulative discharge, erosion in the first few days following the blowout certainly did. The methodology I use here cannot address this early erosion directly, but can instead provide an alternative calculation of flow rates and discharge in the first few weeks based on the times at which various rams were closed. This is described in Appendix I. Here the time between riser collapse on April 22 and the first BOP pressure measurements on May 8 is broken into a number of periods defined by closing the various rams. I then calculate the flow rate and discharge for each period using the difference between the reservoir and ambient sea pressures and the state of the BOP at that time. This yields a cumulative discharge between April 22 and May 8 that agrees with the value from my best-estimate calculation within 0.22 mmstb. Taking into account reasonable flow rates over the 36 hours preceding riser collapse, this discrepancy is reduced to about 0.17 mmstb. From these results, I conclude that uncertainties in conditions before May 8 are not large, contributing at most 3.3% to the overall uncertainty in my estimated cumulative discharge.

VALIDITY OF MODEL AND DATA

To help ensure the accuracy of this model, validity of assumptions and data, and the quality of the parameter estimation, I have undertaken a number of additional calculations and checks. These were intended to verify internal self-consistency of the model, freedom from gross errors, and good agreement between calculated and measured values. To further ensure this integrity, I wrote from scratch a second stand-alone version of portions of the model to confirm there were no undetected errors in the original coding. Flow rates calculated from this were then successfully compared against those of the original code. Highlights of my various validation efforts are described below. These demonstrate that my model, built on several measurements made during and just before shut-in, accurately describes all measurements made in that timeframe, provides consistent estimates of flow rates regardless of which measured pressures are used, and accurately predicts pressures that were measured over the 86 days. My validation efforts also show that my model parameters are consistent with values used by BP during the blowout response and that flow rates calculated by BP are accurately reproduced by my methodology.

Comparison with BP Parameters and Calculations

My best estimate of the productivity index is 43.8 stbd/psi. This value was determined empirically from measurements that characterize true behavior of the flowing well. Nevertheless, it falls very close to the midpoint of the range of values of 37, 45, and 50 stbd/psi used internally by BP.^{12,13} I believe that the BP values were all calculated using the estimated or measured permeability of the reservoir and the wellbore geometry. As such, this comparison serves primarily to confirm that my methodology yields credible results.

¹¹ Assuming that the cement remained reasonably intact, the likely mechanism for progressive failure is erosion. In this case, the rate of failure would not remain constant but would instead increase rapidly as small channels opened and fluid velocities increased. The 9 hour estimate thus very likely represents an upper bound on the time to complete elimination of any resistance to flow by the cement or other down-hole restriction.

¹² "Dynamic Relief Well Kill for Macondo MC252 Blowout," SNL046-082105, O. B. Rygg, ADD Wellflow, AS, June 2010.

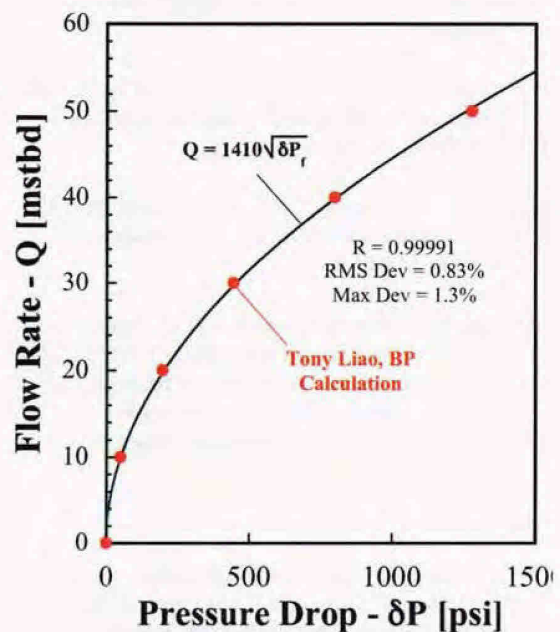
¹³ Value of 37 stbd/psi is obtained from analysis of calculations by Tony Liao of BP presented in "BP-HZN-2179MDL04920969.xls." Value of 45 stbd/psi is from "Liao, Tony_20130111_Ex 11163.pdf." BP internal email from Tony Liao to Maria Nass, June 27, 2010.

My best estimate of the wellbore discharge coefficient is 1152 stbd/psi^{1/2} and again this was determined empirically. Per Table 2 of Appendix C, this is about 18% lower than the roughly 1400 stbd/psi^{1/2} inferred from BP calculation of flow rates along the casing. My value is lower, I believe, because it correctly captures the complex geometry at the bottom of the well whereas the BP calculations did not. If the higher BP value were used, my best estimate of the cumulative discharge would increase by roughly 15%.

Finally, one difference between my empirical methodology and the approach used in general-purpose models of two-phase flow is my use of constant discharge coefficients to relate flow rates of stock-tank oil directly to pressure differences. This is addressed at length in Appendix C. As part of that analysis, I compared flow rates along the wellbore computed using a fixed discharge coefficient with those calculated by BP using the comprehensive PROSPER model of two-phase flow.¹⁴ A constant discharge coefficient reproduces the BP results to within 1.3% for all flow rates from zero to 50,000 stbd. The RMS deviation¹⁵ between the two results is just 0.83% over all flow rates. This is illustrated in Fig. 7.

Figure 7. Comparison of flow rates calculated via a constant discharge coefficient and those calculated by BP using the PROSPER two-phase model of flow along the wellbore.

The BP PROSPER calculations employ the widely-used Beggs and Brill correlations for two-phase flow, a correlation for gas lift, a comprehensive equation of state for the oil based on measured oil properties, and a very detailed description of the geometry of the wellbore casing. My physically-based empirical approach reproduces all of their flow rates to within 1.3%.



Comparisons During Shut-In and Oil Collection (July 15)

During shut-in, the capping stack choke was closed in a series of 15 steps. As shown in Fig. 8 below, my calculated capping-stack pressures agree with the pressures measured by BP to within $\pm 2.6\%$ or ± 120 psi over all 15 steps. Those for the BOP pressures agree within $\pm 1.7\%$ or ± 90 psi. These deviations are considerably smaller than the estimated accuracy of the BOP gauge, ± 200 psi.¹⁶ Such good

¹⁴ From "BP-HZN-2179MDL04920969.xls". Created by Tony Liao, June 24, 2010.

¹⁵ RMS (root mean squared) deviation is the square root of the average square of discrepancies between a model and all measured points. This is a standard indicator of the agreement between a model and observed values. Smaller values indicate better agreement.

¹⁶ "MC252 Sensor Accuracy," Matt Gochmour, BP briefing, July 18, 2010. Exhibit 8684. Estimated accuracy of BOP transducer was $\pm 4\%$ at 25% of full scale (5,000 psi) based on prior calibration.

agreement demonstrates, in part, that the assumptions underlying the model remain valid over a broad range of flow rates and conditions.

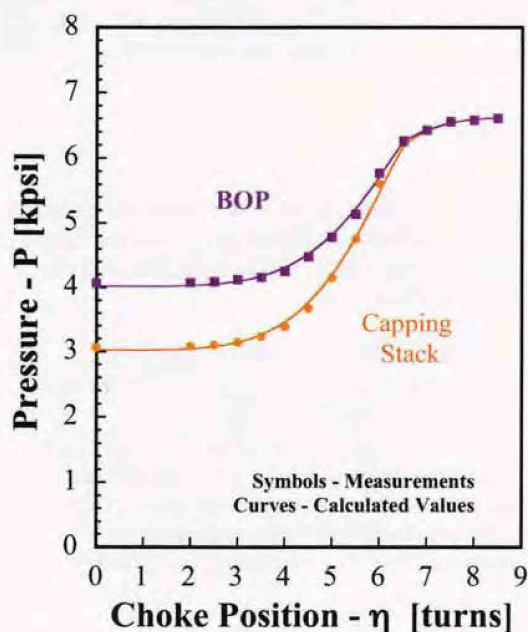
My calculated flow rates during shut-in based on the difference between the reservoir pressure and the measured BOP, capping stack, or ambient pressure agree with one another to within $\pm 3\%$ over all 15 steps of the choke. This demonstrates that changes in the conditions downstream of the BOP are properly accounted for through their influence on BOP pressures, even under dramatically varying conditions. This also confirms validity of this methodology and its ability to yield accurate estimates of historical flow rates that rigorously account for both known and unknown variations in the BOP and riser geometries downstream of the BOP gauge.

Figure 8. Calculated and measured BOP and capping-stack pressures during shut-in. Per Appendix E, measured BOP pressures are corrected by -620 psi.

Calculated BOP pressures (purple curve) agree with the measured values (purple symbols) to within 1.7% or 90 psi for all choke settings.

Calculated capping-stack pressures (orange curve) agree with measured values (orange symbols) to within 2.6% or 120 psi.

Although the measured pressures were used to calculate flow rates in my estimation of the model parameters, these pressures were not fit as part of that process. Instead, the parameters were determined solely by conservation of mass.



I also used my model and parameters to reconcile capping-stack and BOP pressures measured during shut-in. This led to my prediction that the BOP gauge was linear and exhibited the correct sensitivity at the time of shut-in. This prediction, documented in my Sandia Report,¹⁷ was later verified by calibration of the gauge following recovery of the BOP.

On the morning of July 15, oil was collected from the BOP during four one-hour periods. My calculated collection rates using the measured BOP and capping-stack pressures agree with the measured rates within 1.7% for all four periods. This is discussed in Appendix G. This demonstrates good precision in measuring BOP and capping stack pressures and good precision in measuring flow rates of collected oil.

Comparisons During the 86 Days of Flow

BOP pressures that I calculated using just the model parameters and reservoir and ambient pressures agree very well with those actually measured over the 86 days. This calculated history is shown by the

¹⁷ Oil Release from the BP Macondo MC252 Well: Flow Rates and Cumulative Discharge Calculated using Measured Blowout-Preventer Pressures, S. K. Griffiths, Sandia Report SAND2011-3800, June 2011.

black curve in Fig. 5 passing through the BOP pressures. The RMS deviation between these calculated and measured values is just 4.6%, for the period from May 8 to early on July 15, and most of this discrepancy is due to the fact that the calculated pressures are low, on average, by 3.7% or 160 psi as compared to the measured pressures offset by +740 psi. This discrepancy of 160 psi is roughly in the range of uncertainty for my estimate of the BOP gauge offset and is again less than the estimated accuracy of BOP gauge. Because these BOP pressures measured over the 86 days in no way influence my model or the six parameters, such good agreement further demonstrates the accuracy of the model and validates my independent conclusion that the offset in the BOP gauge was -740 psi during this period.

The observed decay in measured BOP pressures between May 8 and July 14 is -5.91 psi/day. This is illustrated by the blue line in Fig. 5. Per Appendix J, my model predicts that the decay rate of the reservoir pressure should be very nearly three times the decay rate at the BOP. This leads to a reservoir decay rate of 17.5 psi/day or 1500 psi total over the period from blowout to shut-in. This agrees remarkably well with my independent estimate of 1540 psi based on the long-term shut-in pressure, as described in Appendix F. This independent estimate does not depend on any measured BOP pressures, so such agreement again indicates validity of my model. It also indicates that the BOP gauge (PT-B) was linear and exhibited the correct sensitivity between May 8 and July 14. Otherwise, the slope of the fit to the measured pressures would be inconsistent with my independent estimate of the decay in reservoir pressure.

INFORMATION REQUIRED BY THE FEDERAL RULES OF CIVIL PROCEDURE

1. This report contains my opinions, conclusions, and reasons therefore.
2. A general statement of my qualifications is contained in the Personal Background section, page 3. A more detailed statement of my qualifications is included in Appendix K.
3. A list of publications authored since 1995 is provided in Appendix L.
4. My compensation for the preparation of this report and any testimony as an expert witness at trial or deposition is as follows: \$180 per hour.
5. I have not previously testified as an expert witness.
6. The facts and data I considered in forming my opinions are listed in Appendix M.

The opinions expressed in this report are my own and are based on the data and facts available to me at the time of writing. Should additional relevant or pertinent information become available, I reserve the right to supplement the discussion and findings in this report.

Appendix A: Main Assumptions

Development of the model required for this approach involves several assumptions. These are that: (1) all flows are fully developed, fully mixed, and quasi-steady; (2) all flows are turbulent, except in the reservoir; (3) flow in the reservoir is laminar; (4) geometry of well from the BOP gauge down is nominally unchanged over the 86 days; (5) two-phase flow through the capping stack choke is adequately described by a constant de-rating factor over the range of conditions of interest; and (6) gas-oil mixture densities at any fixed position along the flow path do not vary significantly with changes in pressure or flow rate over the ranges of interest. For the wellbore, the last of these assumptions can be relaxed to a statement that the mean density along the wellbore does not vary significantly with changes in pressure or flow, again over the range of conditions of interest. As discussed in Appendix C, assumption 6 regarding constant density is not actually required since turbulent discharge coefficients remain relatively constant even when mixture densities and two-phase factors vary significantly.

Assumptions 1 through 3 are readily justified after the fact by examining computational results along with the expected well geometry. Assumption 4 can also be justified after the fact, at least in part, by looking for discrepancies in the results suggesting the something significant and unexplained happened along the way. This can reveal sudden changes in well geometry below the BOP, but slow evolution cannot be discerned. Finally, assumptions 5 and 6 are somewhat intertwined. If the densities are relatively constant, then the de-rating factor for two-phase flow should also be relatively constant provided the overall composition is fixed. As further discussed in Appendix C, these two influences additionally offset one another in their impact on variation in the discharge coefficients.

Pressures in the reservoir and deep in the well always exceed the bubble point value, well below 10,000 psi at the local temperature of about 240 F. As such, the oil-gas mixture in this region is always liquid. Since temperatures here are stable and the compressibility of this mixture is fairly small, densities deep in the well will vary by at most 3.2% as the reservoir pressure decays from roughly 11,850 to 10,310 psi due to reservoir depletion. For laminar flow, mass flow rates are proportional to the fluid density, so this total density variation leads to potential errors in flow rates of $\pm 1.6\%$. The constant-density approximation thus seems well justified here. However, laminar flow rates also vary inversely with dynamic viscosity, and this falls by less than 15% as pressures fall from 11,850 to 10,310 psi.¹⁸ The net effect of this pressure variation is therefore an increase in flow rate of about 12% for a fixed pressure differential as the reservoir pressure decays, leading to a marginal variation of $\pm 6\%$.

Along the wellbore, flow rates are determined chiefly by the pressure differential and mean density,¹⁹ and this varies only slightly over the full range of conditions of interest. For a linear temperature profile from 150 or 180 F to 240 F between the BOP and bottom of the well, calculated mean wellbore specific gravities vary only from 0.52 to 0.56 for BOP pressures between 3,100 and 6,605 psi, reservoir pressures from 11,850 to 10,310 psi, and associated flow rates between zero and 70,000 stbd. Because turbulent flow rates vary in proportion to the square-root of density, this density variation of 7% leads to a total variation in the flow rate of 3.4% and a marginal variation of just $\pm 1.7\%$, with higher densities yielding higher flow rates. Such low variation in the mean wellbore density is important in these analyses because this is the dominant restriction to flow between the reservoir and BOP over all of the 86-day history.

These density variations and the related elevation heads were calculated after-the-fact by computing flow rates, the frictional pressure drop, local pressures and densities along the wellbore, and the resulting mean wellbore density and elevation head using the baseline parameters and a version of the model accounting for the influence of local density variations on both the elevation head and local wellbore discharge coefficient. The equilibrium equation-of-state used in these calculations replicates proprietary tabulations provided by BP for live oil at pressures above the bubble point.²⁰ Fits to later BP tabulations, also proprietary, yield mixture densities roughly 10% below and above the values used in these

¹⁸ From BP file "Information Package 3.doc" under "Black-Oil hydrocarbon fluid properties table used in BP's Prosper models." SNL007-006872. BP proprietary document.

¹⁹ Turbulent flows depend only weakly on viscosity through dependence of friction factors on the Reynolds number.

²⁰ From BP file "Live_Oil_density.xls." SNL059-000136. August 18, 2010. BP proprietary document.

calculations.^{21/22} While the three versions of this equation-of-state yield slightly different mixture densities, the resulting variations in density are nearly identical. Calculated flowing elevation heads are shown in Fig. 1 of Appendix G.

The assumption that local densities do not vary significantly along the wellbore also carries an implied assumption that the elevation head in the wellbore does not change significantly with pressures and flow rates over the range of conditions of interest. This head is also determined by the mean density of the gas-oil mixture between the bottom of the well and the location of the BOP gauge and, as already discussed, this varies by at most 7% over all possible conditions encountered during the 86-day history, including shut-in. This variation in mean density leads to a maximum total variation in elevation head of roughly 220 psi based on calculated nominal head of 3220 psi. For turbulent flow, flow rates vary with the square-root of the pressure difference, so this in turn leads to potential errors in the flow rate of $\pm 2.0\%$ with increasing densities yielding lower flow rates.²³ Because mass flow rates fall with increasing elevation head (due to reduced driving pressure differential) but increase with increasing density (due to role of density in flow rate correlation), the influence on flow rates of density and elevation head tend to offset one another such that flow variations due to wellbore density variations are reduced. It is therefore conservative to treat these density variations and the resulting pressure variations independently in assessing the accuracy of results as this approach will overestimate uncertainties.

During the shut-in process, BOP pressures ranged from roughly 4000 to 6600 psi. Over this range, densities vary by 14% for temperatures between 150 and 180 F, yielding an uncertainty in the flow rate of $\pm 3.4\%$. The range of pressures at the capping stack are even larger, from roughly 3000 to 6600 psi, leading to density variations of nearly 30% and potential errors in flow rates through the capping stack choke of roughly $\pm 7\%$. Further, the estimated equilibrium quality of the mixture (mass fraction vapor) varies by a roughly factor of two. For this reason, it might be advantageous to limit use of the shut-in data to capping stack pressures below 4000 psi, corresponding to the first five turns of the capping-stack choke. Over this range of pressures, from 3000 to 4000 psi, densities vary by at most 20% leading to errors in calculated flow rates of $\pm 4.8\%$. Limiting the shut-in data used to less than five turns of the choke stem also ensures that flow through the BOP and capping stack is always in the two-phase regime, thus also helping to ensure that assumption (5) of a constant choke de-rating factor remains valid for two-phase flows with varying gas and liquid fractions. Over this range of conditions, the calculated equilibrium quality of the gas-oil mixture varies by less than 30%, which should be more consistent with the assumption of a constant de-rating factor. Surprisingly, limiting use of the shut-in data in this manner has very little impact on the calculated historical flow rates, much less than 1%.

Flow rates measured just prior to shut-in also play a role in this approach to estimating historical flow rates. These measurements were made with the capping-stack kill line open over a range of conditions leading to capping-stack pressures (just upstream of kill line) that varied from 2353 to 2400 psi. For temperatures between 150 and 180 F, this range of pressures leads to a variation in density of 7.7%, leading to a marginal variation in kill-line flow rates of $\pm 1.9\%$. Calculated mixture qualities over this range of pressures vary by less than 0.1% for any fixed temperature between 150 and 180 F, so changing two-phase conditions should have negligible impact on kill-line flow rates.

Finally, it is important to note again that these variations and potential errors in flow rate through the BOP, capping stack, and kill line do not translate directly into uncertainties in flow rates calculated over the 86-day period. These flow rates are determined only by the productivity index, wellbore discharge coefficient, densities in the wellbore and reservoir, and pressure differences between the reservoir and BOP. Variations in flow rates through the BOP and capping stack do indeed impact calculated flow rates, but only indirectly through their impact on the estimated values of the productivity index and wellbore discharge coefficient.

²¹ From BP file "Information Package 3.doc", SNL007-006872. Undated. BP proprietary document.

²² From BP file "Black Oil Tables from EOS for All Temps 11June2010.xls", LAL248-009068. June 11, 2010.

²³ This variation is based on a nominal frictional pressure drop along the wellbore of 2650 psi obtained from the average flow rate 62,800 stbd and the baseline wellbore discharge coefficient of 1219 stbd/psi^{1/2}.

Appendix B: Mathematical Model

Flow from the reservoir to the bottom of the well is characterized by an industry-standard productivity index (PI). This index describes laminar (Darcy) flow in the reservoir formation and yields a flow rate that is proportional to the pressure difference between the far-field reservoir and the bottom of the well. The units of the PI are stock-tank barrels per day per psi, so the flow rate is given by

$$Q_{st} = \frac{\dot{m}_{st}}{\rho_{st}} = \kappa \delta P \quad (1)$$

where Q_{st} is the flow rate in stock-tank barrels per day (stbd), \dot{m}_{st} is the mass flow rate of stock-tank oil, ρ_{st} is the stock-tank oil density, κ is the productivity index, and δP is the pressure differential in psi. The units of \dot{m}_{st} and ρ_{st} can be picked in any manner that yields the flow rate in barrels per day.

Under the assumptions above, flows through the well casing, BOP restriction, and other flow paths higher in the well can be described by a similar relation, but in this case the flow is assumed to be turbulent and is also perhaps two-phase. Here the flow rate can be expressed in general as

$$Q_{st} = \frac{\dot{m}_{st}}{\rho_{st}} = \frac{\beta \dot{m}_m}{\rho_{st}} = \frac{A_v \beta f_{2\phi}}{\rho_{st}} \sqrt{\frac{2d \rho_m \delta P}{\lambda L}} = \hat{k} f_{2\phi} \sqrt{\rho_m \delta P} \approx k \sqrt{\delta P} \quad (2)$$

where \dot{m}_m is the mass flow rate of the gas-oil mixture, A_v is the cross-section area along the flow path, $\beta \approx 0.7$ is the mass fraction of the mix that is stock-tank oil, $f_{2\phi}$ is a de-rating factor for two-phase flow, d is the diameter or characteristic lateral dimension of the flow path, L is the path length, ρ_m^* is the mixture density, and λ is the turbulent friction factor for single-phase flow. Note that the next-to-the-last expression on the right of eq. 2 combines all constants for either the BOP or well into a single constant \hat{k} . This expression is still rigorous provided the geometry is fixed; however, the final approximation on the right of eq. 2 employs the two assumptions that a single two-phase de-rating factor adequately addresses all conditions at a given location (i.e. the well, BOP, etc.) and that the density is reasonably constant at any location. Again as discussed in Appendix C, both of these assumptions are not rigorously required. The constant k in eq. 2 is thus a discharge coefficient for turbulent flow that is analogous to the productivity index. For convenience, the units of this constant are taken as stbd/psi^{1/2}, and one such constant (four in total) will describe flow along the wellbore, through the BOP, through the capping stack kill line, and the tubing downstream of the capping stack choke.

The final element of this model is a description of flow through the capping-stack choke. This choke is characterized by a variable valve coefficient, C_V , having the units of gallons (of water) per minute per psi^{1/2}. As such, the flow of oil through the choke can be expressed as

$$Q_{st} = \frac{\dot{m}_{st}}{\rho_{st}} = \frac{\beta \dot{m}_m}{\rho_{st}} = \frac{60 \cdot 24}{42} \frac{\beta f_{2\phi} C_V \sqrt{\rho_m^* \delta P}}{\rho_{st}} = \frac{60 \cdot 24}{42} \hat{f}_{DR} C_V \sqrt{\delta P} \quad (3)$$

where ρ_m^* is the local specific gravity of the gas-oil mixture and $\rho_{st}^* \approx 0.83$ is that of the stock-tank oil. The factor $60 \cdot 24$ accounts for conversion from minutes to days; 42 accounts for conversion from gallons to barrels. The overall de-rating factor is then given by

$$\hat{f}_{DR} = \frac{\beta f_{2\phi} \sqrt{\rho_m^*}}{\rho_{st}^*} \approx 0.8 f_{2\phi} \sqrt{\rho_m^*} \approx f_{DR} \quad (4)$$

In analogy to eq. 2, flow rate through the choke can therefore be expressed as

$$Q_{st} = k_{CK} \sqrt{\delta P} \quad \text{where} \quad k_{CK} = \frac{60.24}{42} f_{DR} C_V \quad (5)$$

The final approximation here again employs the assumptions regarding a single two-phase flow factor for all conditions and relatively constant density at the choke location. As discussed in Appendix C, however, each of these assumptions is not individually required. Instead, the density and two-phase factor may vary significantly while the effective discharge coefficient remains relatively constant.

Because stock-tank barrels are equivalent to mass, conservation along the flow path now requires that

$$\kappa \delta P_{res-BH} = k_{well} \sqrt{\delta P_{BH-BOP}} = k_{BOP} \sqrt{\delta P_{BOP-CS}} = k_{CS} \sqrt{\delta P_{CS-amb}} \quad (6)$$

where the subscript *res* refers to the reservoir, *BH* to the bottom of the well, *CS* to the capping stack, and *amb* to the exit condition at the seafloor. All of these discharge coefficients are (at this point) unknown parameters, except for k_{CS} which is partially tied to the capping-stack choke C_V . This is given by

$$k_{CS} = \left(\frac{1}{k_{CK}^2} + \frac{1}{k_{DS}^2} \right)^{-1/2} \quad \text{or} \quad k_{CS} = k_{kill} + \left(\frac{1}{k_{CK}^2} + \frac{1}{k_{DS}^2} \right)^{-1/2} \quad (7)$$

where k_{DS} is the unknown discharge coefficient for tubing downstream of the choke, joining the choke to ambient conditions at the seafloor, and k_{kill} is the unknown discharge coefficient of the kill line. The first of these is appropriate when the kill line is closed; the second is appropriate when it is open.

More generally, the flow between any two points along a flow path that does not include the reservoir can be written as

$$Q_{st} = k_{eff} \sqrt{\delta P_{i,j}} \quad \text{where} \quad k_{eff} = \left(\sum_{m=1}^j \frac{1}{k_m^2} \right)^{-1/2} \quad (8)$$

where $\delta P_{i,j}$ denotes the pressure difference between the two points. The sum over local discharge coefficients must include all values along the path between the two points of interest. If the path additionally includes the reservoir, then the appropriate expression is

$$Q_{st} = \frac{\theta}{2} \left(\sqrt{1 + \frac{4\kappa \delta \tilde{P}_{i,j}}{\theta}} - 1 \right) \quad \text{where} \quad \theta = \frac{k_{eff}^2}{\kappa} \quad (9)$$

Here a circumflex on the pressure difference indicates that this difference must include that from the reservoir to the bottom of the well, while the sum yielding k_{eff} in eq. 8 is just over those path elements involving turbulent flow. Finally, if the path spans just from the reservoir to the well bottom, then the flow rate is given by eq. 1, where δP in this case is the difference between the reservoir and bottom-hole pressures.

Appendix C: Technical Basis for Constant Discharge Coefficients

Appendix A of this report describes a set of assumptions leading to a correlation in which the turbulent flow rate of stock-tank oil is proportional to the square-root of a pressure difference with a constant of proportionality, the discharge coefficient, that is fixed over the range of conditions of interest. That correlation was derived in the classical manner of simplifying general governing equations through multiple assumptions. As described in Appendix A, these include the assumptions of constant fluid density, constant two-phase factors, etc. However, the model used in these analyses is in fact based on just the single assumption that all turbulent flow rates of stock-tank oil are strictly proportional to the square-root of the pressure difference. This is equivalent to the single assumption that the discharge coefficients for the wellbore, BOP restriction, capping-stack kill line and choke line tubing, and the capping-stack variable choke valve are each independent of the pressure and temperature, again over the range of conditions of interest. In this light, the multiple assumptions of Appendix A may be viewed as a path to the central assumption of constant discharge coefficients for each of the flow elements.

Constant discharge coefficients still represent a fairly strong assumption given that two-phase flows occur over much of the flow path, including a significant portion of the wellbore and the entirety of the BOP and capping stack, at least up to the high pressures encountered just preceding final shut-in. Such two-phase flows are known to depend strongly on a two-phase factor and, in general, the two-phase factor depends strongly on the pressure and temperature through their influence on the quality of the mixture and the densities of the liquid and vapor phases. The model based on constant discharge coefficients nevertheless reproduces all BOP and capping-stack pressures measured during shut-in to within 120 psi or 2.6% and the oil collection rates early on July 15 to within 1.7%. It also correctly predicted that the BOP gauge was linear and displayed the correct sensitivity to within about 1.5% at the time of shut-in. This accuracy (or better) was later verified by post-retrieval calibration of BOP gauge.²⁴

Such agreement between measured and calculated values is remarkable in light of the simplifying assumptions of Appendix A and resulting use of constant discharge coefficients. The purpose of the present analysis is thus to better understand why constant discharge coefficients provide such accurate results and to provide a more rigorous justification for their use. The approach used for this is to formulate the discharge coefficient in terms of well-established two-phase flow correlations. The resulting expression is then used to compute potential variations in the discharge coefficients over various pressures and temperatures of interest. As demonstrated, variations in the discharge coefficients are very significantly lower than variations in fluid densities or two-phase factors owing to tradeoffs between the liquid density, mass fraction of liquid that is stock-tank oil, and the two-phase factor.

The analyses below supporting this observation address first flow through the BOP and capping stack via two-phase correlations appropriate for short pipes, the variable choke and any orifice. The wellbore discharge coefficient is addressed separately through the analysis of flow rates and pressures provided by BP in preparation for shut-in. The productivity index is not considered here because flow in the reservoir is all single phase for the range of conditions of interest.

BOP and Capping Stack Discharge Coefficients

Under the assumption of a constant discharge coefficient, the pressure drop δP across any flow element from the bottom of the BOP through the capping stack to ambient conditions is expressed as

$$\delta P = \frac{Q_{st}^2}{k^2} \quad (1)$$

where k is the fixed discharge coefficient and Q_{st} is the flow rate of stock-tank oil. Because the density of stock-tank oil is fixed for this problem, the flow rate Q_{st} is equivalent to a mass flow rate.

²⁴ From "BOP Pressure-Temperature Sensor Test Data from 6-15 and 6-16 (2011).pdf." Gauge calibration was performed by Det Norske Veritas on recovered PT-B transducer.

A comparable expression for the pressure drop can be written in terms of two-phase flow. Employing a K-factor version of the widely-used Lockhart-Martinelli formulation,²⁵ the two-phase pressure drop is given by

$$\delta P = \frac{1}{2} K \rho_l u_l^2 \phi_l^2 = \frac{K}{2A^2 \rho_l} \dot{m}_l^2 \phi_l^2 \quad (2)$$

where K is a constant based on the geometry and turbulent friction factor, ρ_l is the liquid density, u_l is the liquid superficial velocity, and ϕ_l is the liquid two-phase factor. Note that the right-hand form in eq. 2 is written in terms of the liquid mass flow rate, \dot{m}_l , using the identity $\dot{m}_l = \rho_l u_l A$ where A is the effective total cross-sectional area of flow. Finally, eq. 2 can be further rewritten in terms of the mass flow rate of stock-tank oil, \dot{m}_{st} using the definition $\dot{m}_{st} = \hat{x} \dot{m}_l$ where \hat{x} is the mass fraction of liquid that is stock-tank oil. This yields

$$\delta P = \frac{K \phi_l^2}{2A^2 \rho_l \hat{x}^2} \dot{m}_{st}^2 = \frac{K \phi_l^2 \rho_{st}^2}{2A^2 \rho_l \hat{x}^2} Q_{st}^2 \quad (3)$$

Here the right-hand form utilizes the fact that the mass flow rate of oil is the product of the volumetric flow rate, Q_{st} , and the fixed density of the stock-tank oil, ρ_{st} .

The forms of eqs. 1 and 3 are now identical in that each relates the pressure drop to the flow rate of stock-tank oil. These two expressions therefore can be equated to eliminate the flow rate and pressure drop, yielding an expression for the discharge coefficient, k , in terms of the parameters appearing in the two-phase formulation. Following minor rearrangement, this gives

$$k = \left(\frac{\sqrt{2} A}{\sqrt{K \rho_{st}}} \right) \left(\frac{\hat{x} \sqrt{\rho_l}}{\phi_l} \right) \quad (4)$$

The first term on the right of this expression involves only geometry of the flow path and the density of stock-tank oil and so does not vary with pressure or temperature. Rather, all possible variation in the discharge coefficient is contained in the second term involving the mass fraction of stock-tank oil in the liquid, the liquid density, and the liquid two-phase factor. An important note here is that the two-phase factor must always decrease with increasing pressure, up to the saturation or bubble point pressure, but the mass fraction of oil in the liquid, \hat{x} , and liquid density, ρ_l , also decrease with increasing pressure up to saturation. As such, it is impossible to discern a priori whether the discharge coefficient based on the two-phase formulation increases, decreases, or remains relatively constant with variations in pressure. That the liquid density falls significantly with increasing pressure is of particular note, and this is important contributor to determining any variation in the discharge coefficients. This behavior results from the fact that species of lower molecular weight than the stock-tank oil are increasingly incorporated into the liquid phase as the pressure is increased, driving the overall liquid density down.

Without loss of generality, variation in the discharge coefficient with pressure and temperature can also be expressed in terms of normalized variables. That is

$$k^* = \frac{k}{k_0} = \frac{\hat{x}^* \sqrt{\rho_l^*}}{\phi_l^*} \quad \text{where} \quad k_0 = \left(\frac{\sqrt{2} A}{\sqrt{K \rho_{st}}} \right) \left(\frac{\hat{x}_{sat} \sqrt{\rho_{l,sat}}}{\phi_{l,sat}} \right) \quad (5)$$

²⁵ Lockhart, R.W. and Martinelli, R.C., "Proposed Correlation of Data for Isothermal Two Phase, Two Component Flow in Pipes," Chem. Engr. Progr., 45, 1949.

and

$$\hat{x}^* = \frac{\hat{x}}{\hat{x}_{sat}}, \quad \rho_l^* = \frac{\rho_l}{\rho_{l,sat}}, \quad \phi_l^* = \frac{\phi_l}{\phi_{l,sat}} \quad (6)$$

where the subscript *sat* denotes the value at the saturation pressure or bubble point at the temperature of interest. Note that $\phi_{l,sat} = 1$, so ϕ_l and ϕ_l^* are identical. Also note that \hat{x}_{sat} is independent of temperature. That is, that overall mass fraction of the mixture of liquid and vapor that is stock-tank oil is constant and does not depend on either the pressure or the temperature.

Equation 5 provides a complete formulation stating the discharge coefficient in terms of well-established two-phase flow equations and will describe potential variations in the discharge coefficient with pressure and temperature. All that is required now is an expression for the two-phase factor and an equation of state for the fluid to compute fluid densities and other thermo-physical properties required to evaluate the two-phase factor.

The primary two-phase model used for this analysis is the well-established and widely-used Martinelli formulation in which the two-phase pressure drop is calculated from the pressure drop for the flow of liquid alone and a two-phase factor. Numerous models of this two-phase factor have been developed over the last few decades, and each adequately addresses some set of data. The well-known correlation by Chisholm,²⁶ as later modified by Whalley,²⁷ is used for the majority of this analysis because it has been successfully employed to describe flow in both pipes and orifices. The variable choke valve and BOP restriction are best described as an orifice, while the capping stack kill line is clearly best described as a pipe. The Chisholm-Whalley relation is also relatively simple and so more transparent than many other correlations. Other versions of the two-phase factor are discussed in a later section.

Because Reynolds numbers in all flow elements are very high, the two-phase model appropriate here is that in which both the liquid and vapor exhibit turbulent behavior. Per Whalley, the two-phase factor in this regime is given by

$$\phi_l^2 = 1 + \frac{C}{\chi} + \frac{1}{\chi^2} \quad \text{where} \quad C = \left(\frac{\rho_l}{\rho_v}\right)^{1/2} + \left(\frac{\rho_v}{\rho_l}\right)^{1/2} \quad (7)$$

The variable χ is the Martinelli parameter, discussed below. Note that the value of C in this expression is often and erroneously taken as $C = 20$ for turbulent-turbulent flow based on Chisholm's original work with steam-water mixtures. This value is, however, applicable only to that case and yields large errors when the ratio of the liquid to vapor densities is not large. Whalley later derived the more general expression for C above and showed that it yields a value near 20 for the conditions considered by Chisholm. This expression also correctly recovers the limiting case in which liquid and vapor densities are equal; for this special case, it is required that $C = 2$.

The Martinelli parameter appearing in eq. 7 is related to inter-phase slip and represents the square-root of the ratio of the pressure gradient or pressure differential for the flow of the liquid alone to that for flow of the gas alone. This can be expressed in terms of the liquid and vapor densities and mass flow rates as

$$\chi^2 = \frac{f_l \rho_v \left(\frac{\dot{m}_l}{\dot{m}_v}\right)^2}{f_v \rho_l} = \frac{f_l \rho_v (1-x)^2}{f_v \rho_l x} = \frac{\rho_v}{\rho_l} \left(\frac{1-x}{x}\right)^{7/4} \left(\frac{\mu_l}{\mu_v}\right)^{1/4} \quad \text{or} \quad \frac{\rho_v}{\rho_l} \left(\frac{1-x}{x}\right)^2 \quad (8)$$

where f_l and f_v are liquid and vapor friction factor, ρ_l and ρ_v are phase densities, μ_l and μ_v are viscosities, and x is the mixture quality or mass fraction of the mixture in the vapor phase. Evaluation of this

²⁶ Chisholm, D., "A Theoretical Basis for the Lockhart-Martinelli Correlation for Two-Phase Flow," *Int. J. Heat Mass Transfer.*, 10, 1967.

²⁷ Whalley, P. B., *Two-Phase Flow and Heat Transfer*, Oxford University Press, New York, 1996.

expression and those above requires fluid properties as a function of pressure and temperature, and this requires an equation of state.²⁸

The equation of state used in these calculations was provided by BP in tabular form and is based on a gas-oil-ratio of 2883 scf/stb and overall stock-tank oil mass fraction of $\beta = 0.64$.²⁹ These tabulations include the oil formation volume factor, FVF, and both densities and viscosities for the liquid and vapor phases. Values of these properties at pressures other than those tabulated were computed using quadratic interpolation. Other versions of the equation of state provided by BP yield slightly different results, but overall trends and the conclusions drawn from these trends remain the same.

From these interpolated values, the mass fraction of stock-tank oil in the liquid at any given pressure and a tabulated temperature can be computed from the definition

$$\text{FVF} = \frac{\text{vol liq}}{\text{vol st oil}} = \frac{\rho_{st}}{\rho_l} \left(\frac{\text{mass liq}}{\text{mass st oil}} \right) = \frac{\rho_{st}}{\rho_l} \frac{1}{\hat{x}} \quad \text{or} \quad \hat{x} = \frac{1}{\text{FVF}} \frac{\rho_{st}}{\rho_l} \quad (9)$$

where, as previously discussed, ρ_{st} is the fixed density of stock-tank oil. From interpolation of the tabulations to ambient pressure and 60°F, its value is $\rho_{st} = 53.0 \text{ lb/ft}^3$. The mixture quality can then be calculated directly from the fact that the mass fraction, β , of the liquid and vapor mixture that is stock-tank oil is a constant. This overall mass fraction of stock-tank oil is by definition $\beta = \hat{x}(1-x)$, so the quality is then given by

$$x = 1 - \frac{\beta}{\hat{x}} \quad \text{where} \quad \beta = 0.64 \quad (10)$$

The value $\beta = 0.64$ is obtained from the definition that it is equal to the value of \hat{x} at the saturation pressure, which is included in the tabulated equation of state. All of the variables appearing eqs. 5 through 8 can thus be interpolated directly (densities and viscosities) or by definitions relating various parameters (quality and stock-tank oil mass fraction) to tabulated values.

Calculated values of the normalized discharge coefficient, two-phase factor, stock-tank oil mass fraction, and liquid density computed using the equations above are shown in Figs. 1 and 2. The first of these is for a fixed temperature of 160 F; the second is for 240 F. These temperatures were selected because they almost certainly bound the range of temperature of interest for the BOP and capping stack during shut-in and during oil collection earlier on July 15, 2010.

We seen in Figs. 1 and 2 that variation in the two-phase factor, liquid density, and stock-tank oil mass fraction are indeed rather significant, but variations in the discharge coefficient are much smaller. Over all pressures between the minimum possible value of 2198 psi and a maximum possible of 11,850 the discharge coefficient varies by just 19% at 160 F and by just 23% at 240 F. In contrast, the two-phase factor varies by roughly a factor of two over the same range of pressures. Variations over the range of conditions of interest for each flow element are smaller still. This is illustrated by the points and horizontal lines labeled as choke, BOP and kill. The outer set of points in each case represent the total range of pressures seen at either end of the flow element. For example, the smallest pressure at either end of the choke line was the ambient pressure of 2198 psi and the maximum pressure was 6605 psi measured just at shut-in.

These outer points provide a crude measure of the range of conditions impacting variation in the discharge coefficients, but do not accurately reflect this because flow rates are not determined by the conditions at one end of a flow element or the other. Instead, flow rates are determined by the pressure drop across the flow element and some average or effective discharge coefficient based on the conditions at both ends. There are several approaches to estimating such an effective discharge coefficient, and a common practice is to calculate this based on the geometric mean density at the two ends. Because this is

²⁸ The analysis used in calculating the discharge employs discharge coefficients that were determined from measured pressures and flow rates so no equation of state was required.

²⁹ From BP file "Black Oil Tables from EOS for All Temps 11June2010.xls", LAL248-009068.

two-phase flow, however, a more appropriate method is to base the effective discharge coefficient on the geometric mean of the discharge coefficients at the two ends. Again for example, pressures at the two ends of the choke line are 2198 and 3062 psi at the beginning of shut-in but increase to 2198 and 6605 psi just as shut in is completed. The normalized effective discharge coefficients for these conditions range from 0.8952 to 0.9314 at 160 F, a variation of 4.0 %. This variation is indicated in Fig. 1 by the number in parentheses following the choke line label. Similar variations follow each such label for the various flow elements in Figs. 1 and 2. In addition, the range of equivalent pressures corresponding to this range of discharge coefficients is 2545 to 3084 psi. That is, a pressure of 2545 yields a discharge coefficient of 0.8952; 3084 psi yields 0.9314. These equivalent pressures are indicated by the inner pair of points for each flow element.

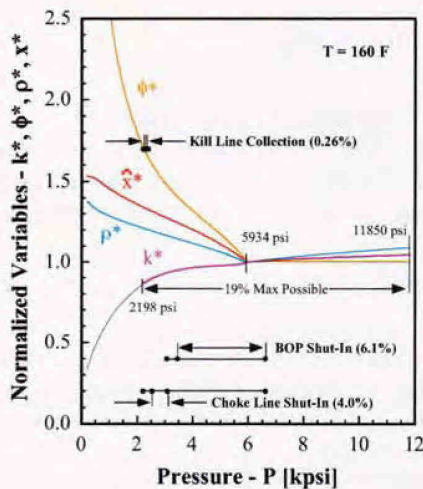


Figure 1. Computed normalized discharge coefficient, stock-tank oil mass fraction in the liquid, liquid density, and two-phase factor at 160 F. Outer dots with bars show the extremes of pressures for each flow element; inner dots show range for effective values.

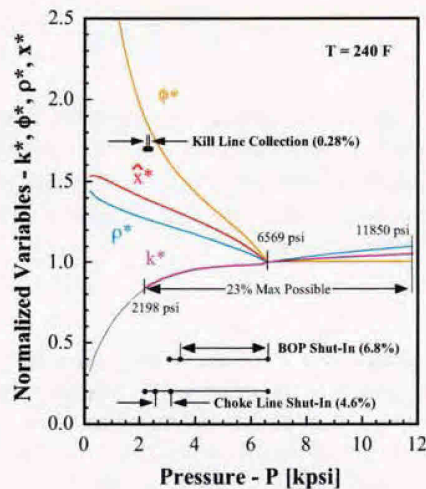


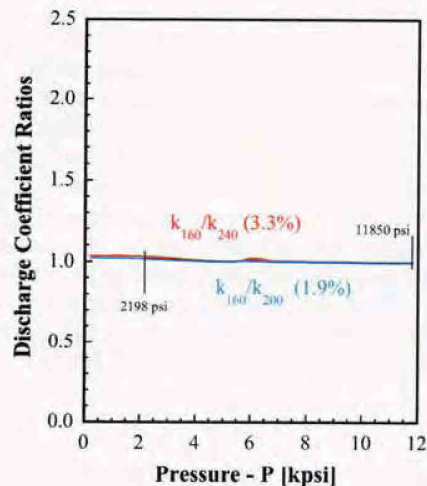
Figure 2. Computed values of the normalized discharge coefficient at 240 F. Higher temperatures yield slightly higher variations in the two-phase factor and normalized discharge coefficient due to higher saturation pressure and as a result a broader two-phase regime.

Additional values of this sort are provided in Table 1 below. The minimum and maximum pair of pressures the ends of each flow element is listed under the element label in the first column. For the kill line, these pressures represent the range observed during collection of oil on the morning of July 15, 2010. For the BOP and choke line, they represent the values observed during shut in. Table 1 thus represents all of the flow elements, except the wellbore, and all of the conditions used in parameter estimation. For each temperature in Table 1, the total variation in the effective discharge coefficient is listed as a percentage. Under these variations is the corresponding range of equivalent pressures. Table 1 also includes results based on the geometric mean density, and it is clear that this alternate method yields very similar results. Variations based on the mean density are for comparison only, however, as those based on the geometric mean discharge coefficient are expected to be more accurate.

	Geometric Mean k			Geometric Mean ρ		
	160 F	200 F	240 F	160 F	200 F	240 F
Kill – Collect 2198-2353 psi 2198-2400 psi	0.3% (2274-2295)	0.3% (2274-2295)	0.3% (2274-2295)	0.3% (2276-2299)	0.3% (2276-2299)	0.3% (2276-2299)
Choke – SI 2198-3062 psi 2198-6605 psi	4.0% (2545-3084)	4.4% (2553-3103)	4.6% (2559-3117)	4.1% (2612-3359)	4.7% (2615-3438)	5.3% (2617-3501)
BOP – SI 3062-4062 psi 6605-6605 psi	6.1% (3451-6605)	6.5% (3456-6605)	6.8% (3464-6605)	5.9% (3507-6605)	6.4% (2514-6605)	6.7% (3521-6605)

Table 1. Calculated percentage variation in capping-stack choke line, kill line and BOP discharge coefficients based on geometric mean discharge coefficient and geometric mean density.

Figure 3. Ratios of discharge coefficients for various temperatures as a function of pressure. The ratio of the coefficients at 160 and 200°F varies by at most 1.9% over the range of pressures from 2198 to 11,850 psi. That for 160 and 240°F varies by at most 3.3%. Variations in discharge coefficients with temperature are therefore negligible over the small range of pressures for each flow element.



Figures 1 and 2 depict only the variations in discharge coefficients that may occur as a result of variations in pressure at a fixed temperature. It is possible, however, that the temperature also varies due to variations in flow rate, time or pressure, especially during shut in. To examine the influence of such temperature variations, it is sufficient to consider the ratio of k^* at one temperature to that at another over the range of pressures of interest. This is illustrated in Fig. 3. Here the ratio of k^* at 160 F to that at 240 F and that at 160 F to that at 200 F are plotted as a function of the pressure. We see that both of these ratios are very nearly constant and very close to unity. The ratio for 160 and 240 F exhibits a maximum deviation from unity of 3.3% for all pressures from 2198 to 11,850 psi. And, the average value of this ratio over this range of pressures is just 1.006. That is, the discharge coefficient at 160 F is on average just 0.6% higher than at 240 F. Maximum deviation in the ratio for 160 F and 200 F is just 1.9% over all possible pressures of interest, and that mean of this ratio is 1.003. The average at 160 F is thus 0.3% higher than at 200 F. These variations are only about 10% of those calculated for variations in pressure as previously seen in Figs. 1 and 2. Given large uncertainties in the two-phase factor, the small likely variation in temperature during oil collection and shut in, and the limited range of pressures of interest for each flow element, variation in all discharge coefficients due to temperature variations appear to be negligible relative to those due to variations in pressure.

All of the results presented so far employ the Lockhart-Martinelli formulation of two-phase flow. This formulation is based on the flow rate of liquid (or gas) only. Since that time, most derivations of two-phase factors have been based on the total mass flow rate. In this case, the liquid two-phase factor, ϕ_{lo} , is defined such that the total mass flow rate is treated as though it were a liquid having the density of the liquid phase. Using the identity $\dot{m}_l = \dot{m}_{tot}(1-x)$ where \dot{m}_{tot} is the total mass flow rate and x is the mixture quality, the flow rate of stock-tank oil can be written as $\dot{m}_{st} = \dot{m}_{tot}\hat{x}(1-x)$ and eq. 4 above can be rewritten as

$$k = \left(\sqrt{\frac{2}{K}} \frac{A}{\rho_{st}} \right) \left(\frac{\hat{x}(1-x)\sqrt{\rho_l}}{\phi_{lo}} \right) \quad (11)$$

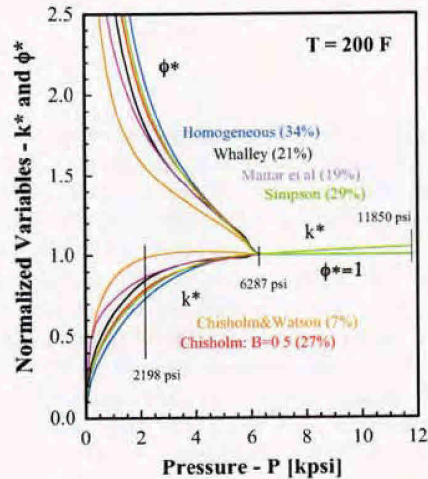
Equation 5 then becomes

$$k^* = \frac{k}{k_0} = \left(\frac{\hat{x}^*(1-x^*)\sqrt{\rho_l^*}}{\phi_{lo}^*} \right) \quad \text{where} \quad \phi_{lo}^* = \frac{\phi_{lo}}{\phi_{lo,sat}} \quad \text{and} \quad 1-x^* = \frac{1-x}{1-x_{sat}} \quad (12)$$

Using this formulation it is possible to compare results like those in Figs. 1 and 2 with alternative two-phase factors describing flow through an orifice or valve that is characteristic of the BOP restriction and the capping-stack variable choke. Results from several such correlations are shown in Fig. 4. Here the two-phase factors for each correlation and the corresponding normalized discharge coefficient are plotted as a function of the pressure for a fixed temperature of 200 F.

Figure 4 clearly shows that there is considerable uncertainty in two-phase factors for supposedly identical geometries, and this represents one of the great challenges in modeling two-phase flows. Such uncertainty, however, does not translate directly into variability in discharge coefficients. Instead, we should expect that each curve in Fig. 4 represents a potentially accurate description of the two-phase factor and resulting normalized discharge coefficient for the problem of interest such that variability in the BOP or choke valve discharge coefficient is properly described by variability along each curve. Variability of this sort is shown in parentheses in Fig. 4. These represent the maximum possible variation over all pressures between 2198 and 11,850 psi.

Figure 4. Normalized discharge coefficient and two-phase factor for various two-phase models of pipe and orifice flows. Orifice and choke flows typically give two-phase factors that are slightly larger than those for pipes. Numbers in parenthesis indicate the maximum possible variation in k^* over the entire pressure range from 2198 to 11,850 psi. As in Figs. 1 and 2, variations over the limited range of pressures associated with each flow element are much smaller. All two-phase factors are presented in the form used by Lockhart and Martinelli.



The various correlations shown in Fig. 4 yield minimum and maximum variation in the discharge coefficient of 7 and 34% over all possible pressures. References for these correlations are: Whalley,³⁰ Mattar,³¹ Simpson,³² Chisholm and Watson,³³ Chisholm,³⁴ and Homogeneous.³⁵

In contrast, the Whalley correlation used in Figs. 1 and 2 yields 21%, placing it near the middle of this range. The maximum variation of 34% occurs for the homogenous two-phase factor. For this case, total variations in the effective discharge coefficient over the ranges of pressure of interest are 0.4% for the kill line, 8.6% for the choke line, and 12% for the BOP. While these values are significantly larger than those in Table 1, they still correspond to relative variation over conditions of interest of at most 6% for the BOP and at most 4.3% for any path through the capping stack choke and kill lines.

Collectively, these results show that the use of constant discharge coefficients to describe two-phase flow through the BOP and the capping-stack choke and kill lines is a well justified for the conditions of interest for each flow element.

Wellbore Discharge Coefficient

The results above describe variation in discharge coefficients with variation in pressure and temperature for an orifice or short pipe as found in the BOP, capping stack, and capping stack variable choke. As such, the two-phase factors used in those analyses are likely not appropriate for the wellbore. Instead, variations in the wellbore discharge coefficient should employ a two-phase factor tailored to a long vertical pipe. Rather than repeating calculations of the sort above, however, it is perhaps more illuminating to examine two-phase flow rates calculated by others and to use these flow rates to determine potential variations in the wellbore discharge coefficient.

In late June of 2010, there was considerable concern about shut-in pressures and the possibility of rupturing burst disks in the well casing. As part of this, BP undertook a number of calculations of the shut in pressure and of pressures along the wellbore at various flow rates. Tony Liao of BP provided detailed calculations of this sort,³⁶ and his results included both frictional pressure drops and pressure drops due to the elevation head as a function of the flow rate.³⁷ His calculated frictional pressure drops were split into two regions: from the bottom of the well to 8969 ft MD TVD, and from 8969 ft to the wellhead. The values he obtained are shown in the first two columns of Table 2 below. The third column is simply the sum of the first two, yielding the total frictional pressure drop along the wellbore. Flowing bottom-hole pressures for these calculations ranged from 8506 to 9837 psi. Wellhead pressures ranged from roughly 4293 to 6496 psi. As such, two-phase flow existed in upper portions of the well for all flow rates greater than 20,000 bpd. At a flow rate of 50,000 bpd, two-phase flow existed in the upper 6900 feet of the casing, slightly more than half the overall height. These flow rates, pressures and two-phase conditions span very nearly the full range encountered during oil collection and shut in on July 15.

³⁰ Whalley, P. B., *Two-Phase Flow and Heat Transfer*, Oxford University Press, New York, 1996.

³¹ L. Mattar, et al., Orifice Metering of Two-Phase Flow, *J. Petrol. Technol.*, 31, 1979.

³² H. C. Simpson, D. H. Rooney and E. Grattan, Two-Phase Flow Through Gate Valves and Orifice Plates, *Proc. Int. Conf. on Physical Modelling of Multiphase Flow*, Coventry, England, 19-21 April 1983.

³³ D. Chisholm and G. C. Watson, *The Flow of Steam/Water Mixtures Through Sharp-Edged Orifices*, Report 213, National Engineering Laboratory, East Killbride, Glasgow, 1966.

³⁴ Chisholm, D., *Two-Phase Flow in Pipelines and Heat Exchangers*, Longman Group Ltd., London, 1983.

³⁵ From: R. B. Schuller, T. Solbakken and S. Selmer-Olsen, Evaluation of Multiphase Flow Rate Models for Chokes Under Subcritical Oil/Gas/Water Conditions. *SPE Production and Facilities*, 18, 2003.

³⁶ Part of the purpose of these calculations appears to be to match the VIP model results to those of Prosper. The Liao results serve as the reference and so appear to be calculated using Prosper.

³⁷ From BP-HZN-2179MDL04920969.xls. Created by Tony Liao, June 24, 2010. Values in Table 2 are taken from upper insert box on the tab labeled "Summary Table." Bottom hole and wellhead pressures are also presented.

Table 2. Calculated frictional pressure drop along the wellbore per Tony Liao of BP (first two columns), along with total pressure drop and effective wellbore discharge coefficient. Effective discharge coefficient varies by at most about 2% for flow rates from 10,000 to 50,000 bpd.

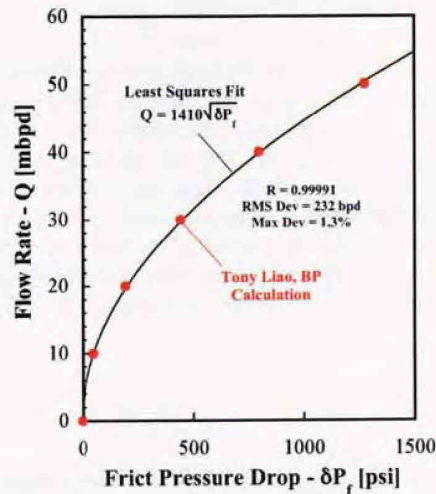
Rate - Q (bpd)	δP Frict to 8969 ft (psi)	δP Frict To WH (psi)	Total δP Friction (psi)	Effective k-well (bpd/psi ^{1/2})
50,000	1124	153	1277	1399
40,000	705	94	799	1415
30,000	394	50	444	1424
20,000	175	21	196	1428
10,000	45	5	50	1421
0	0	0	0	

The fourth column in Table 2 is the effective wellbore discharge coefficient calculated using the frictional pressure drop computed by Tony Liao for the prescribed flow rate. That is,

$$k_{well} = \frac{Q}{\sqrt{\delta P_f}} \quad (12)$$

For example the discharge coefficient for a flow rate 50,000 bpd at a frictional pressure drop of 1277 psi is 1399 bpd/psi^{1/2}. For flow rates over the range from 10,000 and 50,000 bpd, the discharge coefficients calculated in this manner vary only from 1399 to 1428 bpd/psi^{1/2}, a total range of just 2.1%. Thus, for given a prescribed frictional pressure drop, a constant discharge coefficient of just over 1400 bpd/psi^{1/2} should reproduce Liao's flow rates to within about plus or minus 1%.

Figure 5. Flow rates and frictional pressure drops. Red symbols are frictional pressure drops along the wellbore calculated by Tony Liao at prescribed flow rates. These appear to be based on the PROSPER model. The black curve is a least-squares fit to his values using a constant discharge coefficient. The relative RMS deviation between the fit and Liao results is just 0.83% for flow rates from zero to 50,000 bpd.



This is further illustrated in Figure 5. Here the prescribed flow rates of Table 2 are plotted against the frictional pressure drops calculated by Liao. Also shown in Figure 5 is a least-squares fit to his results based on the form $Q = k_{well} \sqrt{\delta P_f}$ such that the discharge coefficient is the only fitting parameter. The result of this fit is a discharge coefficient of 1410 bpd/psi^{1/2}. The resulting goodness of fit is 0.99991, and the RMS deviation between the fit and Liao's results is just 232 bpd. This corresponds to an RMS relative deviation of 0.83% over all flow rates. For all flow rates between zero and 50,000 bpd, the maximum relative deviation is just 1.3%, and this occurs at a flow rate 20,000 bpd. At 50,000 bpd, the deviation is less than 0.8%

The calculations by Tony Liao were used to help assess whether the well could be shut-in safely, with potentially catastrophic consequences if in error, and so likely employed the best computational tools available to BP. Nevertheless, the constant discharge coefficient of 1410 bpd/psi^{1/2} replicates the Liao relationship between flow rate and frictional pressure drop to within 1.3% for all flow rates between zero and 50,000 bpd.³⁸ This observation clearly indicates that a constant discharge coefficient accurately describes flow along the wellbore over the broad range of conditions encountered during shut in. Further, per Table 2, variations in the wellbore discharge coefficient over the range of conditions encountered during shut in are on the order of ±1%. Finally, use of the discharge coefficient obtained from any single condition, as tabulated in Table 2, to describe the flow rate at any other pressure yields discrepancies of at most 2.1% for all flow rates consider by Liao.

As such, use of a constant discharge coefficient to describe flow in the wellbore over the range of relevant conditions appears to be well justified, even for cases spanning single and two-phase flows. Use of a discharge coefficient determined at one pressure to describe flow rates at others is also well justified, and this is fundamental to calculating historical flow rates via the present method.

³⁸ The value of the 1410 bpd/psi^{1/2} for the discharge coefficient obtained here is about 18% larger than the value of 1152 bpd/psi^{1/2} used in calculating my historical flow rates. Direct comparison between these values is not possible, however, because my coefficient includes any influence of the complex geometry at the bottom of the well whereas the Liao calculations do not.

Appendix D: Parameter Estimation

The six unknown parameters appearing in this model are determined in part from pressures measured during shut-in. During this process, spanning about two hours, pressures were measured at both the BOP and capping stack. The ambient pressure at the seafloor was measured earlier using the capping-stack gauge. In addition, all pressures (less head differences) throughout the well must be equal at zero flow, so the reservoir pressure (less head) was also effectively measured at the end of the shut-in process. Again all combinations of these pressures in pairs should yield the same flow rates as the capping-stack choke was closed, so the unknown coefficients can be partially determined by matching flow rates along segments of the flow path using these four measured pressures.

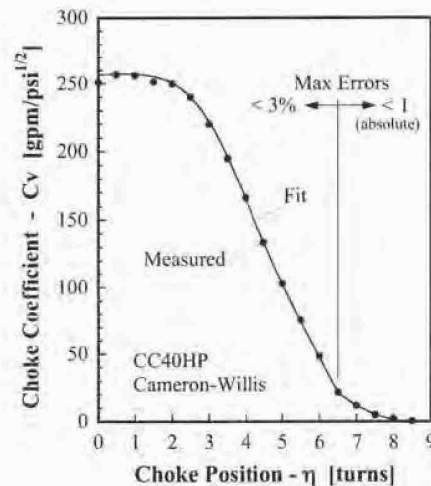
During the shut-in process, the capping-stack kill line was closed and the choke line was closed in a series of steps characterized by turns of the choke stem. A plot of the measured choke valve coefficient, C_V , as a function of the number of turns is shown in Fig. 1.³⁹ This provides values used in eqs. 3 and 5 of Appendix B. Also shown in Fig. 1 is a fit to these values. This fit is used to compute pressures and flow rates as a continuous function of the choke position; it is not used in determining the unknown parameters. Instead, only the discrete measured values (symbols) are used in parameter estimation.

Figure 1. Measured C_V values for the Cameron-Willis CC40HP choke. The fit shown is used only to compute pressures and flow rates as a continuous function of choke position. This is given by:

$$C_V = 387\xi^2 \text{ for } \xi < 0.235$$

$$C_V = 251 \left(\frac{1.714(\xi - 0.185) + 16.36\xi^7}{1 + 16.36\xi^7} \right) \text{ for } \xi \geq 0.235$$

where $\xi = 1 - \frac{2}{17}\eta$



The first step in determining the unknown parameters is to eliminate gauge offsets and any differences in elevation head as these do not contribute to flow. Without loss of generality, the stacking-cap gauge (PT_3K_2) is taken as the reference state. From capping-stack pressures measured before shut-in, this leads to an ambient pressure of 2198 psi⁴⁰ and an implied offset of +614 psi in the BOP gauge. Noting that all pressures less their elevation heads must be uniform in the well at zero flow, the reference capping-stack gauge also yields an implied reservoir pressure of 6605 psi at the time of shut-in, again excluding the elevation head. While this early pressure of 6605 psi corresponds with zero flow from the well when the choke is first fully closed, this is not a true shut-in pressure because the reservoir and wellbore are not yet in equilibrium. As a result, transport internal to the well continues beyond the time of complete choke closure, and the true wellhead shut-in pressure was roughly 7120 psi.⁴¹ The

³⁹ From the manufacturer. Plot of C_V versus stem travel was provided in file "CC40FNR P_C Cv_256.pdf", SNL087-015349. This was converted to turns using a known screw pitch of 4 threads per inch and total travel of 2.125 inches.

⁴⁰ From BP file "MC252_DataDump_071810", SNL087-001206. PT_3K_2: July 13 at 12:58 to July 14 at 02:18.

⁴¹ See Appendix F.

apparent shut-in pressure of 6605 psi is thus most appropriate for use in baseline parameter estimation, but may not be appropriate for calculating historical flow rates.

Using these corrected pressures, a total of 30 residuals and two constraints can be constructed. Fifteen of these are the differences between flow rates computed using pressure drops from the capping stack to ambient and from the BOP to the capping stack, at each of 15 choke positions. Another 15 are the differences between flow rates computed using pressure drops from the reservoir to BOP and the capping stack to ambient. The first constraint is that the flow rate through the BOP must equal the flow rate through the kill line when the capping-stack choke and rams are closed, the kill line is open, there is no oil collection from the BOP, and the capping stack pressure is 2625 psi.⁴² This yields a kill-line coefficient, k_{kill} , that is consistent with all other parameters. The second constraint is that the flow rate between the reservoir and BOP must equal the measured flow rate of collected oil plus the flow rate through the open kill line oil when the flow rate of collected oil is 20,012 stbd and the capping-stack pressure is 2376 psi.⁴³ This collected rate was later updated by BP to 20,296 stbd, and this value is used in my best estimate calculations. An important point here is that the measured BOP and capping-stack pressures during shut-in are not fit in this process. Instead, the various parameters are determined solely by using the measured pressures to determine flow coefficients yielding a model that conserves mass along the flow path. The first constraint serves primarily to set the capping-stack kill line coefficient; the second primarily sets the overall magnitude of the flow rate.

For each of the 30 conditions and 2 constraints, pressures measured at the BOP and capping stack are used in conjunction with the estimated reservoir pressure and ambient sea pressure to calculate the various flow rates. The pressures used in these calculations are averages of the measured values in the plateau region following each incremental step in the variable choke.⁴⁴ In every case, the measured pressures exhibited such a plateau, indicating at least local equilibrium in flow rates.

In practice, all six of the parameters are estimated simultaneously using a non-linear least-squares algorithm, TJMAR1.⁴⁵ The results obtained from this constrained non-linear parameter estimation for the baseline case using a reservoir pressure of 6605 psi for the 30 residuals and the two constraints are as follows. **Productivity Index**, $\kappa=47.2$ stbd/psi; **Wellbore Discharge Coefficient**, $k_{well} = 1219$ stbd/psi^{1/2}; **BOP Restriction**, $k_{BOP} = 1529$ stbd/psi^{1/2}; **Capping-Stack Kill Line**, $k_{kill} = 2482$ stbd/psi^{1/2}; **Capping-Stack Choke Line Tubing**, $k_{DS} = 2511$ stbd/psi^{1/2}; **Wide-Open Variable Choke**, $k_{CV} = 2258$ stbd/psi^{1/2}.

Parameter estimation for my best-estimate conditions follows a similar procedure. Here, however, the pressure of 6605 psi is used for calculating flow rates in the 30 residuals while the reservoir pressure, less a flowing elevation head, of 7260 psi is used in calculating the two constraints. This combination yields consistency of flow rates through the BOP during shut-in while providing a productivity index and wellbore discharge coefficient that most accurately relate flow rates to pressure drops for the higher reservoir pressure over the 86 days of flow. The resulting parameters in this case are: **Productivity Index**, $\kappa = 43.8$ stbd/psi; **Wellbore Discharge Coefficient**, $k_{well} = 1152$ stbd/psi^{1/2}; **BOP Restriction**, $k_{BOP} = 1439$ stbd/psi^{1/2}; **Capping-Stack Kill Line**, $k_{kill} = 2551$ stbd/psi^{1/2}; **Capping-Stack Choke Line Tubing**, $k_{DS} = 2367$ stbd/psi^{1/2}; **Wide-Open Variable Choke**, $k_{CV} = 2124$ stbd/psi^{1/2}.

⁴² From BP file "MC252_DataDump_071810", SNL087-001206. PT_3K_2: July 14, 2010 at 19:00 hours.

⁴³ Pressure from BP file "MC252_DataDump_071810.xls", SNL087-001206. PT_3K_2: July 15, 2010 at 02:00 hours. Flow rate from BP file "Collection rates during well integrity test w_Vx-1.xls" from 01:30 to 02:30 hours. Updated collection rates appear in "Tab 03-BP-HZN-2179MDL07266155.XLS" and "Tab 04-BP-HZN-2179MDL07265827.XLS".

⁴⁴ Pressures are from BP file "MC252_DataDump_071810.xls", SNL087-001206. Timing of the variable choke is from BP file "ACTIVITY LOG Well integrity test Record rev6 7-15.xls", SNL085-001156.

⁴⁵ Jefferson, T. H., "TJMARI-A Fortran Subroutine for Nonlinear Least Parameter Estimation," Sandia National Laboratories Report, SLL-73-0305, 1973.

Appendix E: BOP Gauge Offsets

Accurate BOP pressures are important to calculating historical flow rates and the cumulative discharge, so any offset in the BOP gauge must be well understood and quantified. As discussed in the body of this report, the BOP offset on July 15 at 14:22 was +614 psi based on a reference pressure from PT-3K-2. This offset clearly does not apply at other times, before and after shut in, so understanding the origins and timing of any shift in the offset is also important.

True gauge offsets occur only when the gauge is physically damaged, as by over-ranging, or when one or more reference resistors in the electrical portion of the gauge are damaged or otherwise drift through long-term aging processes. Gauges may also drift due to creep in the diaphragm, though gauges of this type are intended for service lives of many years. There is no indication of over-ranging PT-B during the 86 days or of damage of any other sort, and the period of interest in BOP pressures spans just several months so is quite small compared to the expected service life. It is therefore reasonable to believe that the true offset in PT-B is constant over the 86 days. It is also likely constant for some period prior to the blowout and for some period following shut in.

While the true offset is likely constant over the period of interest, errors of other sorts may additionally occur in pressures reported for PT-B. These include, for example, inaccuracy in converting the PT-B output current to an output voltage via the 250 Ω resistor, incorrect conversion of the resulting gauge voltage to a voltage reported by the Compatt, and incorrect conversion from Compatt output voltage to a pressure. Intentional or unintentional corrections as part of record keeping also represent potential sources of error in pressures reported for PT-B. Errors of this type do not, however, represent true gauge offsets. They simply occur in addition to whatever offset might actually exist.

The goal of this effort is to determine as best as possible the true offset for PT-B, to identify any additional errors or offsets in PT-B pressures, and to establish time periods over which these apply. Uncertainties in PT-B pressures below 100 psi have almost negligible effect on calculated historical flow rates, on the order of 1%, so reducing uncertainty in the offset below this value offers little benefit. As such, small pressure differences due to elevation heads between the PT-B location and the locations of other reference gauges can be ignored.

There are several well-defined occasions for determining the true offset by referencing PT-B pressures to pressures measured simultaneously by other means. These involve reference pressures from five distinct sources: the LMRP gauge PT-A, PT-C and PT-K on the BOP choke and kill lines, PT-3K-2 on the capping stack kill line, and pressures used in calibrating PT-B after it was retrieved. The timeframes and inferred offsets for each of these are described below, along with brief discussion of the merits of each reference condition.

On March 10, 2010, the well was shut in on an annular following an anomaly and was being monitored by way of PT-A on the LMRP and PT-B on the BOP.⁴⁶ Because there was no flow through the well at the time, these should have read the same. However, pressures reported by PT-A ranged from 3430 to 3460 psi while those from PT-B varied from 2690 to 2720 psi. Throughout this period, PT-B showed a nearly constant offset of -740 psi. The main concern about this value is that the accuracy of PT-A is not known, so this offset is subject to some uncertainty. The absence of flow, however, makes this a preferred measurement for use in determining the offset in PT-B.

Between May 25 and May 30, 2010, a series of tests were conducted in association with the top kill effort. Here pressures were measured concurrently using PT-B and either PT-C and PT-K located on the choke and kill line goosenecks leading to the junk shot manifold. BOP valves on the choke and kill lines were configured such that the lines were open to various regions within the BOP, enabling pressures in those regions to be measured remotely. On May 25 the test rams remained closed, separating PT-B from the nearest choke and kill line ports, so measurements then provide at best an indirect estimate of the offset. Measurements on May 26 are likewise problematic because the timing of valves on the BOP are

⁴⁶ "Forensic Examination of the Deepwater Horizon Blowout Preventer: V-II Appendices," Report No. EP030842, pages 222-227, Det Norske Veritas, March 20, 2011.

closely associated with opening the test rams and with pumping mud to kill the well. As a result, all of the measurements of May 26 are at least somewhat corrupted either by pumping, potential hydrostatic head in the riser above the goosenecks, or by rapid changes in valve status such that pressures at PT-B might not be in equilibrium with those at either PT-C or PT-K. Nevertheless, May 26 seems to be the origin of the -966 psi offset for PT-B as proposed by BP.⁴⁷ This value was based on reconciliation to PT-C and PT-K measurements that were in turn reconciled to a calculated head of mud in the choke and kill lines. PT-C in this case was corrected by +103 psi,⁴⁸ but the same transducer was later referenced to the more reliable ambient sea pressure and read that correctly within about 20 psi. The -966 offset is therefore too large (in magnitude) by at least 80 psi even if the May 26 measurements are considered reliable.

Similar measurements were made on May 27, 28 and 30 that appear to suffer fewer such problems. These measurements were also made with the test rams open, but were well separated in time from any pumping, and PT-C and PT-K appear to be isolated (for the most part) from the hydrostatic head of mud in the riser. Relevant pressures measured on May 27 are shown in Fig. 1.⁴⁹ Differences in pressure between PT-B and both PT-C and PT-K are shown in Fig 2. These plots cover times during which various valves on the BOP were opened and closed, as annotated in the two figures.⁵⁰ The periods of interest here are when both lower choke or both lower kill valves are open. This is because PT-C and PT-K pressures at these locations most accurately reflect pressures at the location of PT-B. From Fig 2, the apparent offset in PT-B is -825 psi relative to PT-C and -860 psi relative to PT-K. These values are averages over the appropriate time interval and are noted in Fig. 2.

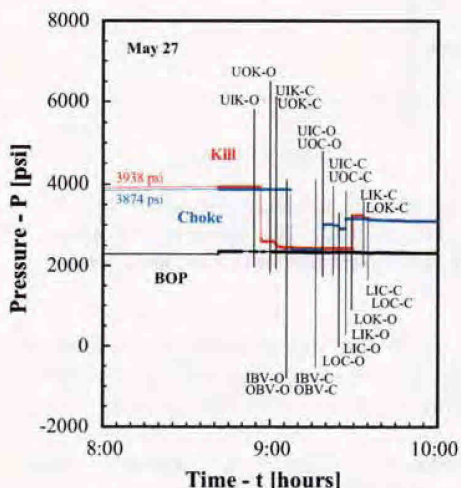


Figure 1. Uncorrected PT-C, PT-K and PT-B pressures on May 27. Annotations show BOP valve positions, e.g. UIC-O denotes opening of the upper inner choke valve; UIC-C denotes closing.

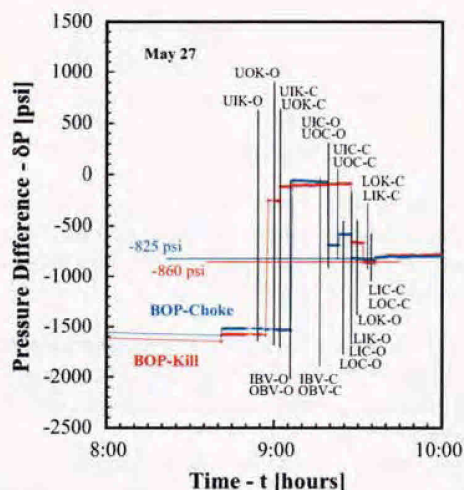


Figure 2. Differences between PT-B and either PT-C or PT-K pressures on May 27, 2010. Values are corrected for differing time base for each of the three gauges.

Comparable plots of the pressures and pressure differences on May 28 and May 30 are shown in Figs. 3 through 6. Both of these dates exhibit some anomalous behavior. The May 28 results indicate a

⁴⁷ The best opportunity to discern offsets on May 26 is between 17:30 and 18:30 as both lower choke and kill lines were open then and there was no mud being pumped. The mean offsets over this period were -860 and -926 psi relative to PT-C and PT-K respectively.

⁴⁸ From BP file BP-HZN-2179MDL05698790-91.

⁴⁹ From "MC252_DataDump_71810.xls", SNL087-001206.

⁵⁰ Timing of the BOP valves is from "BP-HZN-2179MDL06536400-20.pdf," Cameron Controls, May 5, 2010.

slow response in the upper kill line, though lower kill line pressures seem to behave as expected. The May 30 pressures show an additional anomaly in that BOP pressures respond to opening the upper choke line, indicating significant flow of mud through the line. This also occurs briefly on May 28,⁵¹ but is pronounced and prolonged on May 30. In this case the cumulative flow is sufficient to depress pressures at PT-B over the entire period of interest. The issue here is that PT-C and PT-K are intended to measure pressures reflecting those at PT-B, but the measurements themselves are influencing PT-B pressures and so must be treated with some suspicion. This influence is likely the result of significant flow of mud through the choke and/or kill lines due to the hydrostatic head, which will cause PT-C and PT-K to read high relative to PT-B and therefore overestimate the magnitude of the PT-B offset.

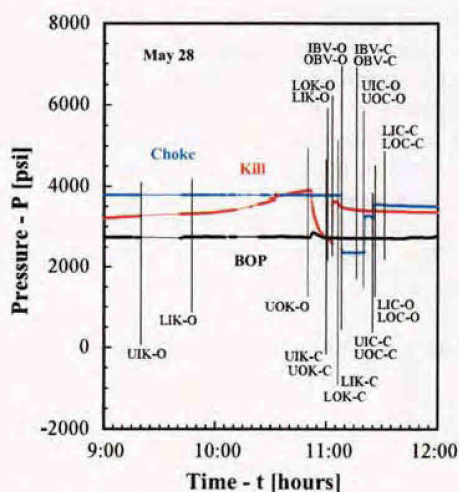


Figure 3. PT-B, PT-C and PT-K pressures on May 28. PT-K pressures for upper kill line exhibit slow response. Note slight perturbation to PT-B when the upper outer kill valve is opened.

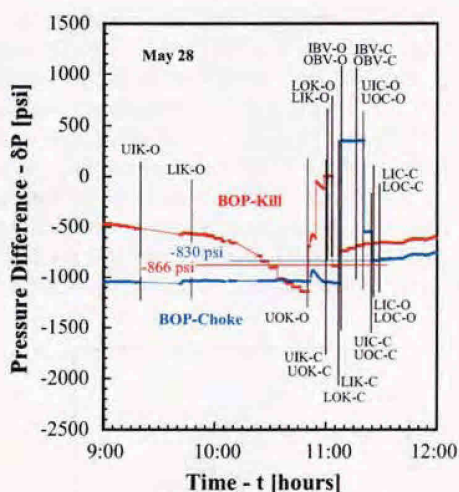


Figure 4. Pressure differences between PT-B and PT-C and PT-K on May 28. Apparent PT-B offsets are -830 and -866 psi relative to PT-C and PT-K, respectively.

Despite these concerns, the PT-B offsets inferred from May 28 and May 30 are quite consistent and are consistent with those of May 27. The values for May 28 are -830 psi relative to PT-C and -866 psi relative to PT-K. Those relative to PT-C and PT-K on May 30 are -825 to -852 psi and -810 psi, respectively.

Consistency between the PT-B offsets inferred from the May 27, 28 and 30 measurements provides no assurance, however, that any of these accurately reflect the true offset. In all of these cases, there is significant continuing flow from the well. And while the open test rams should provide little frictional pressure drop between PT-B below the rams and the choke and kill ports for PT-C and PT-K just above, any acceleration or deceleration of the oil (or mud) flowing between these locations would bias the estimate of the PT-B offset, and this bias would likely be about the same for all results during the May 27 to May 30 timeframe.

Finally, the offset inferred from this period is subject to uncertainties in the accuracy of the reference transducers. BP has estimated at times that PT-K read correctly, and PT-C read low by 63 psi.⁵² This

⁵¹ An additional anomaly on May 28 was that the test rams were briefly closed at 22:14 with both lower choke valves open. PT-B and PT-C showed no response, indicating that the closed test rams provided no resistance to flow. In contrast, when the test rams were finally closed on May 30, PT-B responded promptly (see Fig. 5). Although anomalous, this does not affect the May 28 or May 30 estimates of the offset.

⁵² From "MC252 Sensor Accuracy," slide 17, Matt Gochnour, July 8, 2010, Exhibit 8684.

conclusion is based on reference to the hydrostatic head of mud in the riser. As such, it is subject to uncertainties in the mud density over the entire height of the riser. At other times, BP estimated that PT-C read low by either 32 or 103 psi and that PT-K read low by 40 psi.⁵³ Again, these values seem to be based on reference to the hydrostatic head of mud and so must be considered accordingly. In contrast, PT-C was later referenced to the ambient sea pressure and read 2179 psi. It therefore appears to read low by about 20 psi based on PT-3K-2 measurements of 2198 psi.⁵⁴ In this case, PT-K would be reading high by about 40 psi. Given this small range of uncertainties, it appears appropriate to take the PT-C and PT-K pressures at face value. The PT-B offsets inferred from the May 27 to May 30 measurements therefore span the range from -810 to -866 psi, with a mean value of -840 psi.

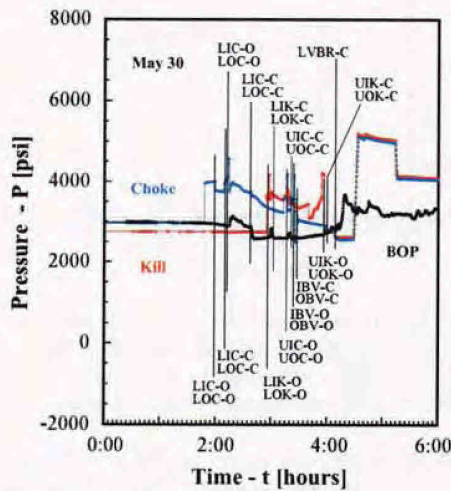


Figure 5. May 30 PT-B, PT-C and PT-K pressures. Note pronounced and prolonged depression of PT-B pressure in response to changes in BOP valve status, indicating mud flow through choke and kill lines.

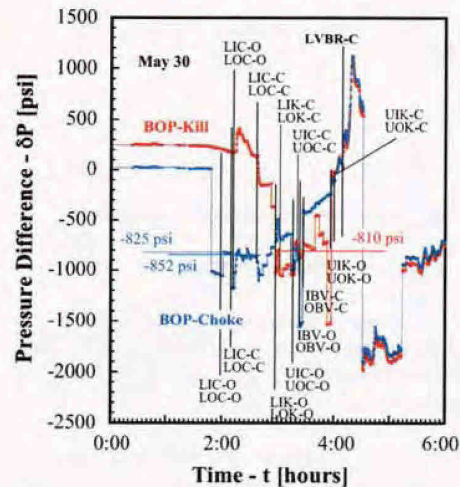


Figure 6. May 30 pressure differences between PT-B and PT-C and PT-K. Consistent with May 27 and 28 values, inferred PT-B offsets are -825 to -852 psi relative to PT-C and -810 psi relative to PT-K.

Additional measurements useful in estimating the PT-B offset were made following shut in on July 15, 2010. Here simultaneous measurements were made using PT-B and PT-3K-2. There was no flow through the well at this time, and PT-3K-2 pressures were later determined to be accurate to within a few psi.⁵⁵ As such, these measurements offer a preferred basis for determining the PT-B offset. The measured pressures are shown in Fig. 7.⁵⁶ Pressure differences between PT-B and PT-3K-2 are shown in Fig. 8.

A notable feature of Fig. 8 is the large change in apparent offset between July 16 and early August. Average offsets for July 16 and 17 are +546 and +576 psi, respectively. From July 15 at 14:22 (shut in) to July 17 24:00, the point-wise differences range from +508 to +641 psi, neglecting two obvious spikes, with a mean of +561 psi and standard deviation of 24 psi. These values are consistent with BP estimates for the offset in this period of +590 psi.⁵⁷ In contrast, the August 1 and 2 averages are -694 and -778 psi. Here the point-wise difference ranges from -576 to -820 psi, with a mean over the two days of -746 psi and a standard deviation of 49 psi. It is clear from Fig. 7 that the PT-3K-2 pressure history is very smooth

⁵³ From BP-HZN-2179MDL02208359. Undated.

⁵⁴ From BP file "MC252_DataDump_71810.xls", SNL087-001206. PT-C value is average for June 22, 2010. PT-3K-2 value is average for July 13, 2010.

⁵⁵ "MC252 Pressure Measurement Reconciliation," Matt Gochnour. Exhibit 8680. Undated

⁵⁶ From BP file "Copy of WIT 14July.xls", BP-HZN-2179MDL07114100. Created by W. Leith McDonald, August 3, 2010.

⁵⁷ From BP-HZN-2179MDL07556778.xls

over both the July and August periods of comparison and that the point-wise variation in both cases results almost exclusively from noise in the PT-B measurement.

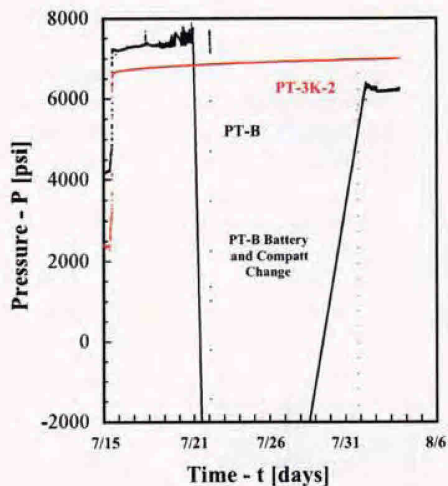


Figure 7. Pressures measured using PT-B and PT-3K-2 following shut-in from July 15 to August 3. The PT-B Compatt began failing just before July 21 and was replaced on July 31 or August 1.

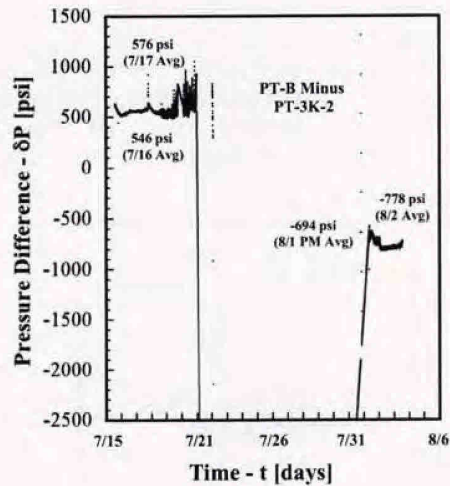


Figure 8. Pressure differences between PT-B and PT-3K-2 following shut in. Of particular note is the shift in apparent offset between July 16/17 and August 1/2 following replacement of the Compatt.

Offsets in early March, mid May and early August are thus all roughly consistent at -740 psi, -840 psi and -746 psi, and all represent valid estimates of the true offset in PT-B. The apparent offset of +561 psi in mid July is clearly an outlier that is associated with the change in Compatt on July 12 and any related change in conversion from voltage to a pressure at the Compatt or system level. The discrepancy between the mid July and early August values is roughly 1300 psi based on the mean values of +560 and -746 psi. It is likely that a large part of this discrepancy is a correction of 966 psi added to PT-B after July 12 but not after July 31. First appearance of this 966 psi correction in the network diagram is July 15, 2010 and so was presumably implemented with the Compatt replacement on July 12.⁵⁸ Other evidence, suggests that the 966 psi correction was not applied at this time.⁵⁹ In addition, dropouts in PT-B output on July 21, 23 and 27 result in reported pressures of -4750 psi whereas the correct reading for zero voltage is -5000 psi. This correct value does appear in a similar PT-B dropout on June 22. A dropout in PT-3K-2 on July 31 also yielded the correct value of -3750 psi for that transducer. This reported dropout pressure of -4750 psi implies that the PT-B pressures at the time were offset by +250 psi. It is not clear whether this condition also existed on July 16 and 17, but if so then this additional error could account for much of the remaining discrepancy between the +560 and -746 psi offsets. Either way, it is clear that the difference between the mid July and early August offsets results from the change in the PT-B Compatt on July 31 or August 1 and/or associated corrections in conversion.⁶⁰ The shift from the -840 psi mean for

⁵⁸ From BP-HZN-2179MDL01514072. BPD187-000521. Exhibit 8690, page 20. July 15, 2010. The 966 psi correction is included in the only conversion presented for PT-B and the associated 301 address.

⁵⁹ BP file "Copy of WIT 14July.xls", BP-HZN-2179MDL07114100, suggests that 966 was not added to PT-B values in "MC252_DataDump_71810.xls", SNL087-001206. This contains both corrected and uncorrected values and the uncorrected values agree with those of "MC252_DataDump_71810.xls." BP-HZN-2179MDL05058495 supports this.

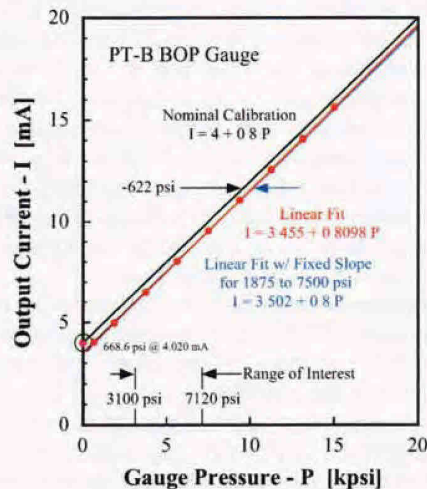
⁶⁰ From "ANI Compatt Tracking 072110.xls." Attachment to email from Jeannie Berube to Matt Gochnour, et al. July 21, 2010. BP-HZN-2179MDL07291679. BPD596-007549. Exhibit 8683, page 6. See also exhibit 8677, July 31, 2010 emails between Matt Gochnour and Deepak Kamidi regarding PT-B trap panel.

the May 27 to May 30 measurements to roughly +560 psi for July 16 and 17 is likewise results from a change in the PT-B Compatt and/or associated corrections on July 12.⁶¹

A final basis for determining the true PT-B offset is calibration of the transducer by Det Norske Veritas following retrieval of the BOP and gauge. This calibration included applied pressures at nine values between 0 and 15 kpsi, with two cycles up and down this range. Gauge output current was thus measured four times at each pressure for a total of 36 values. Results indicated that the transducer exhibited good linearity above 2000 psi, very nearly the correct sensitivity, and no discernable hysteresis. Additional tests showed that cycling the power supply did not induce an offset in the gauge output.

The 36 measured currents are shown in Fig. 9, along with various lines denoting alternative calibration curves.⁶¹ The black line represents nominal behavior for this gauge. Here the output at zero pressure is 4 mA and the sensitivity (slope) is 0.8 mA/kpsi. The red line is a linear least-squares fit to all of the measurements except at zero pressure. In this case, the current at zero pressure is 3.455 mA, and the sensitivity is 0.8098 mA/kpsi. When the gauge was initially ramped to an output of 4.020 mA the measured pressure was 668.6 psi, very close to the value of the fit at that current. This sensitivity is the same as the nominal value to within about 1%. Finally, the blue line in Fig. 9 is a least-squares fit to the measured currents for all pressures between 1875 and 7500 psi, using the nominal sensitivity of 0.8 mA/kpsi. This range encompasses all pressures of interest from April 20 to August 3, 2010. Nominal sensitivity is used here so that the resulting fit is simply shifted from the nominal curve by a fixed offset over all pressures, and the magnitude of this offset is the difference between the initial current at zero pressure of 3.502 mA obtained from the fit and the nominal value of 4 mA. The resulting shift is -0.498 mA, and this corresponds to an offset in pressure of -622 psi that is also uniform across all pressures. That is, pressures reported for PT-B using the nominal calibration curve to convert the output current to a pressure would be low by 622 psi. And this applies even when the output current is first converted to a voltage via the 250 Ω resistor.

Figure 9. Output currents measured by DNV during post-retrieval calibration of the PT-B transducer (symbols). Results show little hysteresis and good linearity with the correct sensitivity above 2000 psi. Least squares fit to the data for pressures from 1875 to 7500 psi indicates an offset in PT-B of -622 psi.



Use of the calibration data in discerning the true PT-B offset is supported by the fact that this is standard practice for characterizing a transducer. The calibration results are also free of any issues related to flow in the well and PT-B co-location with the reference gauge. The main concern about use of the calibration data is not accuracy of the reference, but in PT-B itself. The gauge was removed from its low-temperature subsea environment and was additionally cleaned in preparation for calibration. Either of these could possibly affect the offset.

⁶¹ From "BOP Pressure-Temperature Sensor Test Data from 6-15 and 6-16 (2011).pdf."

Offset values from the several reference sources discussed above are summarized in Table 1, along with brief relevant comments. Reference of PT-B to PT-A (3/10) occurs when there is no flow through the well and so is a preferred measure of the PT-B offset. The main concern here is the unknown accuracy of PT-A. A synopsis of pros and cons for each estimate of the offset follows.

Reference of PT-B to PT-C and PT-K (5/27 to 5/30) occurs only for times during which there is significant flow through the BOP. As a result, the magnitudes of the offsets may be either high or low depending on fluid velocities, orientation of gauge ports with respect to flow, local geometry in the vicinity of gauge ports, and any acceleration or deceleration of the oil or mud passing through the open test rams. The state of the BOP choke and kill valves also influenced PT-B pressures, and this sort of crosstalk should not be present when referencing one gauge to another. The use of PT-C and PT-K as reference pressures is therefore somewhat problematic, and the associated offsets should be discounted.

Near Date	Reference	Offset (psi)	Flow	Comments
3/10/10	LMRP PT-A	-740	No	
5/27/10	PT-C and PT-K	-825 to -860	Yes	Compatt Installed 5/17
5/28/10	PT-C and PT-K	-830 to -866	Yes	
5/30/10	PT-C and PT-K	-852 to -810	Yes	
7/16/10	PT-3K-2	+546 to +576	No	Compatt Change 7/12, 966 Correct
8/2/10	PT-3K-2	-694 to -778	No	Compatt Change ~7/31
6/15/11	DNV Calibration	-622	No	

Table 1. Summary of PT-B offsets determined from various reference pressures.

Reference of PT-B to PT-3K-2 (7/16 and 8/2) again involves no flow and so is a preferred estimator of the PT-B offset. The state of the BOP, LMRP and capping stack are reasonably well known and so present no particular concern, and PT-3K-2 is considered to be highly accurate. The offsets of 7/16 are clearly anomalous, however, and the origin of this is not completely clear. The discrepancy for this offset very likely arises from a correction of +966 psi and an additional offset of +250 psi due either to Compatt reporting or conversion from voltage to pressure at the system level. In any case, the results of 7/16 do not represent the true PT-B offset. In contrast, the offset of 8/2 is highly credible and is consistent with the other estimates, especially the reference to PT-A.

The offset determined via calibration involves no flow and is potentially the most accurate of these estimates. The only concern here is how removal of the gauge from the subsea thermal environment and cleaning may have affected the offset.

From those discussions, the references to PT-A and PT-3K-2 on 8/2 represent the best individual estimates of the PT-B offset. Both of these yield values near -740 psi. Further, every value in Table 1 is within 130 psi of this -740 psi offset, with exception of the 7/16 outlier. The impact of this 130 psi uncertainty on the cumulative discharge is just less than plus or minus 2%. The offset of -740 psi therefore represents a best estimate of the true offset in PT-B over most of the relevant history.⁶² This offset applies to all PT-B pressures from April 20 to July 11. After July 12, but before July 31, the applicable offset is roughly +560 psi, with an observed range of values between +508 to +641 psi. Any value in this range is thus acceptable depending on the use. The offset after July 31 is again -740 psi.

PT-B pressures reported in MC252_DataDump_71810.xls should be corrected by subtracting these offsets from the reported values over the indicated times. The only ambiguous application of these offsets occurs on July 11, 2010. Pressures reported in PT_B Offset 2 15 Jun thru 14 Jul.xls should be corrected in the same manner, but first 966 psi must be subtracted to remove the BP correction already applied. The only ambiguous application here is the period beginning July 9. Starting then, the reported pressures jump abruptly and become very erratic. As such, all pressures for July 9 through July 11 are untrustworthy and are therefore neglected in my analyses.

⁶² I reach the same conclusion whether or not I consider the DNV calibration.

Appendix F: Long-Term Shut In Pressure

The best estimate conditions employ a reservoir pressure history based on a final shut-in pressure of 7120 psi. The basis for this is extrapolation of the wellhead pressures measured using PT-3K-2 to infinite time using a simple model based on single-phase laminar flow in the reservoir.

Consider a region near the bottom of the well. The time derivative of the pressure in this region is proportional to the flow rate of oil into the region from points further into the reservoir. This can be expressed as

$$\frac{dP}{dt} \propto Q_{in} \quad (1)$$

For laminar (Darcy) flow in the reservoir, the flow rate is proportional to a pressures gradient and this pressure gradient is proportional to the difference between the local pressure in the volume and a far-field pressure, and that far-field pressure is roughly the equilibrium pressure within the reservoir attained at infinite time. The flow rate into the volume therefore can be expressed as

$$Q_{in} \propto (P_{eq} - P) \quad \text{such that eq. 1 becomes} \quad \frac{dP}{dt} \propto (P_{eq} - P) \quad (2)$$

For laminar flow, eq. 1 therefore possesses solutions in form

$$P = P_{eq} - ae^{-bt} \quad a > 0, b > 0 \quad \text{for} \quad P_{eq} > P_0 \quad (3)$$

Here P_0 is the initial pressure in the region while a and b are unknown positive constants. This represents simple exponential relaxation to the equilibrium value.

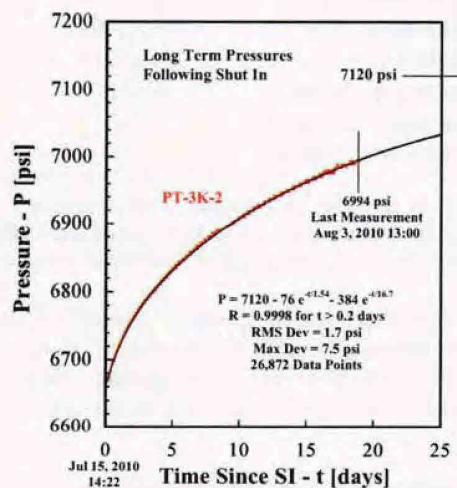
Expressions of this form were used to fit the measured pressures such that values for a , b and P_{eq} are the fitting parameters. Because of the complex geometry, two separate terms representing exponential relaxation are used in this fit. One of these describes rapid relaxation in the vicinity of the wellbore; the second describes relaxation on time scales associated with the reservoir. The result of this two-term fit is shown in Fig. 1. The quality of this fit is extremely good, yielding a goodness of fit of 0.9998 and RMS deviation between the fit and data of just 1.7 psi. The resulting equilibrium pressure is 7120 psi. This yields a reservoir pressure 10,310 psi based on a calculated static head of 3190 psi.

Figure 1. Measured wellhead pressures (red symbols) with two-term fit (black curve). Resulting long-term equilibrium pressure is 7120 psi. Complete fit is shown in the plot frame.

Alternate fits using a single term and subsets of the data indicate that uncertainty in this value is roughly plus or minus 50 psi.

The two exponential terms have short and long time scales of 1.54 and 16.7 days. These represent near-field and far-field relaxation.

PT-3K-2 data are taken from "Copy of WIT 14July.xls", BP-HZN-2179MDL07114100. Created by W. Leith McDonald of BP, August 3, 2010.



Appendix G: Discussion of Uncertainties

Uncertainties in calculated historical flow rates are determined by just several factors. These are uncertainties in the productivity index and wellbore discharge coefficient, variations in fluid densities in the wellbore over the 86 days, similar variations in the density and viscosity in the reservoir, and uncertainties in the pressure differences between the reservoir and BOP. Other parameters in the model have no effect on calculated flow rates, except indirectly. With a few exceptions, uncertainties in the instantaneous flow rate are identical to uncertainties in cumulative discharge from the well. Except as noted, baseline conditions are used in these analyses because they provide the most accurate description of the well at the time of shut-in and so provide the most accurate sensitivity to perturbations affecting the productivity index and wellbore discharge coefficient.

Uncertainties in the productivity index and wellbore discharge coefficient can be quantified by examining variations in flow rates through the kill line, BOP, and capping-stack choke and downstream tubing due to density variations in the gas-oil mixture as occur prior to and during shut-in. The magnitude of these was previously discussed in Appendix A on assumptions. Over the range of relevant conditions, potential variations the flow rate through the kill line are $\pm 1.9\%$. Variations in flow rates through the BOP and capping-stack choke, and tubing downstream of the choke are $\pm 3.4\%$, $\pm 7.0\%$, and $\pm 4.5\%$ respectively. These variations in flow rate are equivalent to variations in the discharge coefficients, so their impact on calculated flow rates can be assessed via a process resembling sensitivity analysis. To make this assessment, the productivity index and wellbore discharge coefficient are estimated as before, but the remaining four parameters are held fixed. Three of these are fixed at their baseline values, while the fourth is perturbed upward or downward by the amounts indicated above. For the variable capping-stack choke, the valve coefficients are perturbed uniformly by a constant. These perturbations result in estimates of the productivity index and wellbore discharge coefficients that deviate from their baseline values and so yield values of flow rates and the cumulative discharge that also deviate from nominal values. The deviation in the estimated cumulative discharge then serves as an estimate of uncertainty in the calculated flow rates.

Case	k_{well} (stbd/psi ^{1/2})	κ (stbd/psi)	Calc Cum (mmstbd)	Dev From BL (%)
Baseline	1219	47.2	5.446	0
1 BOP $\pm 3.4\%$	1194/1247	47.2/47.2	5.359/5.549	-1.6/+1.8
2 Ck DS Tub $\pm 4.5\%$	1245/1194	44.2/50.7	5.464/5.429	+0.3/-0.3
3 Kill Line $\pm 1.9\%$	1070/1504	113.9/28.6	5.431/5.503	-0.3/+1.0
4 Choke $\pm 7\%$	1219/1219	47.2/47.2	5.446/5.446	0/0
5 Choke 2- ϕ Factor	1072	92.8	5.353	-1.7
6 Res Press 7260 psi ⁶³	1152	43.8	5.514	0.6
7 Head Var at Shut-In	1218	45.7	5.410	-0.7

Table 1. Calculated uncertainties in flow rates given uncertainties in conditions during shut-in. Results are obtained by estimating the productivity index and wellbore discharge coefficient with all other parameters fixed at their baseline value except one that is perturbed as indicated.

This is illustrated in Table 1. Here the estimated baseline values of the productivity index and wellbore discharge coefficient are shown, along with the calculated baseline cumulative discharge from the well. Also shown are corresponding values for cases in which one of the discharge coefficients is perturbed. Case 1 of Table 1 shows the impact of perturbations to the BOP discharge coefficients of

⁶³ For consistency, the cumulative discharge was also calculated using the maximum credible (best estimate) reservoir pressure history.

$\pm 3.4\%$ with accompanying variations in the calculated cumulative discharge of -1.6% to $+1.8\%$. Note that variations in the estimated wellbore discharge coefficient are slightly larger than the variations in cumulative discharge because the productivity index is not affected and these two coefficients in series determine flow rates. Also note that the productivity index is not affected in this case because the wellbore and BOP coefficients appear only in series. Because both describe turbulent flow, the scheme used in parameter estimation is free to exchange reductions in one coefficient for an increase in the other without any influence on the estimated productivity index.

Case 2 shows similar results for perturbations to the discharge coefficient of the tubing downstream of the capping-stack choke. Here impact on the calculated cumulative discharge is quite small, $\pm 0.3\%$, despite a rather significant perturbation of $\pm 4.5\%$. This simply confirms that resistance to flow through the choke downstream tubing is relatively unimportant compared to that through the BOP, as was already apparent from the relative magnitudes of their baseline discharge coefficients.

Case 3 describes a perturbation to the kill-line discharge coefficient of $\pm 1.9\%$. Here the impact on cumulative discharge is decidedly asymmetric, leading to a flow rate deviation of -0.3% as the kill-line discharge coefficient is increased and $+1.0\%$ as it is reduced. The estimated productivity index and wellbore discharge coefficient for this case also deviate very significantly from baseline values, but with little net impact on the calculated cumulative discharge. This illustrates perhaps the robust nature of this method.

The effects of variations in flow rates through variable capping-stack choke are shown in Cases 4 and 5 of Table 1. As mentioned before, the first of these is based on uniform perturbation of the choke valve coefficients. This perturbation yields the unexpected result that the productivity index, wellbore discharge coefficient, and calculated cumulative oil discharge are altogether unaffected. This perplexing outcome is simply the result of the main role of the shut-in data in parameter estimation. That is, the shut-in data primarily determines the relative magnitudes of the productivity index and wellbore discharge coefficient through flow rates that vary significantly. When flow rates are low, pressure drops in the reservoir are larger relative to those in the wellbore; when flow rates are high, pressure drops in the wellbore increase relative to those in the reservoir. Magnitudes of the flow rates through the choke are therefore unimportant in parameter estimation, provided that the flow rates vary sufficiently as the choke is closed and that relative flow rates through the choke are determined only by the choke setting. Thus any uniform multiple of the choke valve coefficient (that is near unity) yields identical values of the productivity index and well discharge coefficient when all other parameters are fixed. This, however, presumes that flow rates through the choke vary only with the choke setting and do not also vary with density or quality as the choke is closed, which of course is the real condition. The Case 4 analysis is therefore inadequate to assess uncertainties.

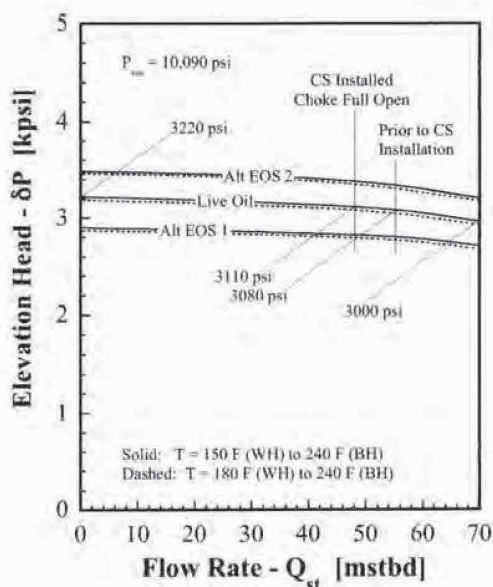
Proper characterization of the impact of uncertain flow rates through the choke requires that the choke flow rate vary in a manner that is not simply proportional to the measured choke coefficients, and this can be accomplished simply by varying the choke de-rating factor. A way to do this that is physically meaningful is to vary the portion of the de-rating factor associated with two-phase flow, as described by Eq. 3 of Appendix B. As previously discussed, the approximate value of this is 0.4 based on the baseline overall de-rating factor of 0.257. This low value clearly describes the two-phase flow expected when the choke is open and the capping-stack pressure is low. As the choke is gradually closed and the pressure increases to the bubble point, however, the two-phase factor should increase to unity assuming that the gas-oil mixture is in an equilibrium state. From the measured pressures, this should occur at some point beyond six turns of the choke for temperatures in the range of 150 to 180 F.

Such a perturbation to the choke two-phase factor is presented as Case 5 of Table 1. Here the two-phase factor is varied quadratically from 0.4 for the open choke to 1.0 at seven turns and beyond.⁶⁴ This produces a variation in flow rate through the choke that varies by a factor of 2.5. Despite this large variation, the impact on cumulative discharge is only modest at -1.7% .

⁶⁴ This quadratic variation roughly approximates a two-phase factor that varies linearly with density as the choke is initially closed.

Case 5 of Table 1 address uncertainties due to the reservoir pressure. Here the cumulative discharge is computed using parameters estimated using the best-estimate reservoir pressure less flowing elevation head of 7260 psi, the best-estimate reservoir pressures history, and the baseline BOP pressures. This leads to an increase in the discharge of 0.6%.

Figure 1. Calculated elevation heads as a function of flow rate. Wellbore temperature profiles are taken as a linear increase from 150 F at the wellhead to 240 F at the bottom (solid) or 180 to 240 F (dashed). The three sets of curves are based on the three distinct equations-of-state discussed in Appendix A. These heads are calculated by specifying the reservoir and wellhead pressures, and varying the flow rate until the sum of the pressure drop through the reservoir, the elevation head, and the frictional drop along the wellbore is equal to the overall pressure differential. During these iterative calculations, the baseline wellbore discharge coefficient is modified by the local density in the wellbore to provide a local discharge coefficient. Integration of local densities along the wellbore is then used to compute the total head. Note that the three equations-of-state yield significantly different values of the head, but variations in head with flow rate are nearly the same for all.



The last uncertainties associated with parameter estimation are due to uncertainties and variations in the elevation head during the shut-in process that affect the pressure differential driving flow in the wellbore. The baseline parameters are based on a reservoir pressure less head of 6605 psi that was measured just as the choke was closed. If the parameters are instead estimated using the best estimate value of 7260 psi, the calculated cumulative discharge is 5.514 mmstb, an increase of 0.6% from the baseline value. This is Case 6 of Table 1. Head variations during shut-in additionally influence parameter estimation because the reservoir pressure, not the pressure less head as assumed, is constant during this process. As shown in Fig. 1, the calculated elevation head falls from 3220 psi at zero flow to 3110 psi at a flow rate of 48,100 stbd (capping stack installed and choke open at start of shut-in). This variation of 110 psi was incorporated into the estimation algorithm by fixing the reservoir pressure and varying the head with flow rate in accordance with Fig. 1. This requires an iterative process such that the head varies with flow rate as the choke is closed and the reservoir pressure less head falls as the flow decreases. The result is a calculated cumulative discharge of 5.410 mmstb, a decrease of 0.7% from baseline. This is Case 7 of Table 1.

The values tabulated in Table 1 represent uncertainties in the calculated historical flow rates due to uncertainties introduced through assumptions in the model and their impact on parameter estimation.

Additional uncertainties in calculated flow rates arise from uncertainties in the measured flow rate used in parameter estimation. This is illustrated in Table 2 showing the BOP and capping-stack pressures measured just prior to shut-in during tests in which oil was also collected from the BOP choke and kill lines upstream of the capping stack.⁶⁵ Recall that a portion of the oil was also discharged from the capping-stack kill line in these tests. The first entry in this table is the baseline case, representing

⁶⁵ From BP file "Collection rates during well integrity test w_Vx.xls", BP-HZN-2179MDL04884268. Values reported are from the Vx meter, as recommended by BP. Pressures were taken from the BP file "MC252_DataDump_071810.xls", SNL087-001206, correlated through time with the collection rates.

parameters estimated using baseline values of the pressures and flow rate of collected oil in parameter estimation. The deviation from baseline in the resulting cumulative discharge is therefore exactly zero in this case. Cases 1 through 4 of Table 2 are identical to the baseline case except for the measured pressures and flow rates used in parameter estimation. Here the values listed for each case are used instead. These cases represent all other results during the same test series for which oil was collected for an hour; this was the maximum duration for such tests and so provides maximum accuracy in the measurement of collected oil. The measured flow rates in these tests vary from somewhat below 18,000 stbd to more than 22,400 stbd, a range of about 22%. Over this range, the resulting uncertainty in the calculated cumulative discharge is just -1.6% to +1.8%. And because all are involved, this range should be viewed as the combined uncertainty introduced by the model, measured pressures, and measured flow rates under the limited conditions of these flow tests. Here BOP pressures were always near 3600 psi and the total flow rate is roughly 53,000 stbd. These conditions are close to those encountered toward the end the 86-day history so provide some assurance that similar uncertainties apply to the historical flow rates and cumulative discharge.

Case	C-Stk P (psi)	BOP P (psi)	Meas Flow (stbd)	Calc Cum (mmstbd)	Dev From BL (%)
Baseline	2376	3586	20,012	5.446	0
1	2400	3605	17,987	5.543	+1.8
2	2353	3567	22,030	5.358	-1.6
3	2386	3617	18,942	5.424	-0.4

Table 2. Calculated cumulative discharge and uncertainties using various values of measured oil flow rates and associated pressures at the BOP and capping stack. Combined uncertainty in the model, measured pressures, and measured flow rates is -1.6% to +1.8% over this limited range of conditions

An alternative to assessing the impact of flow measurement uncertainties is to calculate collected oil flow rates using all of the baseline parameters and the various values of the BOP and capping-stack pressures appearing in Table 2. These calculated rates are then compared with the measured values to obtain an estimate of the combined uncertainty in the model, measured rates, and measured pressures over a narrow range of conditions. Results using this approach are very similar to those in Table 2, showing deviations from the measured collection rates of at most -1.7% to +1.6%.

All of the uncertainties discussed so far are characteristic of conditions just before or during shut-in when the reservoir pressure is more or less fixed. All remaining uncertainties arise from uncertainties over the 86-day history. The first of these are uncertainties due to variations in the oil mixture density in the reservoir. As discussed in Appendix A, the uncertainty in flow rate within the reservoir is less than $\pm 6\%$ due to pressure variations from 10,310 psi to 11,850 psi at a temperature of 240 F. However, because the productivity index is estimated at the end of the 86-day period when the pressure, oil density, and viscosity in the reservoir are lowest, this uncertainty is more appropriately described as the interval -12% to +0%. To describe the impact of this on cumulative discharge, it is therefore appropriate to assume an initial deviation of -12% in the reservoir productivity index with an increase to zero at 86 days. Assuming that this increase is linear in time, the result is a reduction in the calculated cumulative discharge to 5.392 mmstb, a change of -1.0% from the baseline value. This relative insensitivity to a significant time-dependent variation in the reservoir flow rate is due to a combination of two factors: the average deviation over the 86 days is just half of the initial value; and the dominant resistance to flow resides in the wellbore at the flow rates of relevance here, so reductions in the productivity index are reasonably unimportant.

Additional uncertainties in the calculated discharge arise directly from uncertainties in the reservoir pressure history. The initial reservoir pressures was measured at 11,850 psi, and this is taken as correct. Per Appendix F, the final shut-in pressure is 7120 psi, with uncertainty of approximately plus or minus

50 psi. Uncertainty in the reservoir decay over the 86 days is therefore equal to uncertainty in the final pressure, or plus or minus 50 psi. Because the initial measured pressure is taken at face value, this uncertainty begins at zero and grows over the 86 days and so is roughly equivalent to a constant uncertainty of plus or minus 25 psi over the entire period. The result of this is uncertainty in the cumulative discharge of $\pm 0.3\%$.

Variations in flow up the wellbore due to density variations also contribute to uncertainties in the cumulative discharge. These were again discussed in Appendix A and are $\pm 1.7\%$, taking into account the direct effect of density variations on flow rates at a fixed pressure differential, and $\pm 2.0\%$ accounting for the indirect effect of density on the elevation head and its impact on this differential. However, densities and the wellbore head also always decay as the pressures decay, so this again should be expressed as -4.0 to $+3.4\%$. These variations can be treated in a manner analogous to variations in the reservoir, so the wellbore discharge coefficient is varied linearly from its baseline value by -4.0% or $+3.4\%$ initially with a final deviation of zero at 86 days. The result for the first of these is a reduction in the calculated cumulative discharge of -1.3% ; the second yields an increase of 1.1% .

My best estimate of the cumulative discharge of 5.0 mmstb is based on a correction to BOP pressures of +740 psi. Per Appendix E, my uncertainty in this value is ± 130 psi corresponding to a range of corrections from +610 to +870 psi. The impact of this is uncertainty on the cumulative discharge is -1.8% and $+1.9\%$.

Finally, there are uncertainties in the cumulative discharge due to uncertainties in the state of the well prior to the first BOP pressure measurements on May. This is discussed in Appendix I. From that discussion, the uncertainties attributed to this period are -3.3% and $+0.9\%$ based on the reconstruction of events prior to May 8 and credible flow rates during periods following closure of the various rams.

A summary of these uncertainties is provided in Table 1 of the main body of this report. Here uncertainties are listed according to the sources already discussed and grouped by sign. The totals of these are -13.9% and $+9.7\%$, yielding a cumulative discharge between 4.3 and 5.5 mmstb based on my best-estimate nominal value of 5.0 mmstb.

Appendix H: Flow Rates Based on Reservoir and Ambient Pressures

Flow rates from the well using the reservoir and ambient pressures must account for pressure drops in the reservoir and wellbore, as when calculated using the measured BOP pressures, but must additionally account for the pressure drop through the BOP. As such the flow rate can be written as

$$Q_{st} = \frac{\theta}{2} \left(\sqrt{1 + \frac{4\kappa \delta P}{\theta}} - 1 \right) \quad \text{where} \quad \theta = \frac{k_{eff}^2}{\kappa} \quad \text{and} \quad k_{eff} = \left(\frac{1}{k_{well}^2} + \frac{1}{k_{BOP}^2} \right)^{-1/2} \quad (1)$$

Using best estimate values of the productivity index and discharge coefficients, the parameters appearing in eq. 1 are $k_{eff} = 890$ stbd/psi^{1/2} and $\theta = 18450$ stbd.

The total pressure drop in this case is $\delta P = P_{res} - P_{amb}$. Here the reservoir pressure (less elevation head) can also be expressed in terms of its initial value less a decay due to reservoir depletion by a cumulative discharge, Ω . The cumulative discharge is therefore governed by

$$\frac{d\Omega}{dt} = Q_{st} \quad \text{where} \quad \delta P = P_{res}^0 - P_{amb} - R \Omega \quad (2)$$

and R is the apparent incremental modulus of the reservoir expressed in psi/stb. Its value is the inverse of the effective reservoir compressibility divided by the total reservoir capacity. Given calculated flow rates, BOP pressures can also be computed using the relationship between the BOP and ambient pressures. This is given by

$$P_{BOP} = P_{amb} + \left(\frac{Q_{st}}{k_{BOP}} \right)^2 \quad (3)$$

where $k_{BOP} = 1439$ stbd/psi^{1/2}.

Taking $\Omega = 0$ and $P_{res} = P_{res}^0$ at time zero, eq. 2 can be integrated in time to give the instantaneous flow rate, cumulative discharge, and calculated reservoir and BOP pressure histories, provided the reservoir modulus is known. Alternatively, if both the initial and final reservoir pressures are specified, eqs. 1 and 2 become an eigenvalue problem for which only a single reservoir modulus can satisfy both the initial and final values. This value can be determined readily by solving the governing equations using the initial reservoir pressure and a trial value of the modulus. The modulus is then varied in an iterative process until the final calculated pressure matches the target value.

Appendix I: Flow Rates and Discharge Prior to May 8

While no pressures were measured at the BOP prior to May 8, it is possible to reconstruct the sequence of events before then and estimate their impact on flow rates. This sequence of events includes primarily the closure of various rams and collapse of the marine riser.

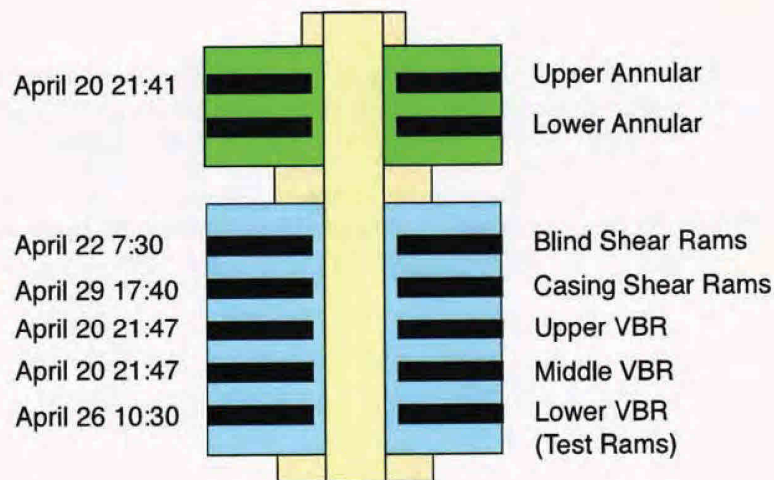
Closure of the rams before May 8 were spread from April 20 (upper annular and two VBRs) to April 29 (casing shear ram).⁶⁶ Each of these rams was closed with the intent to further restrict the BOP and so reduce the flow rate of oil. As such, I might reasonably assume that flow rates from the well decreased continuously up to May 8 in response to each subsequent closure of a ram. In this case, flow rates before May 8 would be at least as large as my calculated rate based on the first measured BOP pressures.

Assuming that flow rates decreased permanently in response to each ram closure does not, however, take into account the possibility of erosion in the rams or captured pipe between the time a ram was activated and the later date of May 8. Such erosion can occur very rapidly when fluid speeds are large, so flow rates may well have increased by May 8 from their values at the time a ram was first closed.

To address this possibility, I have reconstructed events and flow rates before May 8 starting at the condition when the riser had just collapsed. For that state and the states following each subsequent event, I estimated the condition of the BOP in terms of effective discharge coefficients, calculated the flow rate for that condition using the reservoir and ambient pressures, and used that flow rate over the period up to the next event to calculate an incremental cumulative discharge. All of these calculations employ my best-estimate values of the well productivity index and wellbore discharge coefficient. As stated elsewhere in this report, I do not believe that either of these varied significantly over the 86 days, except in the first several hours following the initial explosion.

This process is described below for each period leading up to May 8. A schematic of the BOP and Lower Marine Riser Package is shown in Fig. 1. This indicates the relative positions of the various rams and the time at which each was closed.

Figure 1. Schematic of relative locations of rams in the BOP and annular preventers in the LMRP. Dates and approximate times at which each was closed are shown at the left of the figure.



April 22 10:22 to April 26 10:30

The start of this period is collapse of the marine riser. At this point, the blind shear rams (BSR) had already been activated, severing the drill pipe. The drill pipe had also been severed by erosion and

⁶⁶ From "Expert Report of Forrest Earl Shanks II on BOP Design," October 17, 2011 and BP file Exhibit 8672. Created by BPPassPort User, October 10, 2012.

fracture at the upper annular and was ejected up the BOP prior to riser collapse.⁶⁷ This largely erosive failure of the pipe at the upper annular therefore occurred within 36 hours following blowout. In this state, the region between the BSR and bottom of the riser was open and offered almost no restriction to flow. There is some uncertainty as to when the upper and middle VBRs were closed.⁶⁸ Here I assume that they were closed and still sealed at the beginning of this period such that my estimate of the flow rate provides a lower bound on the true value.

The BSR at this time was partially closed, with an aperture of roughly 1 inch at the side packers and roughly 2 inches across the face, though the BSR blade and recess on the opposing side did appear to overlap.⁶⁹ As such, there were large channels up at least each side of the BSR, and such channels would have provided little resistance to flow. The pressure drop across the BSR was measured on May 25 and May 30 at somewhat less than 100 psi. Upon recovery, the BSR showed very extensive erosion on the sides and under side of the recess, but I do not believe that this erosion significantly reduced the pressure drop across the ram. Instead, I believe that the initial openings were sufficiently large that the pressure drop measured later in May was comparable to that present from its first closure. The extensive erosion resulted simply from the tortuous path through the blade and recess and the focusing of flow from the captured pipe at one side of the two rams. From this I conclude that the discharge coefficient of the BSR at this time was on the order of $6000 \text{ stb/psi}^{1/2}$ based on the roughly 100 psi pressure drop measured in late May and the flow rate at the time of roughly 60,000 stbd.

My inspection of the recovered riser showed little erosion in the kink, except in the vicinity of the several leaks. These leaks clearly originated from cracks that formed due to folding of the riser that were subsequently enlarged by erosion. There was extensive erosion downstream of each leak indicating very significant flow beyond them. Given their reasonably small size and lack of massive enlargement, I conclude that these leaks did not constitute a primary flow path from the riser. The primary path through the riser, with or without leaks, was through the open end some distance for the wellhead. Given that there was no significant erosion in areas away from the leaks, I conclude that the state of the riser as of this time was substantially the same as it was in late May. At that time, the pressure drop through the kinked riser was measured at roughly 300 psi, and this yields an effective discharge coefficient of about $3500 \text{ stbd/psi}^{1/2}$.

Assuming that the middle and upper VBRs were closed and remained perfectly sealed at this point, the pipe hanging below the BOP, the BSR, and riser offered the primary resistance to flow. My estimate of the discharge coefficient for the pipe below the BOP is $640 \text{ stb/psi}^{1/2}$.⁷⁰ The section of pipe above the BSR was already missing so the path through both annulars was open. Using my estimated discharge

⁶⁷ My conclusion is based on the fact that both pipes exiting the top of the BOP were kinked when the riser fell 36 hours following the blowout, and this would not have been possible if the pipe had not already been severed at the upper annular. Pipe positions were described in "Forensic Examination of the Deepwater Horizon Blowout Preventer: VI" Report No. EP030842, page 95, Det Norske Veritas, March 20, 2011. I conclude that pipe sections 83, 1-B-1 and 1-B-2 were already ejected from the BOP at the time of riser collapse, resulting in the kink between 1-B-1 and 1-B-2. This segment of pipe may have been severed on its lower end, between sections 83 and 94, by the blind shear rams, but the failure between sections 1-B-1 and 39 resulted largely from erosion at the upper annular preventer. This dramatic erosion therefore occurred in the first 36 hours following the blowout.

⁶⁸ "2011-10-17 Expert Report of Forrest Earl Shanks F" places closure of the upper and middle VBRs at roughly 21:47 on April 20, 2010. The BP file Exhibit 8672 places closure of the middle VBR at May 8 at approximately 04:00 and closure of the upper VBR at May 26 at roughly 11:00. In each case, I believe that the rams were already closed but leaking extensively due to erosion. Closure of the upper VBR on May 26 required almost no fluid input, but the BOP pressure still increased by approximately 340 psi. This indicates the upper VBR was already closed but leaking badly.

⁶⁹ "Forensic Examination of the Deepwater Horizon Blowout Preventer" Report No. EP030842, page 164, Det Norske Veritas, March 20, 2011.

⁷⁰ This is based on $720 \text{ stbd/psi}^{1/2}$ for the 800 feet of 3.5 inch pipe and $1400 \text{ stbd/psi}^{1/2}$ for the 2500 feet of 5.5 inch pipe as reported on page 12 in "Oil Release from the BP Macondo MC252 Well: Flow Rates and Cumulative Discharge Calculated using Measured Blowout-Preventer Pressures," S. K. Griffiths, Sandia Report SAND2011-3800, June 2011. The two pipes in series yield an effective discharge coefficient of $640 \text{ stbd/psi}^{1/2}$.

coefficient for each of these resistances, I calculate that the flow rate from the well was just over 41,000 stbd. The duration of this period, before the next event, was 4.01 days so the cumulative discharge was 0.17 mmstb.

April 26 10:30 to April 29 17:40

The start of this period is closure of the lower VBR (Test Rams). The test rams were installed in a manner that was not intended to seal the well with elevated pressure below the rams. At this point, however, the pipe was still in place below the BSR, trapped by the closed middle and upper VBRs. Although all of the VBRs were leaking by this time, a lower bound on the flow rate again can be obtained by assuming they were not. In this case, the configuration of the well and BOP were nominally the same as in the previous period. Based on the decaying reservoir pressure, the flow rate in this state was just less than 41,000 stbd. The duration of this period was 3.38 days, yielding an additional cumulative discharge of 0.14 mmstb.

April 29 17:40 to May 8 02:12 (first BOP pressure measurement)

The start of this period is defined by closure of the casing shear ram (CSR). Before this, however, I believe that the drill pipe below the BOP was severely eroded and either perforated or already dropped into the well. This is based on the fact that identical pipe failed at the upper annular, downstream of the closed VBRs, in less than 36 hours. At the start of this period, the test rams had already been closed for more than 3 days, but were not expected to seal, and the upper and middle VBRs had been closed and leaking for over 2 weeks. Given that flow between the pipe and an annular that is not quite sealed would likely resemble the flow between the pipe and a test ram that is not quite sealed, I see no basis for believing that failure at the test rams would not occur in a time scale comparable to failure at the upper annular. At the very least, the pipe in the test rams would have been perforated at this point such that significant flow entered the pipe at the bottom of the BOP. Further, I believe that the pipe below the BOP failed before May 8 as there is no evidence in the BOP pressure history that indicates it failed later. Unless already severely perforated, I believe that this would have been discernable through a significant permanent drop in BOP pressures, and no such drop occurred. Finally, my alternate calculation of the cumulative discharge using the BOP and ambient pressures indicates that the BOP restriction did not vary significantly between May 8 and July 15, and this would preclude additional perforation or complete failure of the pipe below the BOP at any time after May 8.

The CSR showed little erosion except on the bottom face of the upper blade just above the severed pipe. This indicates that the state of the CSR at this time was substantially the same as it was in late May. The pressure drops measured in late May did not isolate the CSR. Instead, the pressure drop across both the upper VBR and the CSR were measured together. Attributing all of this drop to the CSR therefore provides a lower bound on the discharge coefficient for the CSR and so a lower bound on my calculated flow rates. Based on the measured drop on May 25 for both the upper VBR and CSR of about 600 psi, the effective discharge coefficient for the CSR is therefore about $2500 \text{ stbd/psi}^{1/2}$.

In this configuration, I again assume that the VBRs remain perfectly sealed around remaining pipe in the BOP such that a lower bound on the flow rate is obtained. My estimate for the discharge coefficient for this segment is $1800 \text{ stbd/psi}^{1/2}$ based on scaling to the discharge coefficient of the capping stack kill line. The collective resistance of the pipe segment, CSR, BSR and riser yield a calculated flow rate of just over 61,000 stbd. The duration in this case is 8.35 days, and this gives a cumulative discharge of 0.51 mmstb.

Summary

These periods cover all of the time between blowout and the first BOP pressure measurements on May 8, except for the 36 hours before riser collapse. The sum of the incremental discharge from the three periods is 0.82 mmstb. In contrast, my best estimate of a cumulative discharge includes a cumulative at this time of 1.04 mmstb, so there is a discrepancy of 0.22 mmstb or about 4.4% of my total. To make up

this difference, the flow rate over the first 36 hours would need to be roughly 150,000 stbd, and this does not seem credible. However, the flow rate during this period was certainly not zero either. In their calculations, Add Energy concluded that the flow rate through the casing, the drill pipe below the BOP, and the drill pipe to the surface was 36,000 stbd for a net pay zone of 86 feet.⁷¹ Given that this was the likely path for flow at the time and that the down-hole restriction at the cement barrier was failing rapidly, I believe that this represents a reasonable flow rate for the period. Using this value reduces the discrepancy to less than 0.17 mmstb or about 3.3% of my total. Given that leaks in the VBRs would further reduce the discrepancy, this serves as an upper bound on the uncertainty associated with the period before May 8.

In contrast, a reasonable upper bound on of the discharge before May 8 can be had by assuming that the initial estimated flow rate of 63,000 stbd applied over this entire period. Under this condition, the cumulative discharge as of May 8 is slightly above 1.08 mmstb. Here the discrepancy is just over 0.04 mmstb or 0.9% of the total discharge of 5.0 mmstb.

This analysis yields upper and lower bounds on the discharge before May 8 through several conservative assumptions. As a result, I believe that the true discharge during this period would be larger than is represented by my lower bound. I also believe that the true discharge during this period was less than my upper bound. I therefore consider these bounds to be reasonable estimates of uncertainties, but do not feel it is appropriate to alter my best estimate of the total discharge to reflect either of these values.

⁷¹ From "Deepwater Horizon Accident Investigation Report," September 8, 2010. Appendix W, Page 30, Table 3.4,

Appendix J: Correlation of BOP and Reservoir Pressures

Under the mathematical model described in Appendix B, the reservoir and BOP pressures uniquely define a flow rate from the well when both the productivity index and wellbore discharge coefficient are specified. Conversely, if the flow rate and BOP pressure are known, then the reservoir pressure can be inferred. This can be demonstrated by writing each of these pressures in terms of the ambient pressure and flow rate. Without the capping-stack in place, these are given by

$$P_{BOP} = P_{amb} + \left(\frac{Q_{st}}{k_{BOP}} \right)^2 + \delta P_{BOP}^H \quad \text{and} \quad P_{res} = P_{amb} + \frac{Q_{st}}{\kappa} + \left(\frac{1}{k_{BOP}^2} + \frac{1}{k_{well}^2} \right) Q_{st}^2 + \delta P_{res}^H \quad (1)$$

The first of these is derived from eq. 2 of Appendix B; the second comes from eq. 8. Since each of these depends only on the flow rate when the productivity index, discharge coefficients, and ambient pressure are fixed, changes in pressure at the BOP and in the reservoir must likewise depend only on the flow rate. Assuming that elevation heads, δP^H , do not vary with flow rate, this can be expressed as

$$\frac{dP_{BOP}}{dQ_{st}} = \frac{2Q_{st}}{k_{BOP}^2} \quad \text{and} \quad \frac{dP_{res}}{dQ_{st}} = \frac{1}{\kappa} + 2 \left(\frac{1}{k_{BOP}^2} + \frac{1}{k_{well}^2} \right) Q_{st} \quad (2)$$

And since flow rates through the BOP and from the reservoir must be the same in steady state, the ratio of changes in BOP pressures to changes in reservoir pressures can be written as

$$\frac{dP_{BOP}}{dP_{res}} = \frac{1}{1 + \chi} \quad \text{where} \quad \chi = \left(\frac{k_{BOP}}{k_{well}} \right)^2 \left(1 + \frac{k_{well}^2}{2\kappa Q_{st}} \right) \approx 1.575 + \frac{24,750 \text{ stbd}}{Q_{st}} \quad (3)$$

The approximation on the right of this equation is based on the baseline values of $k_{BOP} = 1529 \text{ stbd/psi}^{1/2}$, $k_{well} = 1219 \text{ stbd/psi}^{1/2}$, and $\kappa = 47.2 \text{ stbd/psi}$. Maximum possible variation in the BOP pressure with reservoir pressure therefore occurs when the flow rate is very large, and this is given by $dP_{BOP}/dP_{res} = 0.388$. Parameters for my best-estimate conditions and the corresponding mean flow rate of 58,300 stbd yield $dP_{BOP}/dP_{res} = 0.337$. For this mean flow rate, a decay rate in the BOP pressure of -5.91 psi/day would thus require a decay of -17.5 psi/day in the reservoir pressure or roughly 1500 psi over the 85 days and 17 hours between blowout and shut-in.

Appendix K
Curriculum Vitae for S. K. Griffiths

Stewart K. Griffiths

[REDACTED]
Albuquerque, NM 87122
[REDACTED]



Employment History

Sandia National Laboratories, Albuquerque, NM & Livermore, CA
Senior Scientist (2001-2011 at Retirement)
Distinguished Member of the Technical Staff (1991-2000),
Member of the Technical Staff (1980-1990)
Lawrence Livermore National Laboratory, Livermore, CA
Summer Employee and Consultant (1977-1980)

Education

Ph.D. in Mechanical Engineering, University of Illinois (1980). NSF Graduate Fellow.
M.S. in Mechanical Engineering, University of Illinois (1977). University Graduate Fellow.
B.S. in Mechanical Engineering, University of Illinois (1976). Highest Honors.

Knowledge Base and Technical Skills

Transport phenomena -- fluid dynamics, electro-migration, heat and mass transfer
Numerical and analytical solution of differential and non-linear algebraic equations
Applied optimization and parameter estimation
Reduced-order models of complex phenomena
Analysis and interpretation of data through physically-based mathematical models

Current or Prior Expertise

Transport processes in dielectric and double-layer capacitors
Multi-phase flow and transport in heat pipes
Radiation and electron transport for x-ray lithography
Buoyantly-driven flow and transport during electro-deposition
Dispersion phenomena in electro-kinetic transport processes
Thermal and gravitational stresses in silicon wafers
Chemical vapor infiltration for advanced composite materials
Combustion instabilities in liquid propellants
Gas transfer systems for nuclear weapons
Compressible, incompressible, reacting flows in porous media
Shock propagation in multi-phase, multi-component materials
Multi-phase, multi-component equations of state
Explosives effects and mitigation of explosive dispersal
Fluid-driven fracture propagation in geological materials
Containment of underground nuclear explosions
Heat and mass transfer in electric fields

Recent Research

Optimization of hierarchical porous materials for energy and gas storage

Analysis of failure mechanisms and methods for improved reliability of high-voltage pulse-discharge capacitors

Publications and Patents

Journal publications: 53
Archival proceedings: >15
SNL technical reports: >100
Software copyrights: 2
U.S. Patents: 12

Appendix L
Stewart K. Griffiths
Publications, Reports and Patents

Journal Publications

"Comparison of Molecular Dynamics with Classical Density Functional and Poisson–Boltzmann Theories of the Electric Double Layer in Nanochannels," J. W. Lee, R. H. Nilson, J. A. Templeton, S. K. Griffiths, A. Kung, B. M. Wong, *J. Chem. Theory Comput.*, 8, 2012–2022, 2012.

"Optimization Algorithms for Hierarchical Problems with Application to Nanoporous Materials", P. T. Boggs, D. M. Gay, S. K. Griffiths, R. M. Lewis, K. R. Long, S. Nash, R. H. Nilson, *SIAM J. Optimization*, 22 (4), 1285-1308", 2012.

"Oil Release from Macondo Well MC252 Following the Deepwater Horizon Accident," S. K. Griffiths, *Environ. Sci. Technol.*, 46 (10), 5616–5622, 2012.

"Optimum Inter-Particle Porosity for Charge Storage in a Packed Bed of Nanoporous Particles," S. K. Griffiths and R. H. Nilson, *J Electrochem Soc*, 157 (4) A469-A479, 2010.

"Optimization of Charged Species Separation by Autogenous Electric Field-Flow Fractionation in Nano-Scale Channels," S. K. Griffiths and R. H. Nilson, invited contribution to special edition of *Electrophoresis*, 31, 832-842, 2010.

"Hierarchical Transport Networks Optimized for Dynamic Response of Permeable Energy Storage Materials," R. H. Nilson and S. K. Griffiths, *Phys. Rev. E.*, 80, No. 1, 16310, 2009.

"Optimizing Multiscale Networks for Transient Transport in Nanoporous Materials," R. H. Nilson and S. K. Griffiths, *Nanotechnology 2008*, ISBN: 978-1-4200-8511-2, Vol. 3, Boston, June 2008.

"Optimizing Transport in Materials Having Two Scales of Porosity," R. H. Nilson and S. K. Griffiths, *Phys. Rev. E.*, 79, No. 3, 36304-36314, 2008.

"Influence of mask substrate materials on resist sidewall roughness in deep X-ray lithography," G. Aigeldinger, C.Y.P Yang, D. M. Skala, D. H. Morse, A. A. Talin, S. K. Griffiths, J. T. Hachman, and J. T. Ceremuga, *Microsystem Technologies*, 14, 277-286, 2008.

"Charged Species Transport, Separation and Dispersion in Nano-Scale Channels: Autogenous Electric Field-Flow Fractionation," S. K. Griffiths and R. H. Nilson, *Analytical Chemistry*, 78, 8134-8141, 2006.

"Influence of Atomistic Physics on Electroosmotic Flow: An Analysis Based on Density Functional Theory," R. H. Nilson and S. K. Griffiths, *Journal of Chemical Physics* 125, 164510-23, 2006. (Selected by editor for publication in the web-based *Virtual Journal of Nanoscale Science and Technology*)

"Nucleation and Adhesion of Electrodeposited Copper on Anodized Thin-Film Aluminum for LIGA Microfabrication," M. W. Losey, S. K. Griffiths, and J. T. Hachman, *Journal of The Electrochemical Society*, 153, 177-186, 2006.

"Steady Evaporating Flow in Rectangular Channels," R. H. Nilson, S. W. Tchikanda, S. K. Griffiths, and M. J. Martinez, *International Journal of Heat and Mass Transfer*, 49, 1603-1618, 2006.

"Resist Substrate Studies for LIGA Microfabrication with Application to a New Anodized Aluminum Substrate," S. K. Griffiths, M. W. Losey, J. T. Hachman, D. M. Skala, L. L. Hunter, N. Y. C. Yang, D. R. Boehme, J. S. Korellis, G. Aigeldinger, W. Y. Lu, J. J. Kelly, M. A. Hekmaty, D. E. McLean, P. C. Y. Yang, C. A. Hauck and T. A. Friedmann, *Journal of Micromechanics and Microengineering*, 15, 1700-1712, 2005 (designated by editor as IoP Select).

"The Efficiency of Electrokinetic Pumping at a Condition of Maximum Work," S. K. Griffiths and R. H. Nilson, *Electrophoresis*, 26, 351-361, 2005 (Invited Contribution).

- "Dimensional Errors in LIGA-Produced Metal Structures due to Thermal Expansion and Swelling of PMMA," S. K. Griffiths, J. A. W. Crowell, B. L. Kistler and A. S. Dryden, *Journal of Micromechanics and Microengineering*, 14, 1548-1557, 2004.
- "Axially Tapered Microchannels of High Aspect Ratio for Evaporative Cooling Devices," R. H. Nilson, S. K. Griffiths, S. W. Tchikanda and M. J. Martinez, *Journal of Heat Transfer*, 126, 453-462, 2004.
- "Fundamental Limitations of LIGA X-Ray Lithography: Sidewall Offset, Slope and Minimum Feature Size," S. K. Griffiths, *Journal of Micromechanics and Microengineering*, 14, 999-1011, 2004.
- "Modeling of Pressure and Shear-Driven Flows in Open Rectangular Microchannels," S. W. Tchikanda, R. H. Nilson and S. K. Griffiths, *International Journal of Heat and Mass Transfer*, 47, 527-538, 2004.
- "Analytical Models for High-Temperature Corrosion of Silica Refractories in Glass-Melting Furnaces," R. H. Nilson, S. K. Griffiths, N. Yang, P. M. Walsh, M. D. Allendorf, B. Bugeat, O. Marin, K. E. Spear and G. Pecoraro, *Glass Science and Technology*, 76, 136-151, 2003.
- "Natural Convection in Trenches of High Aspect Ratio," R. H. Nilson and S. K. Griffiths, *Journal of The Electrochemical Society*, 150 (6), 401-413, 2003.
- "Modeling Acoustic Agitation for Enhanced Development of LIGA Resists," R. H. Nilson, S. K. Griffiths and A. Ting, *Microsystem Technologies*, 9, 113-118, 2002.
- "Transport Limitations on Development Times of LIGA PMMA Resists," S. K. Griffiths and R. H. Nilson, *Microsystem Technologies*, 8, 335-342, 2002.
- "Design and Analysis of Folded Channels for Chip-Based Separations," S. K. Griffiths and R. H. Nilson, *Analytical Chemistry*, 74, 2960-2967, 2002.
- "The Influence of X-Ray Fluorescence on LIGA Sidewall Tolerances," S. K. Griffiths and A. Ting, *Microsystem Technologies*, 8, 120-128, 2002.
- "Enhanced Transport by Acoustic Streaming in Deep Trench-Like Cavities," R. H. Nilson and S. K. Griffiths, *Journal of The Electrochemical Society*, 149 (4), 286-296, 2002.
- "Low-Dispersion Turns and Junctions for Microchannel Systems," S. K. Griffiths and R. H. Nilson, *Analytical Chemistry*, 73, 272-278, 2001.
- "Band Spreading in Two-Dimension Microchannel Turns for Electrokinetic Species Transport," S. K. Griffiths and R. H. Nilson, *Analytical Chemistry*, 72, 5473-5482, November 2000.
- "Electroosmotic Fluid Motion and Late-Time Solute Transport at Non-Negligible Zeta Potentials," S. K. Griffiths and R. H. Nilson, *Analytical Chemistry*, 72, 4767-4777, October 2000. Accelerated Article.
- "Conditions for Similitude Between the Fluid Velocity and Electric Field in Electroosmotic Flow," E. B. Cummings, S. K. Griffiths, R. H. Nilson and P. H. Paul, *Analytical Chemistry*, 72, 2526-2532, June 2000.
- "The Influence of Mask Substrate Thickness on Exposure and Development Times for the LIGA Process," S. K. Griffiths, A. Ting and J. M. Hruby, *Microsystem Technologies*, 6 (3), 99-102, February 2000.
- "Hydrodynamic Dispersion of a Neutral Non-Reacting Solute in Electroosmotic Flow," S. K. Griffiths and R. H. Nilson, *Analytical Chemistry*, 71 (24), 5522-5529, December 1999.
- "The Influence of Feature Sidewall Tolerance on Minimum Absorber Thickness for LIGA X-Ray Masks," S. K. Griffiths, J. M. Hruby and A. Ting, *Journal of Micromechanical Microengineering*, 9 (4), 353-361, December 1999 (Featured Article).
- "Condensation Pressures in Small Pores: An Analytical Model Based on Density Functional Theory," R. H. Nilson and S. K. Griffiths, *Journal of Chemical Physics*, 111, No. 9, 4281-4290, September 1999.

- "Scaling of Wafer Stresses and Thermal Processes to Large Wafers," R. H. Nilson and S. K. Griffiths, *Thin Solid Films*, Vol. 315, No. 1-2, 286-293, June 1998.
- "Modeling Electrodeposition for LIGA Microdevice Fabrication," S. K. Griffiths, R. H. Nilson, A. Ting, R. W. Bradshaw, W. D. Bonivert and J. M. Hruby, *Microsystems Technologies*, Vol. 4, No. 2, 98-101, 1998.
- "Optimum Conditions for Composites Fiber Coating by Chemical Vapor Infiltration," S. K. Griffiths and R. H. Nilson, *J. Electrochem. Soc.*, Vol. 145, No.4, 1263-1272, 1998.
- "A Locally Analytic Density Functional Theory Describing Adsorption and Condensation in Microporous Materials," R. H. Nilson and S. K. Griffiths, *Journal of Chemical Physics*, Vol. 108, No. 3, 1162-1174, 1998.
- "Deposition Uniformity, Particle Nucleation and the Optimum Conditions for Chemical Vapor Deposition in Multi-Wafer Furnaces," S. K. Griffiths and R. H. Nilson, *J. Electrochem. Soc.*, 144, No.4, 1399-1410, 1997.
- "The Effect of Elastomeric Liners on High-Pressure Liquid Propellant Combustion Oscillations," S. R. Vosen, R. W. Carling, R. E. Rychnovsky, S. K. Griffiths and R. F. Renzi, *Propellants Explosives and Pyrotechnics*, 20, No. 6, 311-321, 1995.
- "Freezing Flow in a Subcooled Permeable Medium," S. K. Griffiths and R. H. Nilson, *ASME Journal of Heat Transfer*, Vol. 114, 1036-1041, November, 1992.
- "Similarity Analysis of Fracture Growth and Flame Spread in Deformable Solid Propellants," S. K. Griffiths and R. H. Nilson, *Combustion and Flame*, Vol. 88, 369-383, 1992.
- "Wormhole Growth in Soluble Porous Materials," R. H. Nilson and S. K. Griffiths, *Physical Review Letters*, Vol. 65, No. 13, September 24, 1990.
- "Similarity Analysis of Condensing Flows in a Fluid Driven Fracture," S. K. Griffiths and R. H. Nilson, *J. of Heat Transfer*, Vol 110, 754-762, 1988.
- "Hybrid Analytical/Numerical Computation of Heat Transfer in a Gas-Driven Fracture," S. K. Griffiths, R. H. Nilson and F. A. Morrison, Jr., *J. Heat Transfer*, Vol. 108, No. 3, 1986.
- "Similarity Analysis of Energy Transport in Gas-Driven Fractures," R. H. Nilson and S. K. Griffiths, *International Journal of Fracture*, Vol. 30, No. 2, 1986.
- "Hydrogen Combustion In Aqueous Foams," M. R. Baer, S. K. Griffiths and J. E. Shepherd, *Nuclear Science and Engineering*, Vol. 88, 436-444, 1984.
- "Numerical Analysis of Hydraulically-Driven Fractures," R. H. Nilson and S. K. Griffiths, *Computer Methods in Applied Mechanics and Engineering*, Vol. 36, 359-370, 1983.
- "The Fluid Motion and Transport in and about an Assemblage of Drops in an Electric Field," S. K. Griffiths and F. A. Morrison, Jr., *J. of Colloid and Interface Science*, Vol. 94, No. 2, 514-523, 1983.
- "The Reduction of Blast Noise with Aqueous Foam," R. Raspet and S. K. Griffiths, *J. Acoustical Society of America*, Vol. 74, No. 6, 1757-1763, December 1982.
- "The Transport from a Drop in an Alternating Electric Field," S. K. Griffiths and F. A. Morrison, Jr., *Int. J. Heat and Mass Transfer*, Vol. 26, No. 5, 717-726, 1982.
- "On the Transient Convective Transport from a Body of Arbitrary Shape," F. A. Morrison, Jr. and S. K. Griffiths, *J. Heat Transfer*, Trans. ASME, Vol. 103, No. 1, 92-95, February 1981.
- "Low Peclet Number Heat and Mass Transfer from a Drop in an Electric Field," S. K. Griffiths and F. A. Morrison, Jr., *J. Heat Transfer*, Trans. ASME, Vol. 101, No. 3, 484-488, August 1979.

Patents

"Vitreous Carbon Mask Substrate for X-Ray Lithography," G. Aigeldinger, D. M. Skala, S. K. Griffiths, A. A. Talin, C. Y. P. Yang, US Patent Number 7,608,367. Issued October 27, 2009.

"Portable Apparatus for Separating Sample and Detecting Target Analytes," R. Renzi, S. K. Griffiths, et al., US Patent Number 7,452,507. Issued November 18, 2008.

"Apparatus for Producing a Thin Sample Band in a Microchannel System," S. K. Griffiths and R. H. Nilson, US Patent Number 7,371,310. Issued May 13, 2008.

"Axially Tapered and Bilayer Microchannels for Evaporative Cooling Devices," R. H. Nilson and S. K. Griffiths, US Patent Number 6,951,243. Issued October 4, 2005.

"Method for Producing a Thin Sample Band in Microchannel Devices" S. K. Griffiths and R. H. Nilson, US Patent Number 6,770,182. Issued August 3, 2004.

"Method and Apparatus for Reducing Sample Dispersion in Turns and Junctions of Microchannel Systems," S. K. Griffiths and R. H. Nilson, US Patent Number 6,733,730. Issued May 11, 2004.

"Compact Microchannel System," S. K. Griffiths. US Patent Number 6,627,076. Issued September 30, 2003

"Support Apparatus for Semiconductor Wafer Processing," S. K. Griffiths, R. H. Nilson, and K. J. Torres. US Patent Number 6,576,064. Issued June 10, 2003.

"Method and Apparatus for Thermal Processing of Semiconductor Substrates," S. K. Griffiths, R. H. Nilson, B. S. Mattson and S. E. Savas. US Patent Number 6,355,909. Issued March 12, 2002.

"Porous Electrode Method and Apparatus for Electroforming of Detailed Metal Structures or Microelectronic Interconnections," S. K. Griffiths, R. H. Nilson, and J. M. Hruby. US Patent Number 6,355,147. Issued March 12, 2002.

"Method and Apparatus for Reducing Sample Dispersion in Turns and Junctions of Microchannel Systems," S. K. Griffiths and R. H. Nilson, US Patent Number 6,270,641. Issued August 7, 2001.

"Method and Apparatus for Thermal Processing of Semiconductor Wafers," S. K. Griffiths, R. H. Nilson, B. S. Mattson and S. E. Savas, Taiwan Patent Number 129800. Issued July 27, 2001.

"Method and Apparatus for Thermal Processing of Semiconductor Wafers," S. K. Griffiths, R. H. Nilson, B. S. Mattson and S. E. Savas, US Patent Number 6,133,550. Issued October 17, 2000.

Selected Presentations, Proceedings and Reports

"Wall Functions for Incorporation of Atomistic Physics into Continuum Modeling of Electrokinetic Flow," R. H. Nilson and S. K. Griffiths, *Proceedings of Nanotech 2006*, Boston, ISBN 0-9767985-9-X, Vol. 3 (5) 503-506, May 2006.

"Hybrid Atomistic-Continuum Modeling of Electroosmotic Flow in Nanoscale Channels," R. H. Nilson and S. K. Griffiths, *Proceedings of the 9th International Conference on Miniaturized Systems for Chemistry and Life Sciences (μ TAS 2005)*, Boston, Massachusetts, October 9-13, 2005.

"Modeling Nanoscale Flows by Combining Density Functional Theory with Classical Continuum Mechanics," R. H. Nilson and S. K. Griffiths, 8th U.S. National Congress on Computational Mechanics, Austin, TX, July 25-27, 2005.

"3-D Numerical Simulations of Dimensional Errors in LIGA-produced Structures due to PMMA Swelling," N. Bhutani, M. A. Hekmaty, Y. Ohashi, S. K. Griffiths, *Sixth International Conference on High Aspect Ratio Microstructure Technology (HARMST '05)*, Gyeongju, Korea, June 10-13, 2005.

"An aluminum Substrate for Microfabrication by LIGA," S. K. Griffiths, M. W. Losey, J. T. Hachman, D. M. Skala, L. L. Hunter, N. Y. C. Yang, D. R. Boehme, J. S. Korellis, G. Aigeldinger, W. Y. Lu, J. J. Kelly, M. A. Hekmaty, D. E. McLean, P. C. Y. Yang, C. A. Hauck and T. A. Friedmann, SAND2005-2521, April 2005.

"Development of Models and Online Diagnostic Monitors of the High-Temperature Corrosion in Oxy/Fuel Glass Furnaces," M. D. Allendorf, R. H. Nilson, S. F. Rice, S. K. Griffiths, P. M. Walsh, N. Y. Yang, B. Bugeat, M. Usman-Ghani, O. Marin, G. Pecoraro, K. E. Spear, E. Wolfe and M. Velez, SAND2005-1196, April 2005.

"A Modeling and Simulation Investment Strategy for Enabling Microsystems Technologies: An ASC Program Plan," V. Tikare, M. T. Dugger, T. E. Buchheit, S. K. Griffiths, R. C. Schmidt, J. S. Custer, S. N. Kempka, G. E. Sleaf, C. C. Wong, K. A. Peterson, C. A. Applett, R. J. Shul and F. Bitsie, SAND2004-4828, October 2004.

"W80 LEP GTS Peer Review Committee Report (U)," M. F. Hardwick, S. K. Griffiths, J. L. Handrock, B. L. Haroldsen, K. Wally, W. S. Winters, RS-8243/040192, October 2004.

"Modeling Nano-Fluidics with Application to Electrokinetic Pumps," S. K. Griffiths and R. H. Nilson, Fifth International SmallTalk Conference, Association for Laboratory Automation, San Jose, California, July 13-16, 2003. Invited Presentation.

"Fundamental Limitations of LIGA X-Ray Lithography," S. K. Griffiths, Fifth International Conference on High Aspect Ratio Microstructure Technology (HARMST '03), Monterey, California, June 15-17, 2003. Invited presentation.

"Optimization of Electrokinetic Pumps for Chip-Based Chromatographic Separations, S. K. Griffiths and R. H. Nilson, Proceedings of the Sixth International Conference on Miniaturized Chemical and Biological Analysis Systems (μ TAS 2002), Nara, Japan, November 3-7, 2002.

"Stream Function and Vorticity Formulation for Electrokinetic Transport in Microchannel Devices," R. H. Nilson and S. K. Griffiths, Proceedings of the Fifth World Conference on Computational Mechanics (WCCM-V), Vienna, Austria, July 7-12, 2002. Invited Presentation.

"Modeling Electrokinetic Transport for the Design and Optimization of Microchannel Systems," S. K. Griffiths and R. H. Nilson, Fifth International Conference on Miniaturized Chemical and Biological Analysis Systems (μ TAS 2001), Monterey, California, October 21-25, 2001. Invited Plenary Presentation.

"Transport Limitations on Development Times of LIGA PMMA Resists," S. K. Griffiths and R. H. Nilson, Fourth International Conference on High Aspect Ratio Microstructure Technology (HARMST '01), Baden-Baden, Germany, June 17-19, 2001.

"Modeling Acoustic Agitation for Enhanced Development of LIGA Resists," R. H. Nilson, S. K. Griffiths and A. Ting, Fourth International Conference on High Aspect Ratio Microstructure Technology (HARMST '01), Baden-Baden, Germany, June 17-19, 2001.

"Inverted Method for Simulation of Electrokinetic Transport in Microchannel Devices," R. H. Nilson and S. K. Griffiths, Proceedings of the Fourth International Conference on Modeling and Simulation of Microsystems, Hilton Head Island, SC, March 19-21, 2001. MSM2001, Computational Publications, Cambridge, MA, 2001.

"Chemical Vapor Infiltration," S. K. Griffiths and R. H. Nilson, Chapter 6 of Chemical Vapor Deposition, J. H. Park and T. S. Sudarshan, Eds, ISBN 0-87170-692X, ASM International, Materials Park, OH, 2001.

"Dispersion in Turns for Species Transport by Electrophoresis and Electroosmotic Flow," S. K. Griffiths and R. H. Nilson, Proceedings of the SPIE Symposium on Micromachining and Microfabrication, Santa Clara, CA, September 18-20, *Microfluidic Devices and Systems III*, 14177, No. 29, 2000.

"Acoustic Agitation for Enhanced Development of LIGA PMMA Resists," R. H. Nilson and S. K. Griffiths, Proceedings of the SPIE Symposium on Micromachining and Microfabrication, Santa Clara, CA, September 18-20, *Micromachining and Microfabrication Process Technology VI*, 14174, No. 5, 2000.

"Contained Rocket Motor Burn Demonstrations in X-Tunnel: Final Report for DoD/DOE Joint Demilitarization Technology Program," 24 authors including S. K. Griffiths and R. H. Nilson, J. Lipkin, Ed., Sandia National Laboratories Report, SAND2000-8238, printed May 2000.

"Numerical and Analytical Modeling of Gas Transport in the Tritium-Producing Burnable Absorber Rod (U)," R. H. Nilson, S. K. Griffiths and D. F. Cowgill, Sandia National Laboratories CRD Report, SAND2000-8231, printed May 2000.

"Electroosmotic Flow in a Tube or Channel at Non-Negligible Zeta Potentials," S. K. Griffiths and R. H. Nilson, Proceedings of the Third International Conference on Modeling and Simulation of Microsystems, San Diego, California, March 27-29, 2000. MSM2000, Computational Publications, Cambridge, MA, 2000. Also appears as SAND2000-8437.

"Numerical Evaluation of Rapid Thermal Processing Equipment," S. R. Vosen, D. J. Rader, R. H. Nilson and S. K. Griffiths, Sandia National Laboratories Report, SAND99-8261, printed November 1999.

"Application of Cryocycling to Rocket Motor Propellant Size Reduction and Reuse," J. Lipkin, L. Whinnery, S. Griffiths, R. Nilson, J. Kaminska, G. Mower, W. Munson, J. McNair, J. Elliot, NATO Advanced Research Workshop, Moscow, Russia, October 21, 1999.

"LIGA: Metals, Plastics and Ceramics, J. M. Hruby, A. Morales, L. Domeier, W. D. Bonivert, D. R. Boehme, M. A. Bankert, J. T. Hachmann, S. Leith, S. K. Griffiths and A. Ting, Proceedings of the SPIE Symposium on Micromachining and Microfabrication, Santa Clara, CA, September 20-22, *Micromachining and Microfabrication Process Technology*, 3874, No. 02, 1999.

"Irrotationality of Uniform Electro-Osmosis," E. B. Cummings, S. K. Griffiths and R. H. Nilson, Proceedings of the SPIE Symposium on Micromachining and Microfabrication, Santa Clara, CA, September 20-22, *Micro-Fluidic Devices and Systems*, 3877, No. 27, 1999.

"LIGA Micromachining at Sandia National Laboratories," A. M. Morales, J. M. Hruby, T. Bennett, M. Bankert, D. R. Boehme, W. D. Bonivert, J. Hachman, S. K. Griffiths, R. H. Nilson, A. Ting, L. Domeier, P. Keifer, 4th International Conference on the Commercialization of Microsystems, Dortmund, Germany, July 10th, 1999.

"The Influence of Mask Substrate Thickness on Exposure and Development Times for the LIGA Process," S. K. Griffiths, A. Ting and J. M. Hruby, Third International Conference on High Aspect Ratio Microstructure Technology (HARMST '99), Kisarazu Chiba, Japan, June 13-15, 1999.

"Eliminating Silicon Crystal Defects Induced by Thermal and Gravitational Stresses," R. H. Nilson and S. K. Griffiths, *Defects in Silicon III*, The Electrochemical Society, Vol. 99-1, 119-132, 1999. (Invited Paper, 195th Meeting of the Electrochemical Society, Seattle, WA, May 2-7, 1999).

"Hydrodynamic Dispersion of a Neutral Solute in Electroosmotic Flow," S. K. Griffiths and R. H. Nilson, Proceedings of the Second International Conference on Modeling and Simulation of Microsystems, San Juan, Puerto Rico, April 19-21, 1999. MSM99, Computational Publications, Cambridge, MA, 558-561, 1999.

"Optimum Doses and Mask Thickness for Synchrotron Exposure of PMMA Resists," S. K. Griffiths, J. M. Hruby and A. Ting, Proceedings of the SPIE Symposium on Design, Test and Microfabrication of MEM/MOEMS, Paris, France, March 30–April 1, 1999.

"PMMA Development Studies Using Various Synchrotron Sources and Exposure Conditions," M. X. Tan, M. A. Bankert, S. K. Griffiths, A. Ting, D. R. Boehme, S. Wilson and L. M. Balsler, Proceedings of the SPIE Symposium on Micromachining and Microfabrication, Santa Clara, CA, September 20-22, *Materials and Device Characterization in Micromachining* 3512, 1998.

"Modeling Electrodeposition for LIGA Microdevice Fabrication," S. K. Griffiths, R. H. Nilson, R. W. Bradshaw, A. Ting, W. D. Bonivert, J. T. Hachman and J. M. Hruby, Sandia National Laboratories Report, SAND98-8231, printed February 1998.

"Cryocycling of Energetic Materials: Final Report," S. Griffiths, J. Handrock, D. Kasberg, J. Lipkin, R. Nilson, V. Revelli, L. Weingarten and L. Whinnery, edited by J. Lipkin, Sandia National Laboratories Report, SAND97-8280, printed August 1997.

"Optimum Conditions for Maximum Centerline Deposition Rates in Chemical Vapor Infiltration for Composites Manufacturing," S. K. Griffiths and R. H. Nilson, Proceedings of the International Conference on Chemical Vapor Deposition: CVD XIV and EUROCYD 11, 192nd Meeting of the Electrochemical Society, Paris, France, September 1, 1997.

"Molecular-Scale Modeling of Adsorption in Microporous Materials Using a Hybrid Analytical/Numerical Method," R. H. Nilson and S. K. Griffiths, Second SIAM Conference of Mathematical Aspects of Materials Science, Philadelphia, PA, May 12-14, 1997.

"Thermal Processing Issues for 300 mm Silicon Wafers: Challenges and Opportunities," H. R. Huff, R. K. Goodall, R. H. Nilson and S. K. Griffiths, Proceedings of the 191st Meeting of the Electrochemical Society, Montreal, Canada, May 4-9, 1997.

"Scaling of Wafer Stresses and Thermal Processes to Large Wafers," R. H. Nilson and S. K. Griffiths, Proceedings of the 1997 International Conference on Metallurgical Coatings and Thin Films, American Vacuum Society, San Diego, CA, April 22, 1997 (Invited Paper).

"In Situ Bioremediation: A Network Model of Diffusion and Flow in Granular Porous Media," S. K. Griffiths, R. H. Nilson and R. W. Bradshaw, Sandia National Laboratories Report, SAND97-8250, printed April 1997.

"Analyses of Wafer Support and Transport Processes for 300 mm Wafers," S. K. Griffiths and R. H. Nilson, 6th International Conference on 300 mm Wafer Specification, SEMICON/Japan, Tokyo, Japan, December 5, 1996.

"Scaling Batch Processes for Large Wafer Diameters," R. H. Nilson and S. K. Griffiths, Second Large Diameter Wafer Thermal Issues Conference, SEMATECH, Austin, TX, September 25, 1996.

"Reduction of Pressure Oscillations in Liquid Propellant Combustion," R. E. Rychnovsky, R. W. Carling, S. K. Griffiths and S. R. Vosen, Sandia National Laboratories Report, SAND96-8205, printed January 1996.

"Sandia Support for the Textron Rapid Densification IPC Program," S. K. Griffiths, R. S. Larson, R. H. Nilson, L. L. Whinnery, T. Osterheld, M. Allendorf, B. A. Meyer and M. Nichols, ARPA Annual Review of the Textron Specialty Materials RD IPC Program, Chelmsford, MS, August 10, 1995.

"Particle Size Reduction of Propellants by Cryocycling," L. L. Whinnery, S. K. Griffiths, J. Lipkin, R. H. Nilson, S. Goods, D. Dawson, H. Radloff, R. S. Larson, B. Long, J. Swearngen, and J. M. Hruby, Sandia National Laboratories Report, SAND95-8227, printed May 1995.

"Exchange Front Stability in Packed-Column Chromatography," S. K. Griffiths and R. H. Nilson, Proceedings of the 4th Symposium on Multiphase Transport in Porous Media, FED 173/HTD-Vol. 265,

ASME Winter Annual Meeting, New Orleans, LA, November 28-December 3, 1993. Also appears as SAND93-8503.

"Injection Nozzle and Liquid Dispersion Effects in Liquid Propellant Combustion Pressure Oscillations," S. R. Vosen, S. K. Griffiths, R. E. Rychnovsky and R. W. Carling, Proceedings of the Joint 1993 JANNAF Propulsion Meeting and 30th JANNAF Combustion Subcommittee Meeting, Naval Postgraduate School, Monterey, California, November 15-18, 1993.

"The Effect of Elastomeric Liners on High-Pressure Liquid Propellant Combustion Oscillations," S. R. Vosen, R. W. Carling, R. E. Rychnovsky, S. K. Griffiths and R. F. Renzi, Sandia National Laboratories internal report, SAND92-8592, June 1993.

"Propellant Removal from Rocket Motors Containing Double-Base Compositions," L. Whinnery, S. K. Griffiths, J. M. Hruby, R. S. Larson, B. C. Long and J. Lipkin, Proceedings of the 23rd International Conference of Fraunhofer-Institut für Chemische Technologie (ICT) -- Waste Management of Energetic Materials and Polymers, Karlsruhe, Germany, June 30 - July 3, 1992.

"Results from Combustion Chamber Liner Tests in the Liquid Propellant Injector/Combustor," S. R. Vosen, R. W. Carling, R. E. Rychnovsky, S. K. Griffiths and R. F. Renzi, Proceedings of the 28th JANNAF Combustion Subcommittee Meeting, San Antonio, TX, October 28-November 1, 1991.

"Sustained Growth of Multiple Gas-Driven Fractures," S. K. Griffiths, R. H. Nilson and E. J. Halda, Proceedings of the 6th Symposium on Containment of Underground Nuclear Explosions, Reno, NV, September 23-27, 1991.

"Predicted Tritium and Helium Deliveries for Chaps Systems," S. K. Griffiths and J. M. Hruby, JOWOG-12 on Chemistry and Weapons Materials, AWE, Aldermaston, UK, September 10-14, 1990.

"The Effect of Height Stratification on Gravitational Coagulation and Settling of Aerosols," L. A. Mondy and S. K. Griffiths, Sandia National Laboratories Report, SAND87-0645, March 1990.

"Combustion of Liquid Propellant in a High-Pressure Injector/Combustor," R. W. Carling, R. E. Rychnovsky and S. K. Griffiths, Proceedings of the 26th JANNAF Combustion Meeting, Pasadena, CA, October 23-27, 1989. Also appears as SAND89-8719, December 1989.

"Choking Limitations on the Speed of Gas Driven Fractures," 5th Symposium on Containment of Underground Nuclear Explosions, S. K. Griffiths and R. H. Nilson, Mission Research Corporation, Santa Barbara, CA, September 18-22, 1989.

"Analysis of Condensing Flow in a Fluid Driven Fracture - Application to Nuclear Test Containment," S. K. Griffiths and R. H. Nilson, Fourth Symposium on the Containment of Underground Nuclear Tests, Colorado Springs, CO, September 21-25, 1987

"Transient Evaporating Flow in a Fluid Driven Fracture," S. K. Griffiths and R. H. Nilson, First International Multiphase Fluid Transients Symposium, ASME Fluids Engineering Division, Vol 41, 75-83, December 1986. (also appears as SAND86-8827)

"Hydraulic Fractures Driven By Two-Phase Flows," S. K. Griffiths and R. H. Nilson, ASME Winter Annual Meeting, Anaheim, CA, December 1986.

"Gap Leakage in Blast Gun Experiments," S. K. Griffiths, A. E. Lutz and W. S. Winters, Sandia National Laboratories, memo to L. I. Weingarten, July 28, 1986.

"Lethality Test Of Sprint Rocket Motor," S. K. Griffiths, Sandia National Laboratories, memo to F. H. Mathews, July 1, 1986.

"Similarity Analysis of Condensing Flow in a Fluid Driven Fracture, S. K. Griffiths and R. H., Sandia National Laboratories Report, SAND87-8667, March 1986.

- "Gas-Driven Fractures in Nuclear Test Containment," S. K. Griffiths and R. H. Nilson, Sandia National Laboratories Report, SAND85-8686, March 1986.
- "Self-Similar Analysis of Planar Hydraulic Fractures Driven by a Constant Flow Rate," R. H. and S. K. Griffiths, Sandia National Laboratories Report, SAND86-9694, March 1986.
- "Analysis of Fluid/Solid Interaction in Hydraulic Fracturing: Transition Between Laminar and Turbulent Flows," S. K. Griffiths and R. H. Nilson Fluid Transients In Fluid-Structure Interaction, Fluids Engineering Division, ASME, Vol. 30, 31-40, November 1985. (also appears as SAND85-8758)
- "Gas-Driven Fractures in Nuclear Test Containment," S. K. Griffiths and R. H. Nilson, Proceedings of the Third Symposium on Containment of Underground Nuclear Explosions, LLNL CONF-850953, September 1985. (also appears as SAND85-8686)
- "Gas Fracturing: Numerical Calculations and Field Experiments," S. K. Griffiths, C. W. Smith, and R. H. Nilson, Proceedings of the 25th U. S. Symposium on Rock Mechanics, American Institute of Mining, Metallurgical and Petroleum Engineers, Inc., 157-164, 1984.
- "Ignition of AL/FE₃O₄ Thermite Mixtures," S. K. Griffiths and W. F. Hammett, Ninth International Pyrotechnics Society Seminar, Colorado Springs, Co, August 7, 1984.
- "Shock Wave Propagation in Aqueous Foams," S. K. Griffiths, Gordon Research Conference, Plymouth State College, Plymouth, NH, August 2, 1984 (Invited Presentation).
- "Similarity Analysis of Energy Transport in Gas-Driven Fractures," R. H. Nilson and S. K. Griffiths, Sandia National Laboratories Report, SAND84-0469, June 1984.
- "The Permeability of Granular Beds Implaced in a Vertical Drill Hole," S. K. Griffiths and F. A. Morrison, Jr., ASME Fluids Engineering Symposium, Energy-sources Technology Conference, New Orleans, LA, February 12-16, 1984.
- "Numerical Analysis of Hydraulically Driven Fractures: Comparisons with Similarity Solutions and Experimental Results," S. K. Griffiths, C. W. Smith and R. H. Nilson, Proceedings of the Second Symposium on Containment of Underground Nuclear Explosions, Defense Nuclear Agency, Albuquerque, NM, Lawrence Livermore National Laboratory, CONF-830882, Vol. 2, August 2-4, 1983.
- "Hydrogen Combustion in Aqueous Foams," M. R. Baer, S. K. Griffiths, and J. E. Shepherd, 2nd International Symposium on Nuclear Reactor Thermal-Hydraulics, Santa Barbara, CA, January 12, 1983. Also appears as SAND82-0917.
- "Shock Propagation in Solid/Gas Systems," S. K. Griffiths, SUBWOG 29C on Damage Limitation, Atomic Weapons Research Establishment, Aldermaston, UK, April 10 and 14, 1983.
- "Numerical Analysis of Hydraulically-Driven Fractures," R. H. Nilson and S. K. Griffiths, Sandia National Laboratories, SAND81-2618, April 1982.
- "Deliberate Ignition and Water Fogs as H₂ Control Measures for Sequoyah," M. P. Sherman, M. R. Baer, and S. K. Griffiths, Proceedings of the Workshop on the Impact of Hydrogen on Water Reactor Safety, Vol., IV, Sandia National Laboratories, SAND81-0661, September 1981.
- "The Permeability of Emplaced Overton Sand: First Results of the U8e Backfill Experiment," S. K. Griffiths, Lawrence Livermore National Laboratory, ENN-78-44, June 30, 1978.

A	
1	Appendix M: List of Consideration Materials
2	Ex. 3179
3	Ex. 3220
4	Ex. 7219
5	Ex. 8122
6	Ex. 8553
7	Ex. 8664
8	Ex. 8665
9	Ex. 8666
10	Ex. 8666
11	Ex. 8667
12	Ex. 8668
13	Ex. 8669
14	Ex. 8669
15	Ex. 8670
16	Ex. 8670
17	Ex. 8671
18	Ex. 8672
19	Ex. 8672
20	Ex. 8673
21	Ex. 8674
22	Ex. 8675
23	Ex. 8675
24	Ex. 8676
25	Ex. 8677
26	Ex. 8678
27	Ex. 8679
28	Ex. 8680
29	Ex. 8681
30	Ex. 8681
31	Ex. 8681
32	Ex. 8681
33	Ex. 8683
34	Ex. 8683
35	Ex. 8684
36	Ex. 8686
37	Ex. 8687
38	Ex. 8688
39	Ex. 8689
40	Ex. 8690
41	Ex. 8690
42	Ex. 8691
43	Ex. 8692
44	Ex. 8692
45	Ex. 8693
46	Ex. 8694

	A
47	Ex. 8695
48	Ex. 8696
49	Ex. 8697
50	Ex. 8698
51	Ex. 9156
52	Ex. 9256
53	Ex. 9306
54	Ex. 9314
55	Ex. 9315
56	Ex. 9316
57	Ex. 9317
58	Ex. 9320
59	Ex. 9320
60	Ex. 9325
61	Ex. 9325
62	Ex. 9328
63	Ex. 9361
64	Ex. 9402
65	Ex. 9455
66	Ex. 9469
67	Ex. 9490
68	Ex. 9490
69	Ex. 9490
70	Ex. 9490
71	Ex. 9506
72	Ex. 9507
73	Ex. 9508
74	Ex. 9509
75	Ex. 9511-corrected
76	Ex. 9516
77	Ex. 9517
78	Ex. 9522
79	Ex. 9523
80	Ex. 9546
81	Ex. 9890
82	Ex. 9891
83	Ex. 10031
84	Ex. 10443
85	Ex. 10444
86	Ex. 11132
87	Ex. 11133
88	Ex. 11134
89	Ex. 11135
90	Ex. 11136
91	Ex. 11137
92	Ex. 11138

	A
93	Ex. 11139
94	Ex. 11140
95	Ex. 11141
96	Ex. 11142
97	Ex. 11143
98	Ex. 11144
99	Ex. 11145B
100	Ex. 11146
101	Ex. 11147
102	Ex. 11148
103	Ex. 11149
104	Ex. 11150
105	Ex. 11151
106	Ex. 11152
107	Ex. 11153
108	Ex. 11154
109	Ex. 11155
110	Ex. 11156
111	Ex. 11157
112	Ex. 11158
113	Ex. 11159
114	Ex. 11160
115	Ex. 11161
116	Ex. 11162
117	Ex. 11163
118	Ex. 11164
119	Ex. 11165
120	Ex. 11166
121	Ex. 11173
122	Ex. 11174
123	Ex. 11175
124	Ex. 11176
125	Ex. 22740
126	Deposition of Matt Lee Gochnour (20120913)
127	Deposition of Matt Lee Gochnour (20120914)
128	Deposition of Morten H. Emilsen (20111208)
129	Deposition of Stephen Paul Carmichael (20121218)
130	Deposition of Stephen Paul Carmichael (20121219)
131	Deposition of Tony Liao, Ph.D., Volume 1 (20130110)
132	Deposition of Tony Liao, Ph.D., Volume 2 (20130111)
133	BP-HZN-2179MDL00940544 - BP-HZN-2179MDL00940546

	A
134	BP-HZN-2179MDL01587191 - BP-HZN-2179MDL01587201
135	BP-HZN-2179MDL01592779 - BP-HZN-2179MDL01592798
136	BP-HZN-2179MDL01607006
137	BP-HZN-2179MDL01607007
138	BP-HZN-2179MDL01607019 - BP-HZN-2179MDL01607025
139	BP-HZN-2179MDL02208336
140	BP-HZN-2179MDL02208337 - BP-HZN-2179MDL02208357
141	BP-HZN-2179MDL02208358
142	BP-HZN-2179MDL02208359
143	BP-HZN-2179MDL02208359
144	BP-HZN-2179MDL02208359
145	BP-HZN-2179MDL04480747 - BP-HZN-2179MDL04480748
146	BP-HZN-2179MDL04480749
147	BP-HZN-2179MDL04480750
148	BP-HZN-2179MDL04480751
149	BP-HZN-2179MDL04480752
150	BP-HZN-2179MDL04810382
151	BP-HZN-2179MDL04810383
152	BP-HZN-2179MDL04823762
153	BP-HZN-2179MDL04825892 - BP-HZN-2179MDL04825893
154	BP-HZN-2179MDL04827503 - BP-HZN-2179MDL04827504
155	BP-HZN-2179MDL04831001 - BP-HZN-2179MDL04831003
156	BP-HZN-2179MDL04844415 - BP-HZN-2179MDL04844416
157	BP-HZN-2179MDL04851876
158	BP-HZN-2179MDL04851877
159	BP-HZN-2179MDL04859296
160	BP-HZN-2179MDL04869884
161	BP-HZN-2179MDL04869885
162	BP-HZN-2179MDL04877708
163	BP-HZN-2179MDL04884268
164	BP-HZN-2179MDL04896195
165	BP-HZN-2179MDL04896196
166	BP-HZN-2179MDL04917974
167	BP-HZN-2179MDL04918831 - BP-HZN-2179MDL04918832
168	BP-HZN-2179MDL04918833

	A
169	BP-HZN-2179MDL04920968
170	BP-HZN-2179MDL04920969
171	BP-HZN-2179MDL04930320 - BP-HZN-2179MDL04930323
172	BP-HZN-2179MDL05021364 - BP-HZN-2179MDL05021366
173	BP-HZN-2179MDL05021367
174	BP-HZN-2179MDL05021368
175	BP-HZN-2179MDL05050297 - BP-HZN-2179MDL05050299
176	BP-HZN-2179MDL05058495
177	BP-HZN-2179MDL05058495
178	BP-HZN-2179MDL05092120 - BP-HZN-2179MDL05092125
179	BP-HZN-2179MDL05101509 to 1510
180	BP-HZN-2179MDL05698790
181	BP-HZN-2179MDL05698790
182	BP-HZN-2179MDL05698791
183	BP-HZN-2179MDL05698791
184	BP-HZN-2179MDL05710447
185	BP-HZN-2179MDL05710457 - BP-HZN-2179MDL05710470
186	BP-HZN-2179MDL05713321 - BP-HZN-2179MDL05713330
187	BP-HZN-2179MDL05745820
188	BP-HZN-2179MDL05745880
189	BP-HZN-2179MDL05777324
190	BP-HZN-2179MDL05777325
191	BP-HZN-2179MDL05856301 - BP-HZN-2179MDL05856303
192	BP-HZN-2179MDL05857306 - BP-HZN-2179MDL05857308
193	BP-HZN-2179MDL05859638 - BP-HZN-2179MDL05859641
194	BP-HZN-2179MDL05860582 - BP-HZN-2179MDL05860584
195	BP-HZN-2179MDL05864479 - BP-HZN-2179MDL05864483
196	BP-HZN-2179MDL06089077
197	BP-HZN-2179MDL06099534 - BP-HZN-2179MDL06099535
198	BP-HZN-2179MDL06099534 - BP-HZN-2179MDL06099535
199	BP-HZN-2179MDL06126568
200	BP-HZN-2179MDL06336851
201	BP-HZN-2179MDL06495915

A	
202	BP-HZN-2179MDL06536400 - BP-HZN-2179MDL06536420
203	BP-HZN-2179MDL06608850 - BP-HZN-2179MDL06608859
204	BP-HZN-2179MDL06608860
205	BP-HZN-2179MDL06612452 - BP-HZN-2179MDL06612461
206	BP-HZN-2179MDL06612462
207	BP-HZN-2179MDL06876116 - BP-HZN-2179MDL06876144
208	BP-HZN-2179MDL06938097 TO 38105
209	BP-HZN-2179MDL06938106 - BP-HZN-2179MDL06938109
210	BP-HZN-2179MDL06938110
211	BP-HZN-2179MDL06938111
212	BP-HZN-2179MDL06938112
213	BP-HZN-2179MDL06939005 to 9013
214	BP-HZN-2179MDL06959089 - BP-HZN-2179MDL06959092
215	BP-HZN-2179MDL06959093
216	BP-HZN-2179MDL06959094
217	BP-HZN-2179MDL06959095
218	BP-HZN-2179MDL06959096
219	BP-HZN-2179MDL06959097
220	BP-HZN-2179MDL06959098
221	BP-HZN-2179MDL06959333 - BP-HZN-2179MDL0695339
222	BP-HZN-2179MDL06962142 - BP-HZN-2179MDL06962144
223	BP-HZN-2179MDL06962145 - BP-HZN-2179MDL06962152
224	BP-HZN-2179MDL06962153
225	BP-HZN-2179MDL06962198 - BP-HZN-2179MDL06962202
226	BP-HZN-2179MDL06962203 - BP-HZN-2179MDL06962205
227	BP-HZN-2179MDL07012741 - BP-HZN-2179MDL07012742
228	BP-HZN-2179MDL07012941 - BP-HZN-2179MDL07012945
229	BP-HZN-2179MDL07013314 - BP-HZN-2179MDL07013317
230	BP-HZN-2179MDL07013318
231	BP-HZN-2179MDL07013319
232	BP-HZN-2179MDL07013478 - BP-HZN-2179MDL07013483

	A
233	BP-HZN-2179MDL07013664 - BP-HZN-2179MDL07013673
234	BP-HZN-2179MDL07013756 - BP-HZN-2179MDL07013764
235	BP-HZN-2179MDL07014728 - BP-HZN-2179MDL07014729
236	BP-HZN-2179MDL07014730
237	BP-HZN-2179MDL07014731
238	BP-HZN-2179MDL07014732
239	BP-HZN-2179MDL07014733
240	BP-HZN-2179MDL07114100
241	BP-HZN-2179MDL07247552
242	BP-HZN-2179MDL07247752
243	BP-HZN-2179MDL07250945 - BP-HZN-2179MDL07250956
244	BP-HZN-2179MDL07263650
245	BP-HZN-2179MDL07284545 - BP-HZN-2179MDL07284554
246	BP-HZN-2179MDL07284666 - BP-HZN-2179MDL07284673
247	BP-HZN-2179MDL07287056 - BP-HZN-2179MDL07287058
248	BP-HZN-2179MDL07287059
249	BP-HZN-2179MDL07287060
250	BP-HZN-2179MDL07287061
251	BP-HZN-2179MDL07287062
252	BP-HZN-2179MDL07287750 - BP-HZN-2179MDL07287752
253	BP-HZN-2179MDL07287968 - BP-HZN-2179MDL07287969
254	BP-HZN-2179MDL07288901 - BP-HZN-2179MDL07288909
255	BP-HZN-2179MDL07288910
256	BP-HZN-2179MDL07288924 - BP-HZN-2179MDL07288926
257	BP-HZN-2179MDL07289825 - BP-HZN-2179MDL07289828
258	BP-HZN-2179MDL07289829
259	BP-HZN-2179MDL07290599 - BP-HZN-2179MDL07290601
260	BP-HZN-2179MDL07290602
261	BP-HZN-2179MDL07291113 - BP-HZN-2179MDL07291115
262	BP-HZN-2179MDL07291679
263	BP-HZN-2179MDL07291679

	A
264	BP-HZN-2179MDL07299385 - BP-HZN-2179MDL07299386
265	BP-HZN-2179MDL07299431 - BP-HZN-2179MDL07299432
266	BP-HZN-2179MDL07299794 - BP-HZN-2179MDL07299797
267	BP-HZN-2179MDL07300593 - BP-HZN-2179MDL07300597
268	BP-HZN-2179MDL07301891 - BP-HZN-2179MDL07301894
269	BP-HZN-2179MDL07301895
270	BP-HZN-2179MDL07301896
271	BP-HZN-2179MDL07301897
272	BP-HZN-2179MDL07302669 - BP-HZN-2179MDL07302672
273	BP-HZN-2179MDL07302673
274	BP-HZN-2179MDL07304106
275	BP-HZN-2179MDL07304506
276	BP-HZN-2179MDL07306418 - BP-HZN-2179MDL07306429
277	BP-HZN-2179MDL07308227 - BP-HZN-2179MDL07308228
278	BP-HZN-2179MDL07308229 - BP-HZN-2179MDL07308238
279	BP-HZN-2179MDL07308808
280	BP-HZN-2179MDL07308812 - BP-HZN-2179MDL07308816
281	BP-HZN-2179MDL07310116 - BP-HZN-2179MDL07310125
282	BP-HZN-2179MDL07310201 - BP-HZN-2179MDL07310203
283	BP-HZN-2179MDL07347878 - BP-HZN-2179MDL07347883
284	BP-HZN-2179MDL07348831
285	BP-HZN-2179MDL07359111 - BP-HZN-2179MDL07359115
286	BP-HZN-2179MDL07359132 - BP-HZN-2179MDL07359138
287	BP-HZN-2179MDL07459547
288	BP-HZN-2179MDL07459547
289	BP-HZN-2179MDL07556712
290	BP-HZN-2179MDL07556715
291	BP-HZN-2179MDL07556757
292	BP-HZN-2179MDL07556778
293	BP-HZN-2179MDL07557141
294	BP-HZN-2179MDL07568879

A	
295	BP-HZN-2179MDL07585667 - BP-HZN-2179MDL07585712
296	BP-HZN-2179MDL07585755 - BP-HZN-2179MDL07585769
297	BP-HZN-2179MDL07585805 - BP-HZN-2179MDL07585807
298	BP-HZN-2179MDL07633347
299	BP-HZN-BLY00000001-BP-HZN-BLY00000193
300	BP-HZN-BLY00051414 - BP-HZN-BLY00051417; BP-HZN-BLY00051578 - BP-HZN-BLY00051636
301	BP-HZN-BLY00051610
302	BP-HZN-BLY00082874 - BP-HZN-BLY00082914
303	BP-HZN-BLY00396283
304	BP-HZN-CEC017621 - BP-HZN-CEC017629
305	CAM_CIV_0102190 - CAM_CIV_0102202
306	DNV001-0021
307	DNV2011061503
308	DNV2011061504
309	DNV2011061511
310	DNV2011061606
311	DNV-SUPPL-000333
312	DSE003-031366
313	DSE030-330 - 331
314	DSE030-332-333
315	IMT954-011831 - 42
316	IMW014-000878 - IMW014-000906
317	LAL001-000355 - LAL001-000388
318	LAL037-004096 - LAL037-004128
319	LAL037-004192 - LAL037-004266
320	LAL137-027973
321	LAL144-005899 - 005905
322	LAL248-009068 - LAL248-009079
323	LAL278-042744 - LAL278-042746
324	LAL279-020402 - 020411
325	LAL279-20412
326	LAL279-20413
327	LNL020-19910 - 12
328	LNL020-19910 - 12
329	LNL067-4967 - 4978
330	DNV Forensic Examination of the Deepwater Horizon Blowout Preventer vols. I and II (20110320)
331	DNV Forensic Examination of the Deepwater Horizon Blowout Preventer vols. I and II (20110320)
332	NPT001-000125 - NPT0001-000129

	A
333	NPT001-000130
334	OII00041744 - OII00041745
335	SD 0340222; SD 034220; SD 034212
336	SDX004-0007730 - SDX004-0007748
337	SDX005-0026599
338	SDX005-0029904
339	SDX012-0024579
340	SDX012-0031790 - SDX012-0031807
341	SDX012-15870 - SDX012-15874
342	SDX013-0000257 - SDX013-0000268
343	SNL002-1428 - SNL002-1438
344	SNL002-20899 - SNL022-20915
345	SNL002-20933 - SNL022-20956
346	SNL007-6872 - SNL007-2875
347	SNL012-005725 - 005727
348	SNL019-4380
349	SNL019-4813 - SNL019-4829
350	SNL021-7530 - SNL021-7542
351	SNL021-7543 - SNL021-7548
352	SNL022-007753
353	SNL022-007753
354	SNL022-021579 - SNL022-021590
355	SNL022-20993 - SNL022-21012
356	SNL022-21243 - SNL022-21245
357	SNL022-21246 - SNL022-21248
358	SNL022-23742 - SNL022-23743
359	SNL022-23807 - SNL022-23807
360	SNL041-1436 - SNL041-1440
361	SNL042-019507 -
362	SNL043-006027 - SNL043-006076
363	SNL044-15512
364	SNL044-2450
365	SNL044-387
366	SNL045 - 998
367	SNL045-13567 - SNL045-13579
368	SNL045-13593 - SNL045-13600
369	SNL045-13673 - SNL045-13701
370	SNL045-1793 - SNL045-1817
371	SNL045-1833 - SNL045-1844
372	SNL045-1857 - SNL045-1860
373	SNL045-1878 - SNL045-1881
374	SNL045-1964 - SNL045-1979
375	SNL045-1996 - SNL045-2003
376	SNL045-2004 - SNL045-2012
377	SNL045-2013 - SNL045-2021
378	SNL045-2022 - SNL045-2023

	A
379	SNL046-082640
380	SNL046-71976
381	SNL046-82105- SNL046-82141
382	SNL047-13178 - SNL047-13222
383	SNL048-5360 - SNL048-5373
384	SNL048-705 - SNL048-731
385	SNL059-00136
386	SNL075-948 - 966
387	SNL084 - 003280 - SNL084-003286
388	SNL084-000111
389	SNL084-000259
390	SNL084-002132 -SNL084-002146
391	SNL084-002148
392	SNL084-002149 - SNL084-002154
393	SNL084-002155 - SNL084-002162
394	SNL084-002163 - SNL084-002166
395	SNL084-002176 - SNL084 - 003230
396	SNL084-003231 - SNL084-003248
397	SNL084-003249 - SNL084-003263
398	SNL084-003264 - SNL084 - 003278
399	SNL084-005091
400	SNL084-005092 - SNL084-005114
401	SNL084-005115
402	SNL084-005116
403	SNL084-008718 - SNL084-008757
404	SNL084-008718 - SNL084-008757
405	SNL084-008801 - SNL084-008814
406	SNL084-008878 - SNL084 - 008717
407	SNL084-0112
408	SNL084-0113
409	SNL084-0114
410	SNL084-016920
411	SNL084-016921
412	SNL084-016922
413	SNL084-016933 - SNL084-016938
414	SNL084-046793
415	SNL084-046794
416	SNL084-046795
417	SNL084-046796
418	SNL084-046797
419	SNL084-046798
420	SNL084-046799
421	SNL084-046800
422	SNL084-046801
423	SNL084-046802
424	SNL084-046803

	A
425	SNL084-046804
426	SNL084-046805
427	SNL084-046806
428	SNL084-046807
429	SNL084-046808
430	SNL084-046809
431	SNL084-046810
432	SNL084-046811
433	SNL084-046812
434	SNL084-046813
435	SNL084-046814
436	SNL084-046815
437	SNL084-046816
438	SNL084-046817
439	SNL084-046818
440	SNL084-046819
441	SNL084-046820
442	SNL084-046821
443	SNL084-046822
444	SNL084-046823
445	SNL084-046824
446	SNL084-046825
447	SNL084-046826
448	SNL084-046827
449	SNL084-046828
450	SNL084-046829
451	SNL084-046830
452	SNL084-046831
453	SNL084-046832
454	SNL084-046833
455	SNL084-046834
456	SNL084-046835
457	SNL084-046836
458	SNL084-046837
459	SNL084-046838
460	SNL084-046839
461	SNL084-046840
462	SNL084-046841
463	SNL084-046842
464	SNL084-046843
465	SNL084-046844
466	SNL084-046845
467	SNL084-046846
468	SNL084-050560 - 050577
469	SNL084-050560 - 050577
470	SNL084-06267

	A
471	SNL084-074525
472	SNL084-08758
473	SNL084-1571
474	SNL084-1579 - SNL084-1599
475	SNL084-1600 - SNL084-1626
476	SNL084-1627 - SNL084-1653
477	SNL084-1654 - SNL084-1680
478	SNL084-16553
479	SNL084-1682 - SNL084-1693
480	SNL084-1699 - SNL084-1727
481	SNL084-1728 - SNL084-1756
482	SNL084-2062 - SNL084-2071
483	SNL084-2072 - SNL084-2081
484	SNL084-2082 - SNL084-2091
485	SNL084-46784
486	SNL084-59000- SNL084-59003
487	SNL084-69040-SNL084-69043
488	SNL085-001149 - SNL085-001150
489	SNL085-001156 - SNL085-001173
490	SNL085-001174 - SNL085-001179
491	SNL085-042632 - SNL085-042644
492	SNL085-042858 - SNL085-042859
493	SNL085-042860 - SNL085-042885
494	SNL085-04287 - SNL085-042830
495	SNL087-001101 - SNL087-001103
496	SNL087-001145 - SNL087-001148
497	SNL087-001172- SNL087-001173
498	SNL087-001206 - SNL087-005671
499	SNL087-015349
500	SNL087-015349
501	SNL088-072912
502	SNL094-4714 - SNL094-4719
503	SNL110-1522 - 1534
504	SNL117-23918 - 23943
505	SNL148-1385 - SNL148-1398
506	SNL511-7730 - SNL511-7748
507	SNL512-15977 - SNL512-15982
508	SNL519-1701
509	WW-MDL-00022183 - WW-MDL-00022220
	L. Mattar, et al., Orifice Metering of Two-Phase Flow, J.
510	Petrol. Technol., 31, 1979. (19790000)
511	PT.2010.06.30_05.56-TO-2010.06.30_06.10.csv
512	1.3 Item 2 Top Hat 4 03 JUN 1130.pdf
	2.5.3.3.7 Beggs-Brill Correlation for 65953891 Pipeline
513	Production Zoltan
514	229_194_124 - kill and choke lines pictures

A	
515	229_194_126 - kill and choke lines pictures 1
	3.2 RFI 04 Bottom Kill REPORT 10 SEP V4
516	FINAL.webarchive
517	4 - 20 mA PRESSURE TRANSMITTER ATM. 1ST, STS
518	7.2 Item 02 RFI (Well Integr.textClipping
	9.2 Item 2 Design BOP Stack BoP and Wel Not to Scale2
519	22 April 2010.pdf (20100422)
	9.2 Item 2 Design BOP Stack BoP and Wel Not to Scale2
520	22 April 2010-1.pdf (20100422)
	9.2 Item 2 Design BOP Stack BoP and Wel Not to Scale2
521	22 April 2010-2.pdf (20100422)
522	A COUPLED WELLBORE/RESERVOIR SIMULATOR TO MODEL MULTIPHASE FLOW AND TEMPERATURE DISTRIBUTION, Peyman Pourafshary, 12/00/07 (20071200)
523	A Critical Review of Advanced Experimental Techniques to Measure Two-Phase Gas/Liquid Flow, the Open Fuels & Energy Science Journal, 2009
524	A NUMERICAL MODEL FOR MULTIPHASE FLOW ON OIL PRODUCTION WELLS, Sergio P. Ferro & Marcela B. Goldschmit
525	A theoretical basis for the Lockhart-Martinelli correlation for two-phase flow
526	Advances in Fixed-Area Expansion Devices, X. Fang, 08/00/99 (19990800)
527	An Evaluation of the Effects of Valve Body Erosion on Motor-Operated Valve Operability, Thomas H. Hunt & Michael E. Nitzel, 05/00/93 (19930500)
528	An Improved Two-Phase Pressure Drop Correlation for 180° Return Bends, Piotr A. Domanski & Christian J. L. Hermes, 05/21-23/06 (20060521 - 20060523)
529	APPLICATION OF MECHANISTIC MODELS IN PREDICTING FLOW BEHAVIOR IN DEVIATED WELLS UNDER UBD CONDITIONS, Faisal Abdullah ALAdwani, 05/00/03 (20030500)
530	Assessment of the erosion resistance of steels used for slurry handling and transport in mineral processing applications, H. Mcl. Clark, R.J. Llewellyn, 2001 (20010000)
531	Asymptotic Generalizations of the Lockhart-Martinelli Method for Two Phase Flows, Y.S. Muzychka & M.M. Awad, 03/00/10 (20100300)
532	Beggs and Brill method

	A
533	BOP Forensic Phase II Lab Notebook 4.19.11 Book 1 page 4 - BOP P-T Sensor data (20110419)
534	BOP Kill Side - w PT Sensor 12-2-2010_MG_0317 (PT Sensor Sign Augmented).jpg, 12/02/10 (20101202)
535	BOP Kill-Port Side view 11-17-2010 FBI_DSC0004 cropped.JPG, 11/17/10 (20101117)
536	BOP Stack Kill Side - photo from internet.jpg
537	CAMERON Fully Welded Ball Valves
538	CC40 Cv Curve.pdf
539	CFD Analysis of Effect of Elbow Radius on Pressure Drop in Multiphase Flow, Quamrul H. Mazumder
540	Chap 4-9 The Blowout Preventer Except page 210
541	Chapter 2 History of the Nevada Test Site and Nuclear Testing Background, National Cancer Institute
542	Chapter 3 Unsteady Flow
543	Chisholm, D., "A Theoretical Basis for the Lockhart-Martinelli Correlation for Two-Phase Flow," Int. J. Heat Mass Transfer., 10, 1967. (1967)
544	Chisholm, D., Two-Phase Flow in Pipelines and Heat Exchangers, Longman Group Ltd., London, 1983. (19830000)
545	Chokes
546	Control Valve Erosion Solutions, SEVERE SERVICE JOURNAL, Volume 11, Issue 4, 10/00/11 (20111000)
547	CORE-ANNULAR FLOWS, Annu. Rev. Fluid Mech., 1997 (1997000)
548	Critical and Subcritical Flow of Multiphase Mixtures Through Chokes, T.K. Perkins, 12/00/93
549	D. Chisholm and G. C. Watson, The Flow of Steam/Water Mixtures Through Sharp-Edged Orifices, Report 213, National Engineering Laboratory, East Killbride, Glasgow, 1966. (19660000)
550	Department of Chemical Engineering Fluids 4 - Two Phase Flow
551	Dynamic Modeling of Two-Phase Expansion During Operation of Absorption Refrigerators, A. Nouri-Borujerdi, A. Mirzaei
552	Equations of State (Ahmed) Front matter - FINAL.pdf

	A
553	EROSION AND CORROSION IN PIPING SYSTEMS FOR SEA WATER, DNV GUIDELINES No. 15, 08/00/04 (20040800)
554	Erosion in Long-Radius Elbows and Straight Pipes, The Erosion/Corrosion Research Center, 1998 (19980000)
555	Erosion Measurements in Linear, Oscillatory and Combined Oscillatory and Linear Flow Regimes, Richard Jepsen, Jesse Roberts & Joseph Gailani, 2004 (20040000)
556	Erosive Wear of Potential Valve Materials for Coal-Conversion Plants, L. Garner McDonald & John E. Kelley
557	Example Analysis: (Lee text (1st edition), Example 2.2)
558	Experimental and theoretical investigation on the discharge characteristic of stratified two-phase flow, B.A. Shannak, R.A. Damseh & A. Azzi, 11/04/10 (20101104)
559	Experimental investigation of contraction in single- and two-phase flow through sharp-edged short orifice, B. Shannak, L. Friedel, M. Alhusein, A. Azzi, 1999 (20101104)
560	Experimental study of two and three phase flows in large diameter inclined pipes, International Journal of Multiphase Flow 29, 2003 (20030000)
561	Frictional pressure drop of gas liquid two-phase flow in pipes, Nuclear Engineering and Design 238, 2008 (20100000)
562	Fundamentals of Multiphase Flows, Christopher E. Brennen, 2005 (20050000)
563	H. C. Simpson, D. H. Rooney and E. Grattan, Two-Phase Flow Through Gate Valves and Orifice Plates, Proc. Int. Conf. on Physical Modelling of Multiphase Flow, Coventry, England, 19–21 April 1983. (19830419 - 19830421)
564	HANDBOOK OF MULTIPHASE FLOW METERING, Revision 2, Tekna, 03/00/05 (20050300)
565	HCG037-005979 - 005980
566	HEAT TRANSFER AND FLOW PATTERN IN TWO-PHASE LOOPS: AN EXPERIMENTAL INVESTIGATION, Alessandro Franco, 2008 (20080000)

A	
567	http://books.google.com/books?id=ijRejo5uYc8C&pg=PA113&lpg=PA113&dq=martinelli+nelson+two+phase&source=bl&ots=Z1jRnkHO2c&sig=pVGNtAM0mgbTbeYMW TzoytgzIVY&hl=en&sa=X&ei=vojCUlicO6ztiQKB_4DwCw&ved=0CEoQ6AEwAw#v=onepage&q=martinelli%20nelson%20two%20phase&f=false
568	http://excelcalculations.blogspot.com/2012/02/flow-regime-map.html
569	http://ip-science.thomsonreuters.com/mjl/
570	http://wenku.baidu.com/view/b905f2956bec0975f465e24d.html###
571	http://www.onepetro.org/mslib/servlet/onepetroprevie w?id=00014285
572	http://www.scribd.com/doc/58159358/BP-Multi-Phase-Design-Manual
573	http://www.scribd.com/doc/75669647/65953891-Pipeline-Production-Zoltan
574	http://www.spec2000.net/16-dst.htm
575	http://www.sts-sensors.com/us/Home/Products/Pressure/tabid/401/Default.aspx
576	http://www.youtube.com/playlist?list=PL55798FA5584A9C48
577	Improving the Lockhart and Martinelli Two-Phase Flow Correlation by SAS, Adel Hemeida and Faisal Sumait, 1988 (19880000)
578	INDUSTRIAL 4 - 20 mA PRESSURE TRANSMITTER ATM
579	INDUSTRIAL 4 - 20 mA PRESSURE TRANSMITTER, STS
580	Influence of nozzle wear on flow rate and stream droplets size, V. Duvnjak, D. Banaj, R. Zimmer & V. Guberac, 1998 (19980000)
581	Instruction Manual for Oscillating Flow, ibidi, Version 1.5.0, 2011 (20110000)
582	INVESTIGATION OF EROSION WEAR OF DUCTILE MATERIALS WITH AND WITHOUT COATING, Rakesh Kumar, 07/00/11 (20110700)
583	Investigations of sand-water induced erosive wear of AISI 304L stainless steel pipes by pilot-scale and laboratory-scale testing, RJK Wood & TF Jones
584	IPM Brochure

	A
585	Letter from: Minnie Adame To: J. Robert Warren Re: Deposition of Tony T. Liao, Ph.D., Volume 1 (BP) (2010228)
586	Letter from: Minnie Adame To: J. Robert Warren Re: Deposition of Tony T. Liao, Ph.D., Volume 2 (BP) (20130228)
587	Liquid-Vapor Equilibrium Curves for Methane System by Using Peng-Robinson Equation of State, K. Ghanbari & S. Davoodi Majd, 2004 (200400000)
588	Lockhart, R.W. and Martinelli, R.C., "Proposed Correlation of Data for Isothermal Two Phase, Two Component Flow in Pipes," Chem. Engr. Progr., 45, 1949. (19490000)
589	Macondo - Well Control efforts, Dr. Ole B. Rygg, add energy, 03/03/11 (20110303)
590	Measurements of specific energies for erosive wear using a Coriolis erosion tester, Hector Mcl. Clark, John Tuzson, Kien K. Wong, 03/26/98 (19980326)
591	Multiphase Flow Models Range of Applicability, CTES, L.C., 05/18/98 (19980518)
592	Multiphase Flow Production Model (PROMOD1) THEORY AND USER'S MANUAL, DEA 67 PHASE I, 01/00/94 (19940100)
593	MULTIPHASE FLOW, B.J. Azzopardi
594	Natural sloshing frequencies and modes in a rectangular tank with a slat-type screen, Journal of Sound and Vibration, 2011 (20110000)
595	Nozzle Wear As it Affects Output in Spraying, R. P. Cromwell & D. S. Harrison
596	Numerical simulation of gas-liquid two-phase flow and convective heat transfer in a micro tube, Koji Fukagata, Nobuhide Kasagi, Poychat Ua-arayaporn, 2007 (20070000)
597	Numerical simulation of the Macondo well blowout reveal strong control of oil flow by reservoir permeability and exsolution of gas, PNAS, 03/31/11 (20110331)
598	Oil and gas production handbook, An introduction to oil and gas production, ABB, 04/00/10 (20100400)
599	On Productivity Index in Pseudo-steady and Boundary-dominated Flow Regimes, Akif Ibragimov

	A
600	P- T Sensor Orifice at Base of BOP 04-19-2011.png, 04/19/11, (20110419)
601	Part 3 Cavitation in Control Valves, Samson, 03/00/11 (20110300)
602	Perforating - When Failure Is the Objective, Oilfield Review, 08/00/09
603	Performance of a two-phase gas / liquid flow model in vertical wells, C.S. Kabir & A.R. Hasan, 1990 (19900000)
604	Petro 424 Section I PI, IPR Curves
605	Photographs - MG_0018.JPG
606	Photographs - MG_0020.JPG
607	Photographs - MG_0022.JPG
608	Photographs - MG_0026.JPG
609	Photographs - MG_0028.JPG
610	Photographs - MG_0034.JPG
611	Photographs - MG_0038.JPG
612	Photographs - MG_0043.JPG
613	Photographs - MG_0044.JPG
614	Picture (Device Independent Bitmap) 1.jpg
615	Pipe Erosion Measurement INTRODUCTION, MPM Technologies, Inc.)
616	PIPE FITTING FRICTION CALCULATION, FLUIDE DESIGN
617	Pipe Roughness Values, FLUIDE DESIGN, 02/00/03 (20030200)
618	PIPESIM Suite User Guide, Schlumberger, 2005 (20050000)
619	PNL002-000091 - PNL002-000120
620	Port Side view 12-21-2010 Talas TEI0066 cropped.JPG (20101221)
621	Prediction of Pressure, Temperature, and Velocity Distribution of Two-Phase Flow in Oil Wells, Journal of Petroleum Science & Engineering, 11/16/04
622	PREDICTION OF SAND EROSION IN PROCESS AND PIPE COMPONENTS, Asmund Huser & Oddmund Kvernfold, 03/22/00 (20000322)
623	Pressure Drop During Two-Phase Flow of Refrigerants in Horizontal Smooth Tubes, ACRC, 10/00/92 (19921000)
624	Pressure Drop Models Evaluation for Two-Phase Flow in 90 Degree Horizontal Elbows, Ingenieria Mecanica, Vol. 3, No. 3, 2010 (20100000)

A	
625	PRESSURE OSCILLATIONS CAUSED BY MOMENTUM ON SHUT IN OF A HIGH RATE WELL IN A FRACTURED FORMATION, Sanjay Bhatnagar, 06/00/89 (19890600)
626	Pressure Temperature (PT) Sensor, FLOW ASSURANCE PRODUCTS, TELEDYNE OIL & GAS
627	Pressure Transient Analysis (PTA), WIRELINE AND PERFORATING SERVICES, 12/00/07 (20071200)
628	PSC-MDL2179-005354
629	P-T Sensor on Hand Cart 06-13-2011 (1).png, 06/13/11, (20110613)
630	P-T Sensor on Hand Cart 06-13-2011 (2).png, 06/13/11, (20110613)
631	P-T Sensor Orifice and P-T Sensor at Base of BOP 4.19.11.png, 04/19/11 (20110419)
632	P-T Sensor Removed in Front of Orifice 04-19-2011.png, 04/19/11, (20110419)
633	PT.2010.06.29_08.06-TO-2010.06.29_08.39.xlsx
634	Relied-Upon Modeling Runs and code
635	Reproducing slugging oscillations of a real oil well, Florent Di Meglio, Glenn-Ole Kaasa, Nicolas Petit & Vidar Alstad, 12/15-17/10 (20101215 - 20101217)
636	Reproductive accuracy of two-phase flow pressure loss correlations for vertical 90° bends, A. Azzi, L. Friedel, R. Kibboua, & B. Shannak, 2002 (20020000)
637	Reservoir and Injection Technology and Heat Extraction Project Fifth Annual Report, R.N. Horne, H.J. Ramey, Jr., F.G. Miller, W.E. Brigham, Paul Kruger, 12/00/89 (19891200)
638	Review of flow rate estimates of the Deepwater Horizon oil spill, PNAS, 07/27/01 (20010727)
639	Sektion 5 a Renewable energy and district heating, Estimation and validation of models two phase flow from geothermal wells, 10th International Symposium on District Heating and Cooling, 09/05/06
640	SIZING OF RELIEF VALVES FOR TWO-PHASE FLOW IN THE BAYER PROCESS, QUOC-KHANK TRAN & MELISSA REYNOLDS, 2002 (20020000)
641	Solid Particle Erosion in Turbulent Flows Past Tube Banks, Joseph A.C. Humphrey, 02/00/90 (19900200)
642	SPE Production and Operations Symposium 2012, Volume 1 of 2, 05/14-16/12 (20120514 - 20120516)

A	
643	Stipulated Facts Concerning Source Control Events - Rec. Doc 7076, 08/09/2012. (20120809)
644	Table of Integrals, 2012 (20120000)
645	Technical Notes, Technical Note 2.116 Re: Abrasion Resistance of Piping Systems, J.B. Goddard, 11/01/94
646	The local resistance of gas - liquid two-phase flow through an orifice, Int. J. Heat & Fluid Flow, 1986 (19860000)
647	The Norsk Hydro Multi Phase Flow Loop. A high pressure flow loop for real three-phase hydrocarbon systems, Flow Measurement and Instrumentation 17, 2006 (20060000)
648	The scaling law of piping erosion, Bonelli Stephane, Brivois Olivier & Lachouette Damien, 2007 (20070000)
649	THE SKIN EFFECT AND ITS INFLUENCE ON THE PRODUCTIVE CAPACITY OF A WELL, A. F. VAN EVERDINGEN, Vol. 198, 1953 (19530000)
650	THEORETICAL UNCERTAINTY OF ORIFICE FLOW MEASUREMENT, DANIEL MEASUREMENT AND CONTROL WHITE PAPERS, EMERSON Process Management
651	Throttled Valve Cavitation and Erosion, Don Casada, 12/00/91 (19911200)
652	Time Dependence of Solid-Particle Impingement Erosion of an Aluminum Alloy, P. Veerabhadra Rao & Donald H. Buckley, NASA Technical Paper 2169, 08/00/83 (19830800)
653	TJMAR1-A Fortran Subroutine for Nonlinear Least Parameter Estimation, Jefferson, T. H., Sandia National Laboratories Report, SLL-73-0305, 1973. (1949)
654	TOPHAT.PT.20100628_034204_TO_20100628_041337 GRAPH.xlsx
655	Two-phase flow characteristics in multiple orifice valves, Experimental Thermal and Fluid Science 34, 2010 (20100000)
656	TWO-PHASE FLOW HEAT TRANSFER MEASUREMENTS AND CORRELATION FOR THE ENTIRE FLOW MAP IN HORIZONTAL PIPES, A. Ghajar, J Kim & C Tang
657	Two-phase flow through pressure safety valves, Experimental investigation and model prediction, Chemical Engineering Science 60, 06/13/05 (20050613)

	A
658	Two-Phase Friction
659	Two-Phase Frictional Pressure Drop Multipliers for SUVA R-134a Flowing in a Rectangular Duct, P Vassallo & K Keller, 12/13/04 (20041213)
660	Two-Phase Pressure Drop of Refrigerants During Flow Boiling in Small Channels: An Experimental Investigation and Correlation Development, T.N. Tran, M.C. Chyu, M.W. Wambasganss, D.M. France, 07/18-23/99 (19990718 - 19990723)
661	WATERJET NOZZLE MATERIAL TYPES, D. Wright, J. Wolgamott & G. Zink, 08/17-19/03 (20030817 - 20030819)
662	Whalley, P. B., Two-Phase Flow and Heat Transfer, Oxford University Press, New York, 1996. (19960000)